8-2012

Subsurface Planetary Investigation Techniques and Their Role for Assessing Subsurface Planetary Composition

Ahmed Elshafie
University of Arkansas, Fayetteville

SUBSURFACE PLANETARY INVESTIGATION TECHNIQUES AND THEIR ROLE FOR ASSESSING SUBSURFACE PLANETARY COMPOSITION.

SUBSURFACE PLANETARY INVESTIGATION TECHNIQUES AND THEIR ROLE FOR ASSESSING SUBSURFACE PLANETARY COMPOSITION

A dissertation submitted in partial fulfilment
of the requirements for the degree of
Doctor of Philosophy in Space and Planetary Science

By

Ahmed Mohamed ElShafie
Bachelor of Space Science, 2005
Cairo University

August 2012
University of Arkansas

ABSTRACT

Subsurface planetary investigation techniques are of high interest and importance for the scientific community. Not only they can enhance our knowledge of the history of planetary formation but also can lead to information about its future. Whether the investigation is being conducted remotely using imagers, radars or physically using penetrometers or drills, a pre-existed knowledge of the mechanical and electrical properties of the subsurface regolith should be acquired for better data interpretation and analysis. Therefore, the main objective of this work is to investigate the mechanical and electrical properties of planetary analogs, understand their role for assessing the subsurface structure and identify their character for subsurface investigation techniques. Through-out this research, we investigated the mechanical and electrical properties of regolith analogs with emphasis on testing the feasibility of using penetrometer to explore the subsurface of planetary bodies and estimate their structure and layering. We found probe's diameter and regolith density are the most dominant factors which affect penetration forces. We correlated the mechanical and electrical properties of regolith analogs to geomorphological shape formation. An increase in gully total length corresponds to an increase in dielectric constant, friction angle and formation bulk density which will enhance previous, current and future modelling, interpretation and analysis of optical imagery and radar data. We performed dielectric permittivity and hardness measurements for volcanic rocks in order to provide a cross relation between the dielectric constant of the investigated material and its hardness property. A linear increase in dielectric constant observed along with an increase in rock hardness. This will enhance characterization of the shallow subsurface when investigated using radar and drill/penetrometer.

This dissertation is approved for recommendation

to the Graduate Council.

Dissertation Director:

_____

(***Dr. Vincent Chevrier, Dr. Rick Ulrich)***

Dissertation Committee:

_____

(Dr. Derek Sears)

_____

(Dr. Mark Arnold)

DISSERTATION DUPLICATION RELEASE

I hereby authorize the University of Arkansas Libraries to duplicate this thesis when needed for research and/or scholarship.

Agreed _____

(Ahmed Mohamed ELShafie)

ACKNOWLEDGMENTS

I would like to acknowledge several people whom without their help; this dissertation would not see light. Dr. Vincent Chevrier, my graduate advisor, who stood beside me during harsh and good time, for sharing with me my research interest and providing guidance and support through my graduate work, who gave me the freedom to explore on my own, and at the same time the guidance to recover when my steps faltered and most importantly, his friendship during my graduate research. Dr. Rick Ulrick, my graduate co-advisor, for guidance and support my research for the past several years.

I am also indebted to my committee members, Dr. Derek Sears, Dr. Mark Arnold, Dr. Claud Lacy, for their constant assistance and support during my entire graduate research and for their guidance in forming my future. Dr. William Olvier and Dr. Larry Roe, for providing necessary directions during my graduate studies. Our program coordinators Hazel Sears, Dr. Rick Ulrick and Dr. John Dixon. Walter Graupner for technical and laboratory assistance and our program administrators Jessica Park and Kate Dreier.

I would like to express my gratitude to Dr. Essam Heggy, my internship supervisor, for guidance and support, who gave me the opportunity to work on a mission related experiment over NASA/Jet Propulsion Laboratory.

Most importantly, none of this would have been possible without the love and patience of my family. My immediate family, to whom this dissertation is dedicated to, has been a constant source of love, concern, support and strength all these years. I would like to express my heart-felt gratitude to my parents, Mohamed ElShafie and Inas ElGharini, my sisters, Amira, Amani, Tahani, my father and mother in law, Mahmoud ElSenousy and Samira and all my family, friends for supporting and encouraging me during my PhD life. I would like to thank Dr. Hafez

Elkordy and Dr. Farouk El-Baz for their faith in me and for keeping me ambitious during my PhD work.

Finally, and most importantly, I would like to thank my wife Amira and my daughter Jana for their support, encouragement, quiet patience and unwavering love were undeniably the bedrock upon which my PhD have been built. Their tolerance of my occasional vulgar moods is a testament in itself of their unyielding devotion and love.

DEDICATION

This dissertation is dedicated to all people and researchers who are interested in space science. I also dedicate this work to my parents Mohamed and Inas, my wife Amira, and my daughter Jana and my sisters, Amira, Amani, Tahani. There is no doubt in my mind that without their continued support and counsel I could not have completed this process.

TABLE OF CONTENTS

LIST OF PAPERS

ElShafie, A., V. F. Chevrier, R. Ulrich and L.Roe. 2010. Penetration testing for the Optical Probe for Regolith Analysis (OPRA). Advances in Space Research, 46, 327–336.

ElShafie, A., V. F. Chevrier, R. Ulrich. 2010. Penetration testing for subsurface regolith probes in Martian analog material. Proceedings of the International Planetary Probe Workshop, Barcelona, Spain, 370.

ElShafie, A., V. F. Chevrier. Mechanical Properties of Planetary Analog Materials and its Application for Subsurface Investigations. Submitted and in review for Planetary and Space Science (PSS).

ElShafie, A., E. Heggy. Dielectric and Hardness Measurements of Planetary Analog Rocks in Support of In Situ Subsurface Sampling. Submitted and in review for Planetary and Space Science (PSS).

CHAPTER 1: INTRODUCTION

1.1. Regolith on planetary bodies

Investigation of the physical and mechanical properties of regolith is highly important for in situ planetary exploration. Planetary regolith is a layer of loose, incoherent, fragmental materials of whatever origin that cover most of our planetary bodies (Gary et al., 1972). Under this definition, cratered planetary bodies formed by impacts are enveloped by regolith layers due to the transform of coherent surfaces to fragmental debris (Pike, 1980). Since most of our planetary bodies have signs of impacts, therefore, regolith layers are observed on most them, Mercury (Matson et al., 1977; Langevin, 1997; Killen et al., 2004), Venus (McGill et al., 1983; Sprague et al., 1995), Mars and its satellites (Thomas, 1979; Veverka and Burns, 1980; Fanale et al., 1982; Plumb et al., 1989), the Moon (Heiken et al., 1981; McKay et al., 1991), satellites of Jupiter and Saturn (Simonelli et al., 1997) and asteroids (Housen et al., 1979; Housen and Wilkening, 1982).

Geomorphological processes such as gullies and crater formation, erosion (Schultz, 2002; Sullivan et al., 2011) landslides and lithology of the subsurface layers (Lucas and Mangeney, 2007; Perko et al., 2006) are observed on most of our planetary bodies. Their formation is still speculative; however, their current form and stability depend on the mechanical properties of the regolith on which they are developed.

Stability of water ice, salts and some volatiles on planetary bodies is affected by regolith mechanical properties (Zolotov and Shock, 2001; Mellon et al., 2004). Diffusion of volatiles from the subsurface layers on Mars is affected by regolith porosity and tortuosity where both parameters are being strongly function of regolith compaction (Bryson et al., 2008; Chevrier et

al., 2007; Chevrier et al., 2008; Hudson et al., 2007). Therefore, understanding the mechanical properties of regolith analogs can help models of water ice stability.

Planetary regolith strength is commonly described in terms of regolith density, porosity and angle of internal friction (Schofield and Wroth, 1968). These parameters are relevant for understanding science issues concerning regolith origin, history, layering, regolith characteristics and composition. The angle of internal friction, is term used to describe the degree of regolith compaction (Gibson, 1953), is measured from the tangent of the slope of shear stress versus normal stress curve when the regolith fails (Terzaghi et al., 1996).

1.2. Regolith mechanical properties of the Moon

The Surveyor program successfully sent seven landers to the Moon in the period of 1966 to 1968 (Fragments, 1969). The main objective of the program was to investigate and demonstrate the feasibility of soft landing on the Moon (Scott and Roberson, 1969). Five out of the seven landers reached the surface of the Moon while Surveyor 2 crashed and Surveyor 7 lost its contact (Rennilson and Whitaker, 1969). Most of the Surveyor landers housed the Soil Mechanics Surface Sampler Experiment (SMSSE) which was used to investigate the mechanical properties of the subsurface of the Moon (Turkevich et al., 1967). Using the robotic arm as a penetration device, the robotic arm penetrated the subsurface of the Moon to a depth of 3 cm and the required force to reach that depth was about 30 N (Fig. 1.1) (Scott and Roberson, 1969). Estimation the angle of internal friction ranged from 35 to 37° from trench analysis and the regolith density was 1500 kg m^{-3} from picking up and weighting regolith (Scott and Roberson, 1969).

Russia designed and launched four rovers to the Moon in the period 1969 to 1977 to determine the feasibility of supporting manned missions to the Moon (Leonovich et al., 1971). Lunokhod 1 was destroyed during launch and Lunokhod 1977 was never launched (Leonovich et al., 1972). Both of the other two Lunokhods were equipped with a cone penetrometer called PROP to investigate the mechanical properties of the lunar soil (Leonovich et al., 1972). The penetrometer was cone in shape with a diameter of 5 cm and 60° apex angle (Cherkasov and Shvarev, 1973). During instrument penetration, information about the regolith bearing capacity, the ratio of vertical load to the area of the penetration of the cone, and density was recorded (Leonovich et al., 1976). From the forces of penetration, information about the subsurface stratigraphy as well as subsurface density was determined. Lunokhod 1 conducted penetration testing into the crater wall (curve 1), penetration into the crater slope (curve 2), penetration into a crater rim (curve 3) and penetration into an area covered with small rocks (curve 4, Fig. 1.2 A, Leonovich et al., 1972). Penetration into the crater wall was observed to have the minimum penetration resistance ~26 N with a maximum penetration depth of ~8 cm while the maximum force of penetration was recorded when penetrating into an area covered with small rocks (~38 N) with the minimum penetration depth (~6 cm).

Lunokhod 1 performed another penetration experiment in order to study the effect of packing of the lunar soil through multiple penetration of the penetrometer at the same point (Fig. 1.2 B, Leonovich et al., 1972). The regolith resistance increased significantly with repeated penetration. After the first penetration, the maximum force of penetration was ~22 N corresponded to a depth of ~8 cm. After repeating the penetration at the same point, the same maximum force was achieved at ~3 cm deep for the second and third trials. Lunar regolith

quickly compacted after the first penetration and roughly reached its maximum compaction state (Fig 1.2 B).

Lunokhod 2 conducted some penetration experiments on the surface of the Moon using the same technique to allow comparing the results obtained at different time and localities (Leonovich et al., 1976). Figure 1.3 shows the results obtained by the PROP penetrometer on-board Lunokhod 2 after penetrating at 6 different places (Leonovich et al., 1976). Curve 4 corresponds to penetration into a homogeneous regolith layer as shown by the linear increase in force along the penetration depth. Penetration into two different density levels was observed in curve 3 and 5 from the character of the penetration curve. For curve 3, the force of penetration increased at the beginning of penetration and then became constant while for curve 5, force of penetration showed steady increase up to 4 cm in depth then an abrupt increase in the force was observed after 4 cm. Curve 6 showed a steady increase of force as a function of depth. Curve 2 had a high penetration force due to high subsurface density. In some cases, the penetrometer managed to destroy subsurface aggregates and penetrate through the subsurface as shown in curve 1 at a depth of 1 – 3 cm (Leonovich et al., 1976).

The Apollo Simple Penetrometer (ASP) and Apollo Self-Recording Penetroemter (SRP) were used to investigate the mechanical properties of the lunar surface and subsurface on Apollo14, 15 and 16 missions (Mitchell et al., 1971). ASP was part of the Apollo 14 Lunar Surface Experiment Package (ALSEP) which landed in the Fra Mauro highlands 500 km from the edge of the Imbrium Basin. The ASP was a metal rod 68 cm long and 0.95 cm in diameter with a 30° cone angle (Fig. 1.4 A). The ASP was used in three penetration tests by manually pushing it into the lunar subsurface. The ASP reached depths of 42, 44 and 50 cm and the penetration force was in the range of 70–135 N using one hand. A second deployment of the

ASP reached a depth of 62 cm and required a force of 225 N using both hands (Mitchell et al., 1971). From the analysis of the penetration results conducted by Apollo 14 ASP, a clear distinction in the penetration forces as a function of depth is observed. A change in the subsurface density between the first deployment and the second one can be seen from the difference in penetration forces. An increase in the subsurface density as a function of depth can be concluded from the increase of the penetration forces between both deployments.

The Self-Recording Penetroemter (SRP) was used on the Apollo 15 and 16 missions. Apollo 15 mission landed in Hadley-Apennine region is the main boundary of the Imbrium Basin while Apollo 16 mission landed in western edge of the Descartes Mountains approximately 50 km west of the Kant Plateau. The SRP was a rod with a cone at the end pushed manually by the astronaut into the subsurface of the Moon (Fig. 1.4 B). The depth of penetration was recorded by a scriber on a metal cylinder in the upper housing assembly. The drum rotation was proportional to the amount of force exerted on the penetrometer. The independent motion of the drum and stylus produced a continuous force-depth curve on the surface of the drum (Carrier et al., 1991). At a maximum depth of 76 cm, the Apollo 15 SRP recorded a force of 111 N and the Apollo 16 SRP recorded a maximum force of 215 N (Mitchell et al., 1974). At the same depth of penetration, penetration forces increased from Apollo 15 to Apollo 16 which can be accounted for an increase in the subsurface density. From penetration forces conducted by ASP and SRP, the estimated angle of internal friction of the lunar regolith ranged from 46.5 to 50° and the regolith density associated with these parameters ranged from 1.9 to 2 gm cm^{-3} (Mitchell and Houston, 1974).

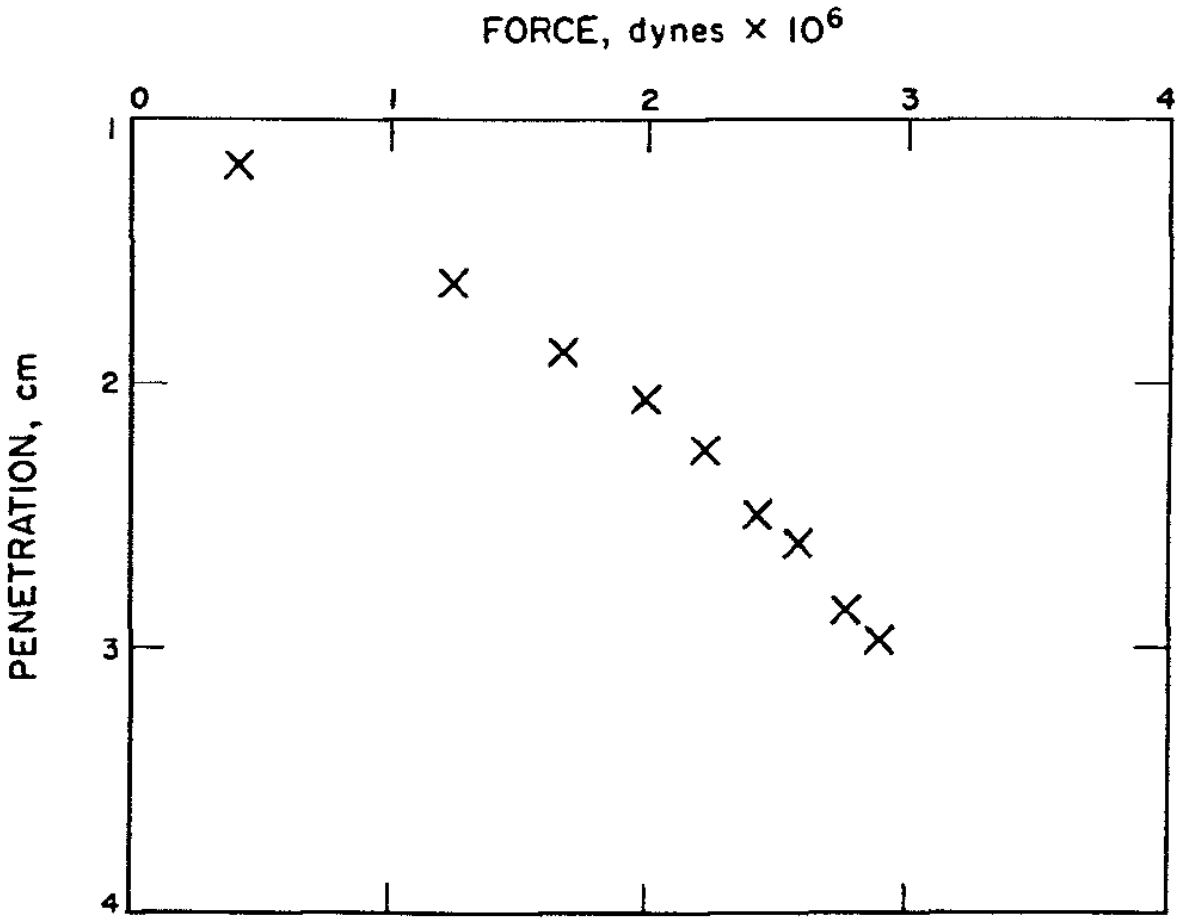

Figure 1.1. Penetration force as a function of depth using the robotic arm on board Surveyor 4 (Scott and Roberson, 1969).

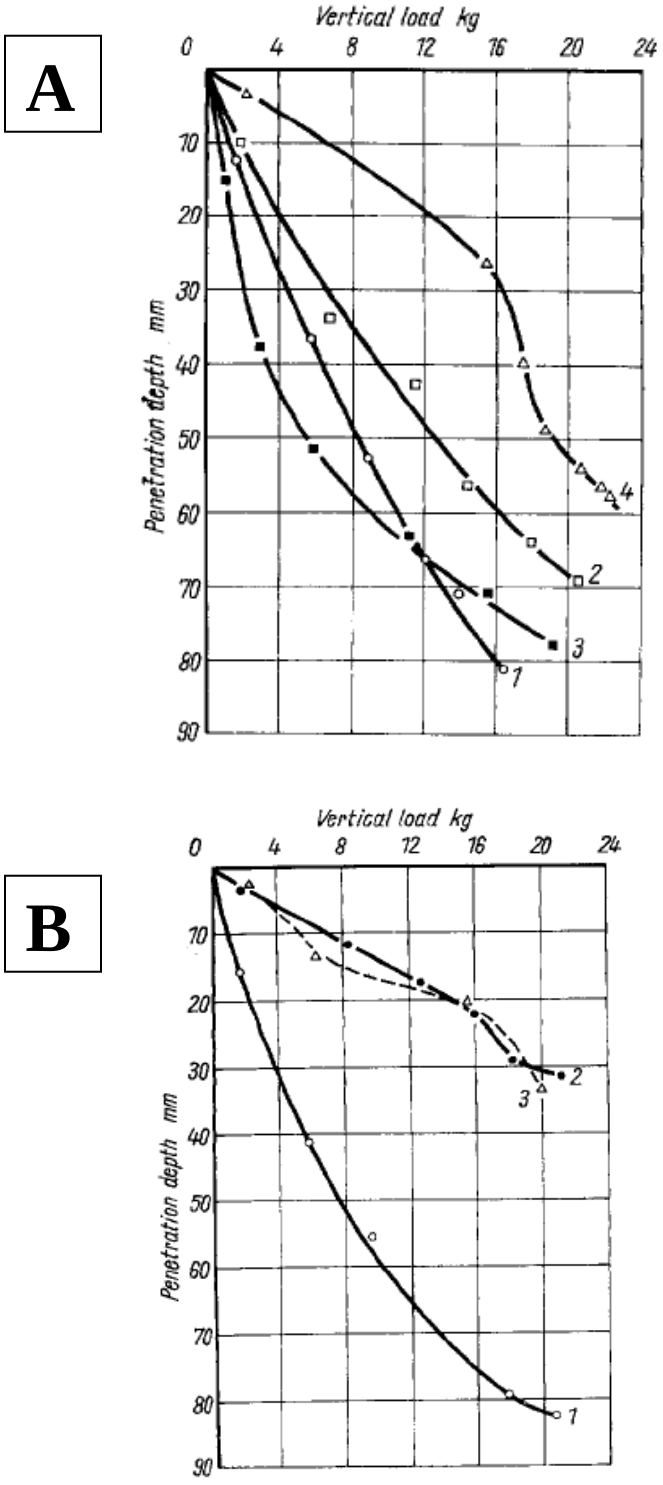

Figure 1.2 A. Penetration forces of cone penetrometer into lunar regolith (Leonovich et al., 1976). B. Penetration forces during investigation of lunar regolith packing capacity (Leonovich et al., 1976).

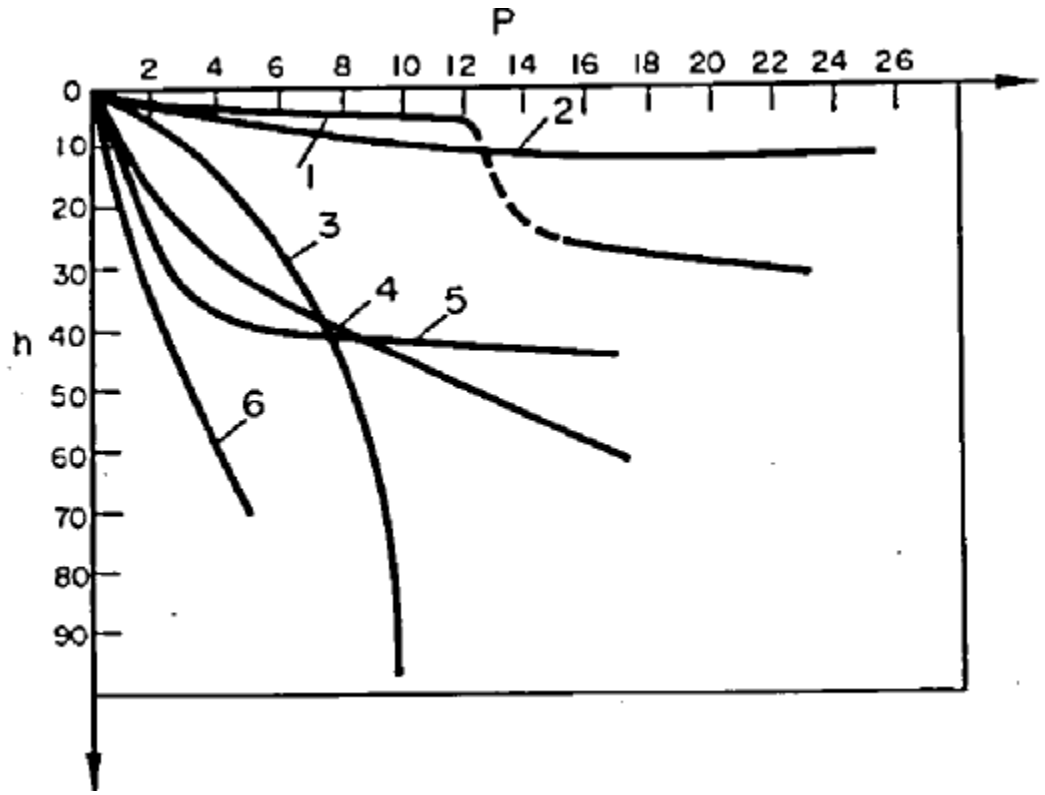

Figure 1.3. Penetration forces using Prop penetrometer: P, vertical load (kg); h, penetration depth (mm). 1, destruction of stone; 2, outcroppings of a hard base; 3, soil with enhanced passing-through capacity; 4, homogeneous layer of soil; 5, layer of loose soil on a hard base; 6, loose soil (Leonovich et al., 1976).

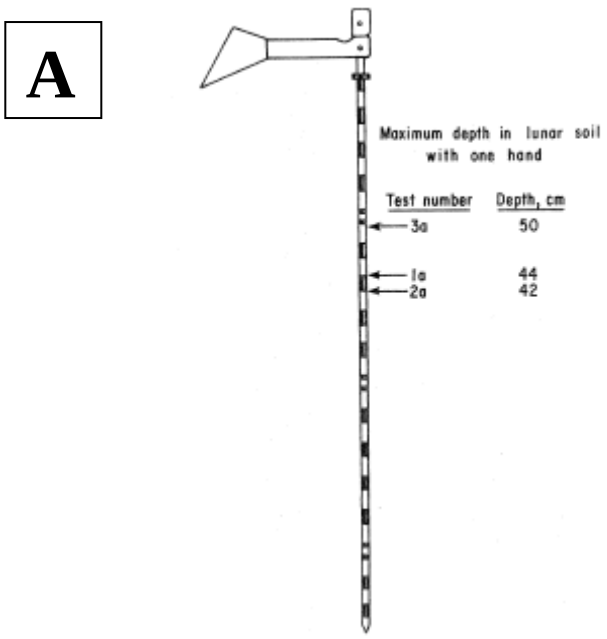

Figure 1.4 A. Apollo Simple Penetrometer (ASP) (Mitchell et al., 1971).

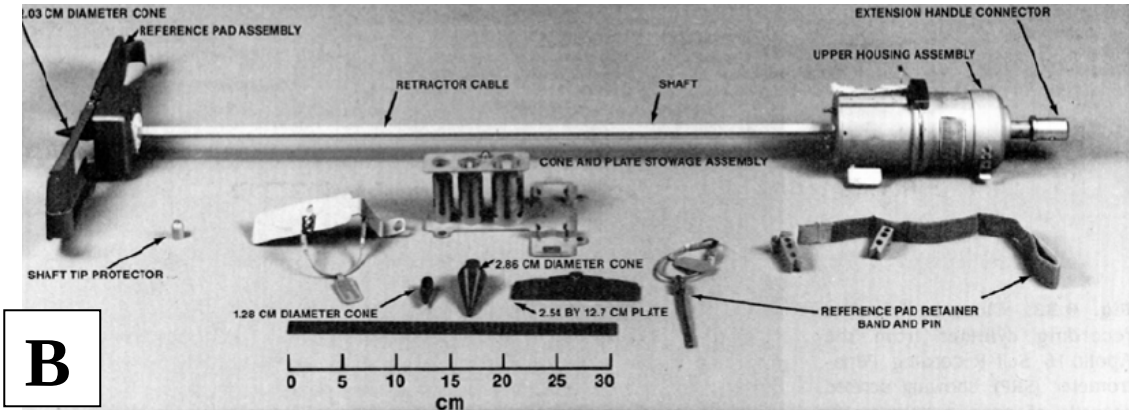

Figure 1. 4 B. Apollo Self-Recording Penetroemter (SRP) on board Apollo 15 and 16 (Carrier et al., 1991).

1.3. Regolith mechanical properties of Mars

Some of the mechanical measurements of the Martian surface and subsurface were conducted using the Viking (VL-1 and VL-2) landers footpad and surface sampler (Levin and Straat, 1976; Moore et al., 1977). VL-1 landed at a velocity of 2.3 m/s where the landers footpads measured the penetration forces and its corresponding depth. For VL-1, footpad 1 was not visible while footpad 2, 3 penetrated a depth of 16.5 and 3.6 cm and the penetration forces were ~4000 N and ~6000 N for footpad 2 and 3 respectively (Fig. 5 A) (Moore et al., 1977). VL-2 landed at a velocity of ~ 1.9 m/s, footpad 1 was not visible while footpad 2 and 3 penetrated a depth of 2.3 and ~ 0 – 0.3 cm. VL-2 landed on rocky material which explains the shallow depth of penetration and no information about penetration forces was recorded (Moore et al., 1977). Drift, blocky and crusty to cloddy are three different surface materials proposed at Viking landing sites (Moore and Clow, 1982). Several trenches formed using the landers surface sampler through excavation. Some of the mechanical properties of the Martian surface were estimated from the dimensional analysis of trenches. The angle of internal friction for drift and crusty to cloddy materials were 14° – 21° and 28° – 39° while a friction angle of 27° – 33° was estimated for blocky materials based on trench analysis (Fig. 5B, Moore and Clow, 1982).

The Sojourner rover was on board the Mars Pathfinder lander (Rover team, 1997). The mission aimed to investigating and analyzing the Martian atmosphere, climate, geology and the composition of its rocks and regolith (Bell III et al., 2000). Using the rover wheels as a trenching, excavating and scraping tool, some mechanical measurements were conducted at the landing site (Rover team, 1997). The friction angle of the Martian deposits was estimated from the correlation of the electric current in the wheel motor during a digging and trenching experiment.

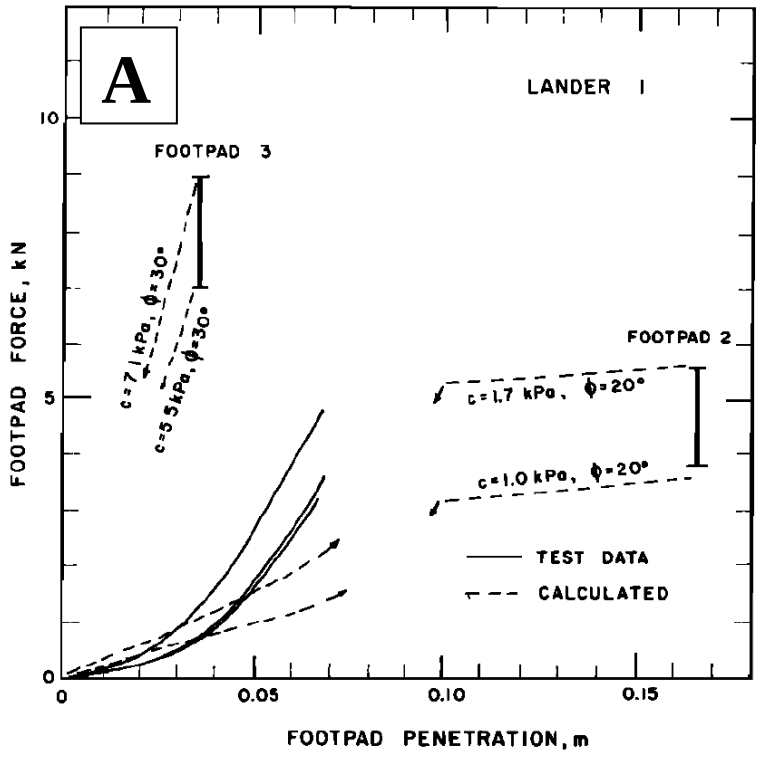

Figure 1.5 A. Footpad penetration force as a function of penetration depth for VL-1 (Moore and Clow, 1982).

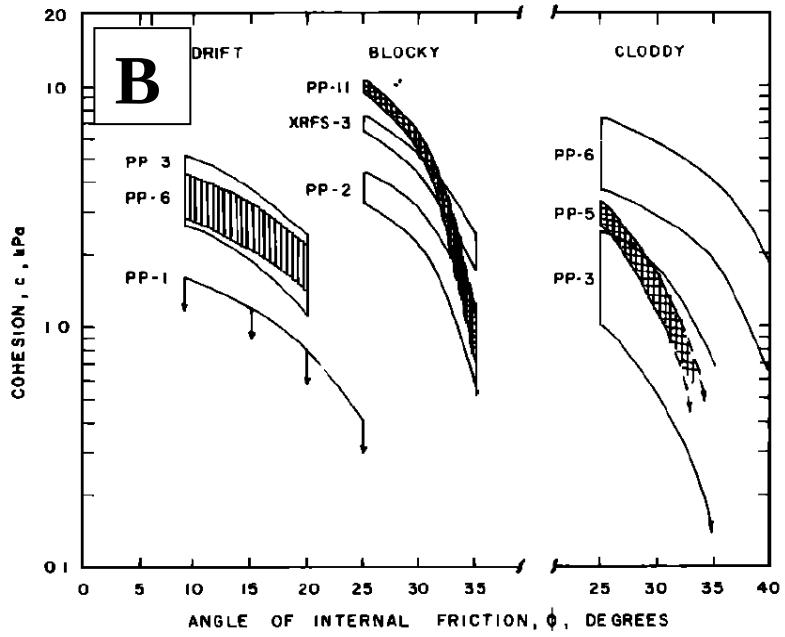

Figure 1.5 B. Cohesion versus angle of internal friction for sample trenches (Moore and Clow, 1982).

Drift and mixed materials showed low (28.2°) to moderate (34° – 38°) angle of internal friction while cloddy materials showed higher values (33.3° – 42.4°) assuming the angle of internal friction is equal to the angle of repose (Rover team, 1997).

Mars Exploration Rover (MER) mission used two rovers, Spirit and Opportunity to investigate and explore the Martian surface and geology with the main goal of searching for clues of past water activity on Mars (Rieder et al., 2003). The rover wheels was used as a shear device which allowed estimation of the regolith angle of internal friction which ranged from 30° – 37° (Sullivan et al., 2011).

The Mars Phoenix Lander launched in May, 2008 and operated until November, 2008 (Smith et al., 2008). The Phoenix Lander objected to search for environments suitable for microbial life, and to research for the history of water on Mars (Arvidson et al., 2008). The lander was equipped with a 2.4 m robotic arm that used to excavate and acquire samples from the subsurface of Mars and deliver it to other on-board instruments for analysis (Bonitz et al., 2008). The angle of internal friction was estimated by the Phoenix lander robotic arm based on the assumption of the slope of dump piles equal to the angle of internal friction and it was estimated to be 38° ± 5° (Shaw et al., 2009).

1.4. Regolith mechanical properties of Titan

The Cassini-Huygens mission objected to investigate Saturn and its largest satellite Titan (Matson et al., 2002). The Huygen probe housed instruments to explore the surface and the subsurface of Titan, the Surface Science Package (SSP, Fig. 1.6 A, Zarnecki et al., 2002). Among the instruments and sensors on board the SSP, the ACC-E penetrometer (Fig 1.6 B), was assigned to measure the mechanical properties of the surface and the subsurface of Titan (Lorenz

et al., 1994). From the impact force profile of the thumb-size sensor (mass of 15 g) the density, cohesion and particle size distribution of the subsurface materials were estimated during the first 40 mm of penetration (Zarnecki et al., 2002). Figure 1.7 shows the penetration force as a function of depth measured by ACC-E penetrometer (upper panel) and the other three panels for other laboratory tests conducted in pebble, crust and sand materials. The results indicate that the surface has a weak crust and, beneath that, a structure consisting of wet sand and embedded with pebbles (Zarnecki et al., 2005).

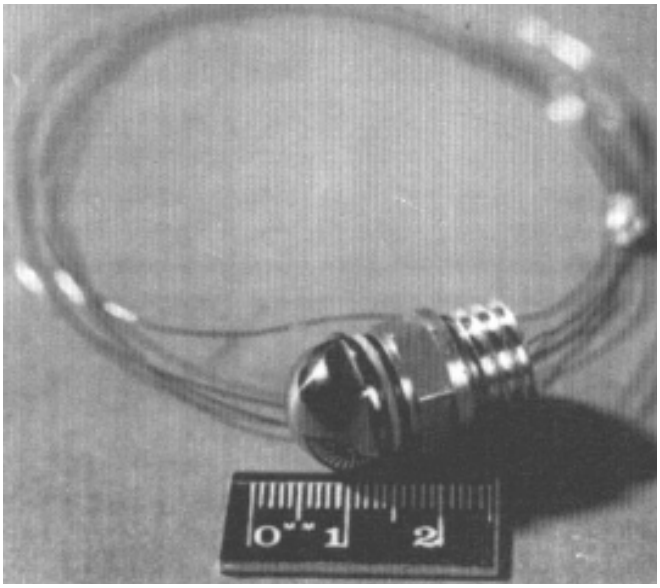

Figure 1.6 A. ACC-E penetrometer sensor head (Lorenz et al., 1994).

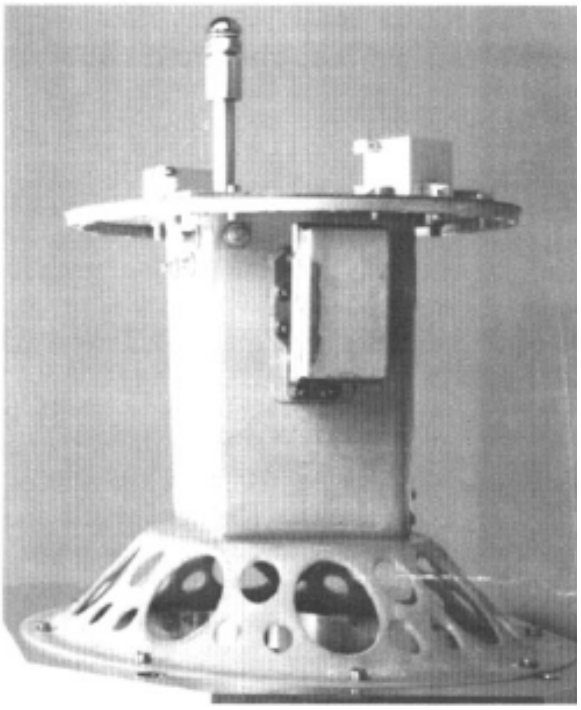

Figure 1.6 B. ACC-E penetrometer mounted on the Surface Science Package (Lorenz et al., 1994).

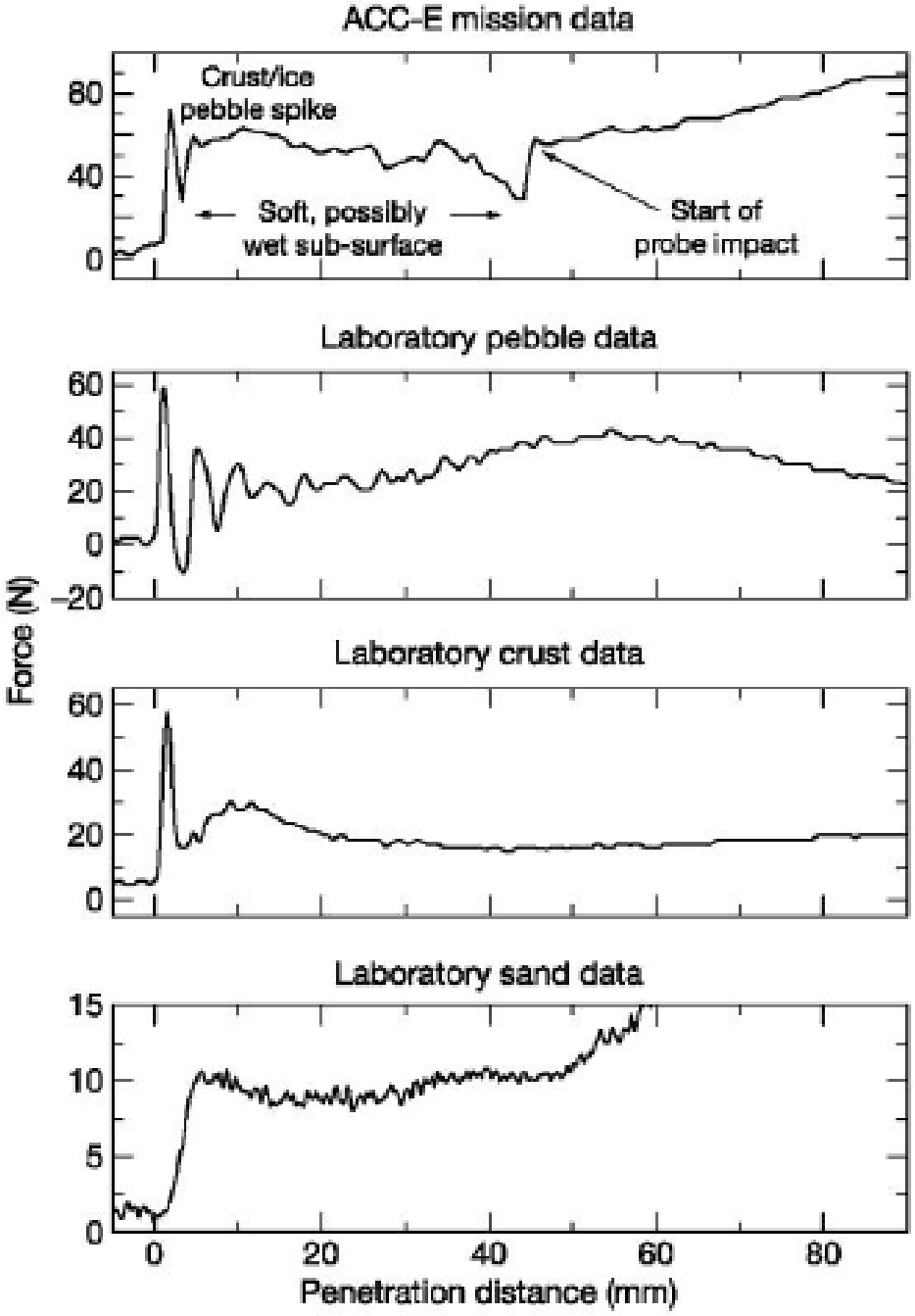

Figure 1.7. Penetration force as a function of depth measured by ACC-E penetrometer (upper panel) and the other three panels for other laboratory tests conducted in pebble, crust and sand materials.

1.5. References

Arvidson, R., D. Adams, G. Bonfiglio, P. Christensen, S. Cull, M. Golombek, J. Guinn, E. Guinness, T. Heet, and R. Kirk. 2008. Mars exploration program 2007 phoenix landing site selection and characteristics. *Journal of Geophysical Research* 113 (E3): E00A03.

Bell III, JF, HY McSween, JA Crisp, RV Morris, SL Murchie, NT Bridges, JR Johnson, DT Britt, MP Golombek, and HJ Moore. 1900. Mineralogic and compositional properties of martian soil and dust- results from mars pathfinder. *Journal of Geophysical Research* 105 : 1721-55.

Bonitz, R. G., L. Shiraishi, M. Robinson, R. E. Arvidson, PC Chu, JJ Wilson, KR Davis, G. Paulsen, AG Kusack, and D. Archer. 2008. NASA mars 2007 phoenix lander robotic arm and icy soil acquisition device. *J.Geophys.Res* 113 : E00A01.

Cherkasov, II, and VV Shvarev. 1973. Soviet investigations of the mechanics of lunar soils. *Soil Mechanics and Foundation Engineering* 10 (4): 252-6.

Fanale, F. P., J. R. Salvail, W. Bruce Banerdt, and R. Steven Saunders. 1982. Mars: The regolith-atmosphere-cap system and climate change. *Icarus* 50 (2): 381-407.

Fragments, R. R. 1969. 14 surveyor: Program results. *Surveyor Program Results*(184): 13.

Gary, M., and R. Mcafee. y wolf, CL–1972-glossary of geology. *American Geological Institute, Washington, 560pp*.

Gibson, RE. 1953. Experimental determination of the true cohesion and true angle of internal friction in clays. Paper presented at 3rd ICSMFE, .

Heiken, G., D. Vaniman, and B. M. French. 1991. *Lunar sourcebook: A user's guide to the moon*Cambridge Univ Pr.

Housen, KR, and L. L. Wilkening. 1982. Regoliths on small bodies in the solar system. *Annual Review of Earth and Planetary Sciences* 10 : 355-76.

Housen, KR, LL Wilkening, CR Chapman, and RJ Greenberg. 1979. Regolith development and evolution on asteroids and the moon. *Asteroids* 1 : 601-27.

Killen, RM, and D. Crider. 2004. Depth of regolith cover on mercury's polar volatile deposits as a function of time. Paper presented at AGU Fall Meeting Abstracts, .

Langevin, Y. 1997. The regolith of mercury: Present knowledge and implications for the mercury orbiter mission. *Planetary and Space Science* 45 (1): 31-7.

Leonovich, AK, VV Gromov, AD Dmitriev, VA Lozhkin, VN Penetrigov, PS Semionov, IN Grannik, VP Grushevskii, and VV Shvariov. 1976. Investigation of the physical and mechanical properties of the lunar sample brought by luna-20 and along the route of motion of lunokhod 2. *In: Space Activity Impact on Science and Technology.(A76-35711 17-12) Oxford, Pergamon Press, Ltd., 1976, p.321-332.* 1 : 321-32.

LEONOVICH, AK, VV GROMOV, AV RYBAKOV, VK PETROV, PS PAVLOV, II CHERKASOV, VV SHVAREV, and Joint Publications Research Service, Washington, DC. 1971. *Determining Geometric Dimensions and Distribution with the Self-Propelled Lunokhod-1(Structure, Strength, and Deformation Properties of Lunar Surface Along Path of Lunokhod Vehicle)*.

Leonovich, AK, VV Gromov, AV Rybakov, VN Petrov, PS Pavlov, II Cherkasov, and VV Shvarev. 1972. Investigations of the mechanical properties of the lunar soil along the path of lunokhod 1. Paper presented at Space Research, .

LEVIN, G. V., and P. A. N. N. STRAAT. 1976. Viking labeled release biology experiment: Interim results. *Science* 194 (4271): 1322-9.

Lorenz, RD, M. Bannister, PM Daniell, Z. Krysinski, MR Leese, RJ Miller, G. Newton, P. Rabbetts, DM Willett, and JC Zarnecki. 1994. An impact penetrometer for a landing spacecraft. *Measurement Science and Technology* 5 : 1033.

Matson, D. L., L. J. Spilker, and J. P. Lebreton. 2002. The Cassini/Huygens mission to the saturnian system. *Space Science Reviews* 104 (1): 1-58.

Matson, DL, TV Johnson, and GJ Veeder. 1977. Soil maturity and planetary regoliths-the moon, mercury, and the asteroids. Paper presented at Lunar and Planetary Science Conference Proceedings, .

McGill, GE, JL Warner, MC Malin, RE Arvidson, E. Eliason, S. Nozette, and RD Reasenberg. 1983. Topography, surface properties, and tectonic evolution. *Venus* 1 : 69-130.

McKay, D. S., G. H. Heiken, A. Basu, G. Blanford, S. Simon, R. Reedy, B. M. French, and JJ Papike. 1991. The lunar regolith. *Lunar Sourcebook* 5 (1).

Mellon, M. T., W. C. Feldman, and T. H. Prettyman. 2004. The presence and stability of ground ice in the southern hemisphere of mars. *Icarus* 169 (2): 324-40.

Mitchell, JK, LG Bromwell, WD Carrier III, NC Costes, and RF Scott. 1971. Soil mechanics experiment, apollo 15 preliminary science report. *NASA Spec.Publ.SP-272*: 87-108.

Mitchell, JK, and WN Houston. 1974. Static penetration testing on the moon. Paper presented at preprint for European Conference on Penetration Testing, Garston Engineering and Building Research Establishment, Stockholm, Sweden, .

Moore, H. J., R. E. Hutton, R. F. Scott, C. R. Spitzer, and R. W. Shorthill. 1977. Surface materials of the viking landing sites. *Journal of Geophysical Research* 82 (28): 4497-523.

Moore, HJ, GD Clow, and RE Hutton. 1982. A summary of viking sample-trench analyses for angles of internal friction and cohesions. *Journal of Geophysical Research* 87 (B12): 10043,10,050.

Pike, R. J. 1980. Formation of complex impact craters: Evidence from mars and other planets. *Icarus* 43 (1): 1-19.

Plumb, R. C., R. Tantayanon, M. Libby, and W. W. Xu. 1989. Chemical model for viking biology experiments: Implications for the composition of the martian regolith.

Rieder, R., R. Gellert, J. Brückner, G. Klingelhöfer, G. Dreibus, A. Yen, and SW Squyres. 2003. The new athena alpha particle X-ray spectrometer for the mars exploration rovers. *J.Geophys.Res* 108 (7): 1-7.

Schofield, A. N., and P. Wroth. 1968. Critical state soil mechanics.

Scott, RF, and FI Roberson. 1969. Surveyor: Program results. *NASA SP-184*: 171.

Shaw, A., R. E. Arvidson, R. Bonitz, J. Carsten, HU Keller, M. T. Lemmon, M. T. Mellon, M. Robinson, and A. Trebi-Ollennu. 2009. Phoenix soil physical properties investigation. *J.Geophys.Res* 114 : E00E05.

Simonelli, D. P., J. Veverka, and A. S. McEwen. 1997. Io: Galileo evidence for major variations in regolith properties. *Geophysical Research Letters* 24 (20): 2475-8.

Smith, PH, L. Tamppari, RE Arvidson, D. Bass, D. Blaney, W. Boynton, A. Carswell, D. Catling, B. Clark, and T. Duck. 2008. Introduction to special section on the phoenix mission: Landing site characterization experiments, mission overviews, and expected science. *J.Geophys.Res* 113 : E00A18.

Sprague, A. L., D. M. Hunten, and K. Lodders. 1995. Sulfur at mercury, elemental at the poles and sulfides in the regolith. *Icarus* 118 (1): 211-5.

Terzaghi, K., R. B. Peck, and G. Mesri. 1996. Soil mechanics. *New York: John Wiley & Sons*.

Thomas, P. 1979. Surface features of phobos and deimos. *Icarus* 40 (2): 223-43.

Turkevich, A. L., E. J. Franzgrote, and J. H. Patterson. 1967. Chemical analysis of the moon at the surveyor V landing site. *Science* 158 (3801): 635-7.

Veverka, J., PC Thomas, M. Robinson, S. Murchie, C. Chapman, M. Bell, A. Harch, WJ Merline, JF Bell III, and B. Bussey. 2001. Imaging of small-scale features on 433 eros from NEAR: Evidence for a complex regolith. *Science* 292 (5516): 484-8.

Zarnecki, JC, MR Leese, JRC Garry, N. Ghafoor, and B. Hathi. 2002. Huygens' surface science package. *Space Science Reviews* 104 (1): 593-611.

Zolotov, M. Y., and E. L. Shock. 2001. Composition and stability of salts on the surface of europa and their oceanic origin. *J.Geophys.Res* 106 (32): 815-32.

CHAPTER 2: PENETRATION TESTING FOR THE OPTICAL PROBE FOR REGOLITH ANALYSIS (OPRA)

2.1. Introduction

Much of the history of rocky planetary bodies is revealed by studying the records of past events that are preserved in their surface geology. Younger layers are present on the top of older layers, based on the principle of superposition, which reveals the chronological order of geological events. According to the principle of original horizontality, each layer is formed horizontally but their orientation can be modified by various processes that can result due to uplifting and folding (Longwell and Flint, 1962).

Investigating microgravity planetary bodies (i.e. comets, asteroids) is of high interest since they are remnant of the solar system. Not only could they provide information about the history of the solar system but also they could enhance our understanding of its evolution. Due to space weathering, surface compositions of asteroids are altered from its internal structure. Therefore, telescopic measurements of asteroids rarely match laboratory reflectance spectra. Regolith layer on asteroids vary according to the size of the asteroids. For moderate size (100 – 300 km diameter) asteroids, they have about 1 km depth of regolith material (Housen et al., 1982).

A penetrometer is a cone on the end of a cylinder which is used to investigate the surface and subsurface of planetary bodies by pushing it into granular material (Lunne et al., 1997). Cone Penetration Testing (CPT) is the technique of measuring the resistance force which encountered by a penetrometer. CPT is widely used for terrestrial applications. CPT was earlier named the static penetration test, quasi-static penetration test and Dutch sounding test. The first

Dutch cone penetrometer test was made in 1932 by P. Barentsen in Holland and it was pushed down by hand where the penetrometer had a cone diameter of 10 cm^2 and 60° tip angle . However, CPT can be used to determine subsurface stratigraphy, estimate some geotechnical parameters and to predict future changes of the soil due to loading (Lunne et al., 1997). In fact, two American Society for Testing and Materials (ASTM) (ASTM D3441 - 05) and (ASTM D5778 – 07) are describing the methodology of CPT.

2.1.1. Apollo 14 (ASP) and Apollo 15, 16 (SRP)

The Apollo Simple Penetrometer (ASP) was part of the Apollo 14 Lunar Surface Experiment Package (ALSEP) and was used to investigate soil mechanics on the moon. ASP was a metal rod 68 cm long and 0.95 cm in diameter with a 30 degree cone angle. ASP was used in three penetration tests by manually pushing it into lunar soil by an astronaut. ASP reached to a depth of 42, 44 and 50 cm and the penetration force was in the range of 70 to 135 N using one hand. A second deployment of ASP reached a depth of 62 cm and required a force of 225 N using both hands (Mitchell et al., 1971).

A Self-Recording Penetroemter (SRP) was used on the Apollo 15 and 16 missions. This instrument was connected to a recording drum which recorded the force versus depth. At a maximum depth of 76 cm, the Apollo 15 SRP recorded a force of 111 N and the Apollo 16 SRP recorded a maximum force of 215 N (Mitchell et al., 1974).

2.1.2. Example of Impact Penetrometer (Huygens Probe)

ACC-E is a piezoelectric force sensor (impact penetroemter) which was part of the Surface Science Package (SSP) onboard the Huygens probe which is used to investigate the subsurface of Saturn's moon Titan (Lorenz et al., 1994). From the impact force profile of the thumb-size sensor (mass of 15 g) an estimation of the density, cohesion and particle size

distribution of the subsurface materials was estimated during the first 40 mm of penetration (Zarnecki et al., 2002). The results indicated that the surface had a weak crust and, beneath that, a structure consisted of wet sand and embedded pebbles (Zarnecki et al., 2005).

2.1.3. Example of Dynamic Penetrometer (PLUTO Mole)

Planetary Underground Tool (PLUTO) mole, was an instrument on-board the Beagle 2 lander, was part of the Mars Express mission to Mars (Richter et al., 2002). It was considered as a dynamic penetrometer (Stoker et al., 2003). The mole was capable of delivering a maximum force of 50 N per shock where it reached to a depth of 3.9 mm in loose sand and 0.8 mm in stiffish sand on earth (Kochan et al., 2001).

2.2. The Optical Probe for Regolith Analysis

OPRA (Optical Probe for Regolith Analysis, Fig. 2.1A) is a static penetrometer with vertically-stacked windows that would be inserted from either a lander or rover into regolith or unconsolidated ices on the surface of a planet, asteroid, moon or comet. These windows are connected by fiber optics to an IR spectrometer located in the body of the spacecraft. The spectrometer will address each window individually, providing swept frequency illumination to subsurface material outside the window and simultaneously returning the reflected signal to the unit. The result will be a spectral composition profile of the subsurface material sampled every couple of centimeters down to a maximum depth of about 50 cm. If a borehole is already available, OPRA could be lowered into it. The accuracy of subsurface investigation will depend on the diameter of the borehole, and in turn the distance between the embedded sensors inside OPRA and the borehole wall. Because the probe will be thin and since the heat-producing electronics are in the spacecraft, disturbance of the subsurface layers should be minimal. There are no moving parts in the probe and all electronics may be located in the warm-box within the rover or spacecraft body. The spectral range of the instrument is nominally 0.5 to 5 μm (20,000 – 2000 cm^{-1}) which is suitable for the mineralogical and chemical characterization of the subsurface, including the water band at ~ 3 μm and various ices (CO_2, clathrates)

In order to meet intended science objectives, OPRA will have the shape of a penetrometer with windows placed laterally along the side (Fig. 2.1B). These windows will protect the fiber optic cables from being in direct contact with subsurface material. Some fibers will carry illumination to the windows and others will carry the returning signal to the IR instrument. The number of windows is a function of the probe diameter, length and fiber optic diameter (Pilgrim et al., 2009).

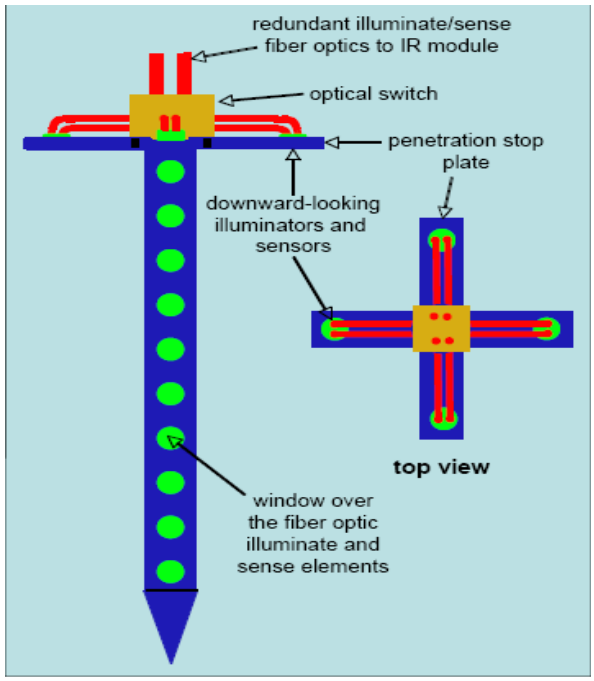

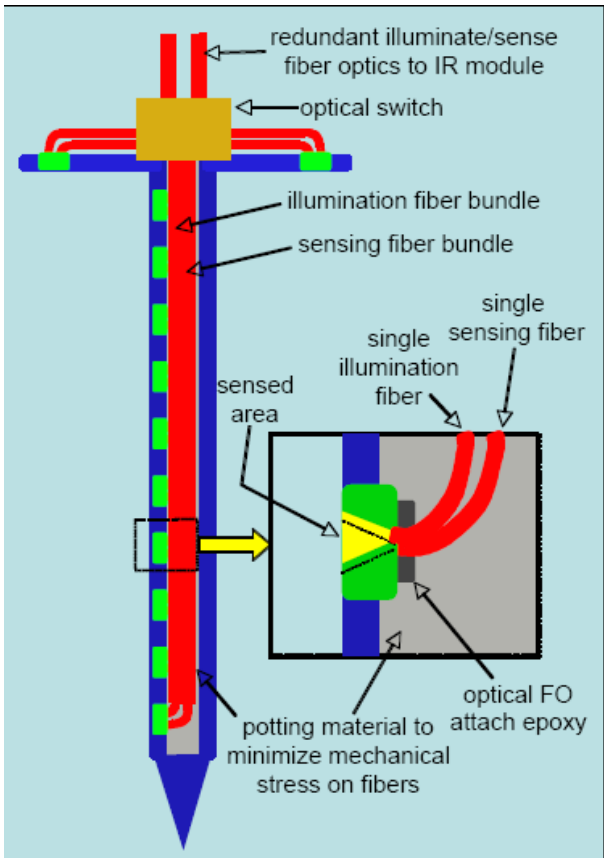

Figure 2.1 A. The Oprical Probe for Regolith Analysis (OPRA). B. OPRA as a penetrometer like shape with windows placed on the side.

2.2.1. Purpose of Research

The principal objective of the experiments described in this work is to determine the optimized diameter and tip angle which correspond to minimum insertion and withdrawal forces of OPRA. This is done by measuring the amount of force needed to insert and extract various probes covering a range of these key variables into unconsolidated material. Sand was our choice of analogue material because it is a well-studied material, has a bulk density and particle size distribution similar to that is found on some planetary bodies such as Mars and the Moon. Apollo 11 reported a minimum and maximum bulk densities of 1360 and 1800 kg/m^3 on the moon (Mitchell et al., 1974). On Mars, an average bulk density of 1520 kg/m^3 is indicated by Mars Pathfinder rover (Matijevic et al., 1997). Many valid models such as bearing capacity model which is used in geotechnical engineering can be applied to sand in the essence of explaining the penetration resistance (Terzaghi, 1943), (Vesic, 1963), (Hansen, 1970) and (Puech et al., 2002). In addition to the engineering requirements to minimize the force necessary to insert the probe, key properties of the regolith can be inferred from the force measurements, including density, compaction and porosity. Table 2.1 shows symbols used through the work and their definition.

Table 2.1. List of symbols used in the paper

Symbol	Def.
A_c	Area of the cone (m^2)
A_s	Area of the sleeve (m^2)
B	Cone diameter (m)
D	Probe diameter (cm)
D_r	Relative density (dimensionless)
e	Void ratio (dimensionless)
e_{max}	Maximum possible void ratio (loosest condition)
e_{min}	Minimum void ratio (densest condition)
f_s	Sleeve friction ($N\ m^{-2}$)
F_T	Total resistance force (N)
K	Coefficient of lateral pressure at rest (dimensionless)
Kp	Passive coefficient of lateral stress (dimensionless)
L	Lateral extension of the slip lines (m)
m_s	Mass of sand (kg)
Nq	Bearing capacity factor (dimensionless)
q_c	Cone resistance ($N\ m^{-2}$)
V_S	Volume of solid particles (m^3)
V_T	Total volume (m^3)
V_v	Volume of voids(m^3)

Z	Penetration depth (m)
γ	Effective unit weight of sand (N m^{-3})
φ	Friction angle of sand (degree)
ρ_s	Particle density of sand (kg m^{-3})

2.3. Experimental Apparatus

A list of probes was used to simulate the OPRA probe in the penetration tests. We used sixteen different probes categorized into four groups (Table 2.2). These probes vary in diameter, length and tip apex angle to envelop most of the variables potentially affecting the penetration force. They cover the expected size ranging from (0.9 – 1.9 cm diameter), and tip angle ranging from (30, 60, 90 and 120°).

A specific apparatus was designed and built to measure the insertion and withdrawal forces of the OPRA probe in unconsolidated materials. A general illustration of the setup is shown in Figure 2.2. A parallel shaft gear motor drives a lead screw. The lead screw housing is made of steel with an outside diameter of 4 cm, thickness of 5 mm and length of 80 cm. The role of the housing is to move up and down in correspondence with the forward and backward movement of the motor. The housing is equipped with two reflective laser sensors, one at the top of the housing and the other one is at the bottom as shown in Figure 2.3 A, to stop the automated program if one of the lasers hits the reflective plates. This constraints the range of positions (depth) in which our apparatus can be safely operated. The motor is capable of working in reversible modes. The coupling between the motor and the lead screw is realized by using a two-way metal sleeve connector. The coupling piece provides high holding capacity between the motor shaft and the lead screw as seen in Figure 2.3B.

A Transducer Techniques compression load cell (MLP-1K), with a capacity of 450 kg, is attached at the bottom of the housing. A DPM-3 output panel is used as the load cell meter and calibrated to give output reading in kg with an accuracy of 0.01%. An ultrasonic depth sensor is placed on the top of the penetration stand. By measuring the distance between the sensor and the top of the regolith, the penetration distance of the probe into the regolith is measured

Table 2.2. List of probes

Series	Diameter (cm)	Length (cm)	Tip length (cm)	Tip angle (°)
Series 1				
Probe 1	0.9	50.8	1.8	30
2	0.9	50.8	0.9	60
3	0.9	50.8	0.6	90
4	0.9	50.8	0.3	120
Series 2				
Probe 1	1.2	51	2.4	30
2	1.2	51	1.2	60
3	1.2	51	0.7	90
4	1.2	51	0.4	120
Series 3				
Probe 1	1.9	50.8	3.4	30
2	1.9	50.8	1.7	60
3	1.9	50.8	1	90
4	1.9	50.8	0.6	120
Series 4				
Probe 1	2.5	51	4.6	30
2	2.5	51	2.2	60
3	2.5	51	1.35	90
4	2.5	51	0.8	120

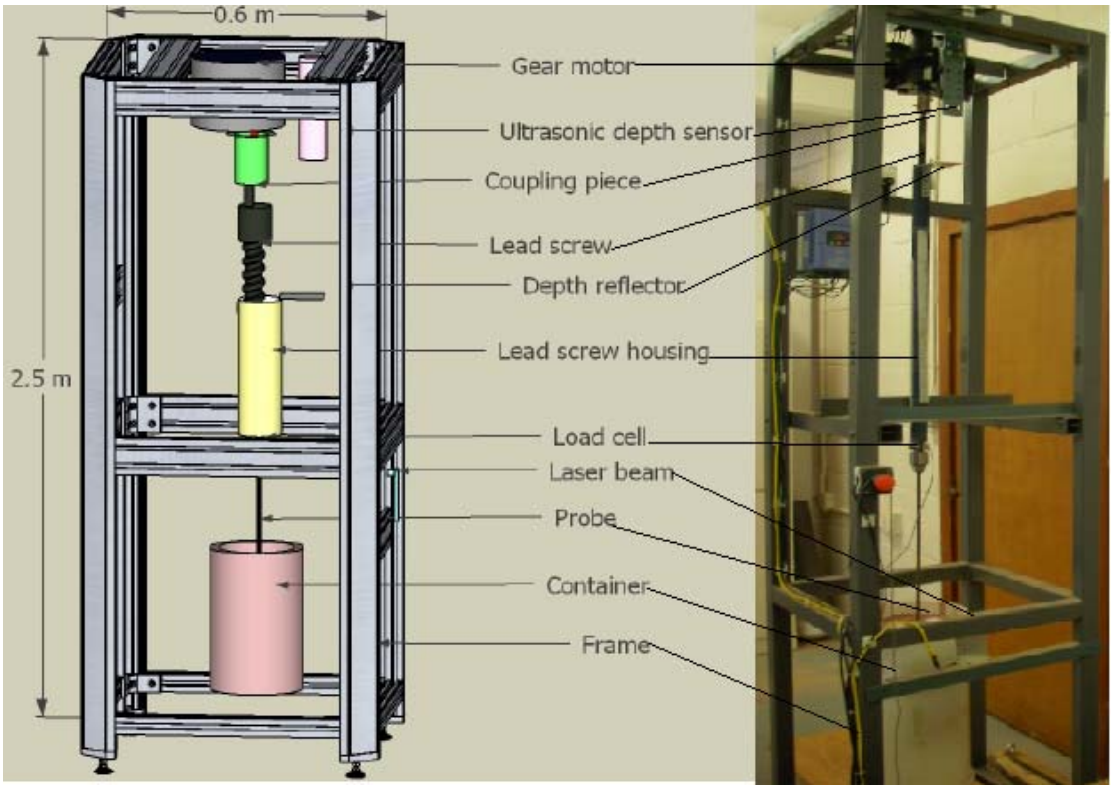

Figure 2.2. The OPRA penetration testing apparatus.

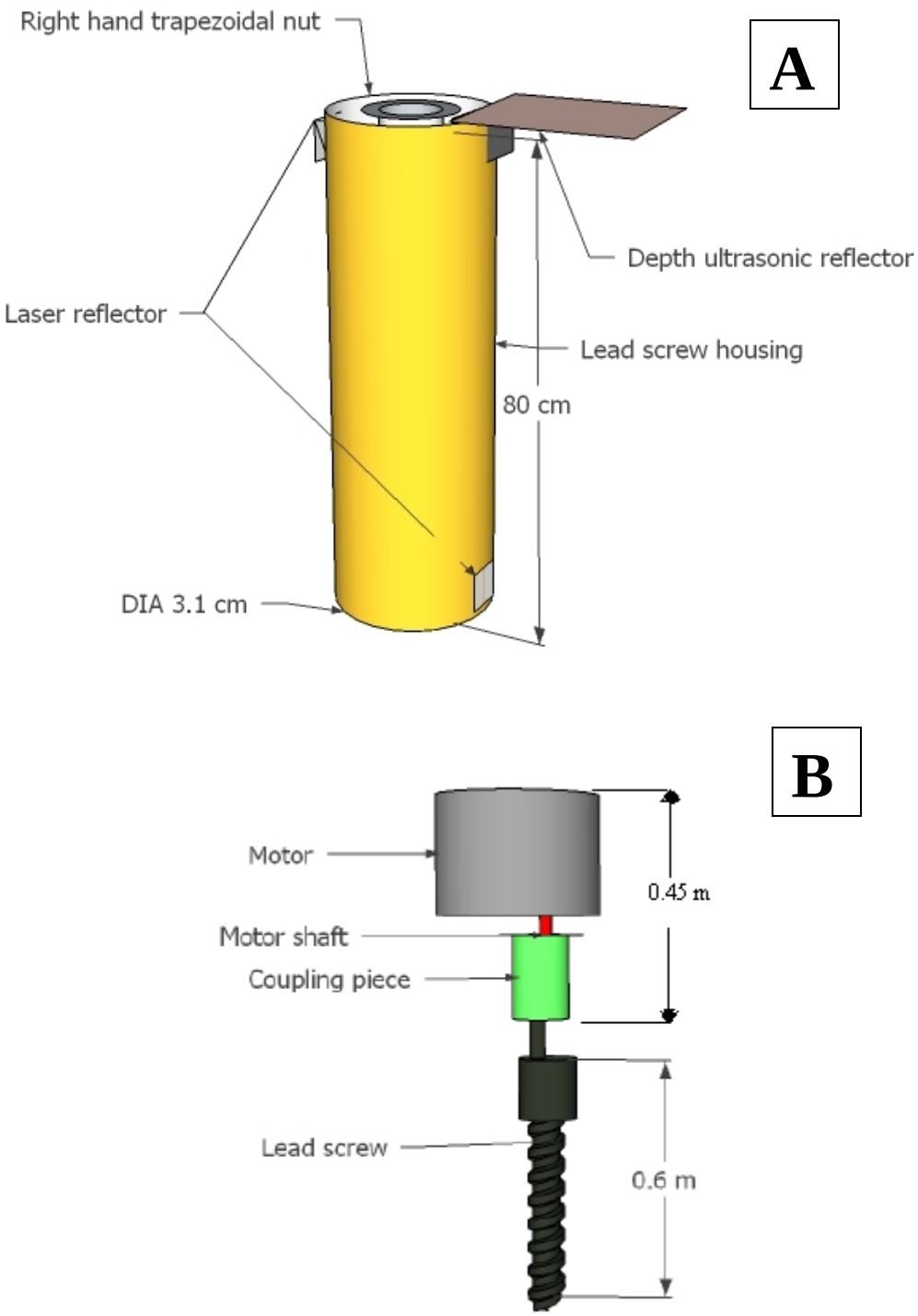

Figure 2.3 A. The lead screw housing with the laser reflectors, trapezoidal nut and depth reflector. B. coupling piece connecting the gear motor to the leas screw.

continuously. At the top of the housing, a reflective aluminium surface is mounted in order to reflect the ultrasonic waves generated by the sensor.

An automated control system was designed using a logic micro-controller (PLC) programmed using a ladder logic program Proficy HMI/SCADA-CIMPLICITY [IC200UAL006] which has a Human Machine Interface (HMI) where the whole penetration experiment can be monitored and controlled through a personal computer. During penetration two parameters are being monitored: the penetration force and penetration depth. The Graphical Human Interface (GHI) of the data collecting software is composed of one main screen with three other sub-screens. Three outputs are shown in the main screen, the motor speed in mm/sec, the penetration depth in cm and penetration force in Newton (Fig 2.4). The Insert/Remove buttons activate the probe downward and upward movement. The insert probe condition is deactivated when the probe reaches a desired depth configured by the user. The remove probe button stops its functionality when the probe is fully removed. The results of the penetration experiment are automatically saved in an Excel file.

2.4. Experimental Procedures

Before starting the experiments, Force displayed on GHI screen is calibrated by comparing it to the compression forces measured out of a balance. Balance output reading in kg is converted to Newton. A probe attached to the load cell is pushed down at different forces against a 200 kg-capacity balance placed on the floor. The plot of force measured by the load cell (GHI screen) versus force measured by the balance shows a slope equal to 1 (Fig. 2.5) indicating that the load cell gives accurate readings and is thus perfectly calibrated for further experiments. Moreover, the error from the load cell is small enough (~1%) to be ignored.

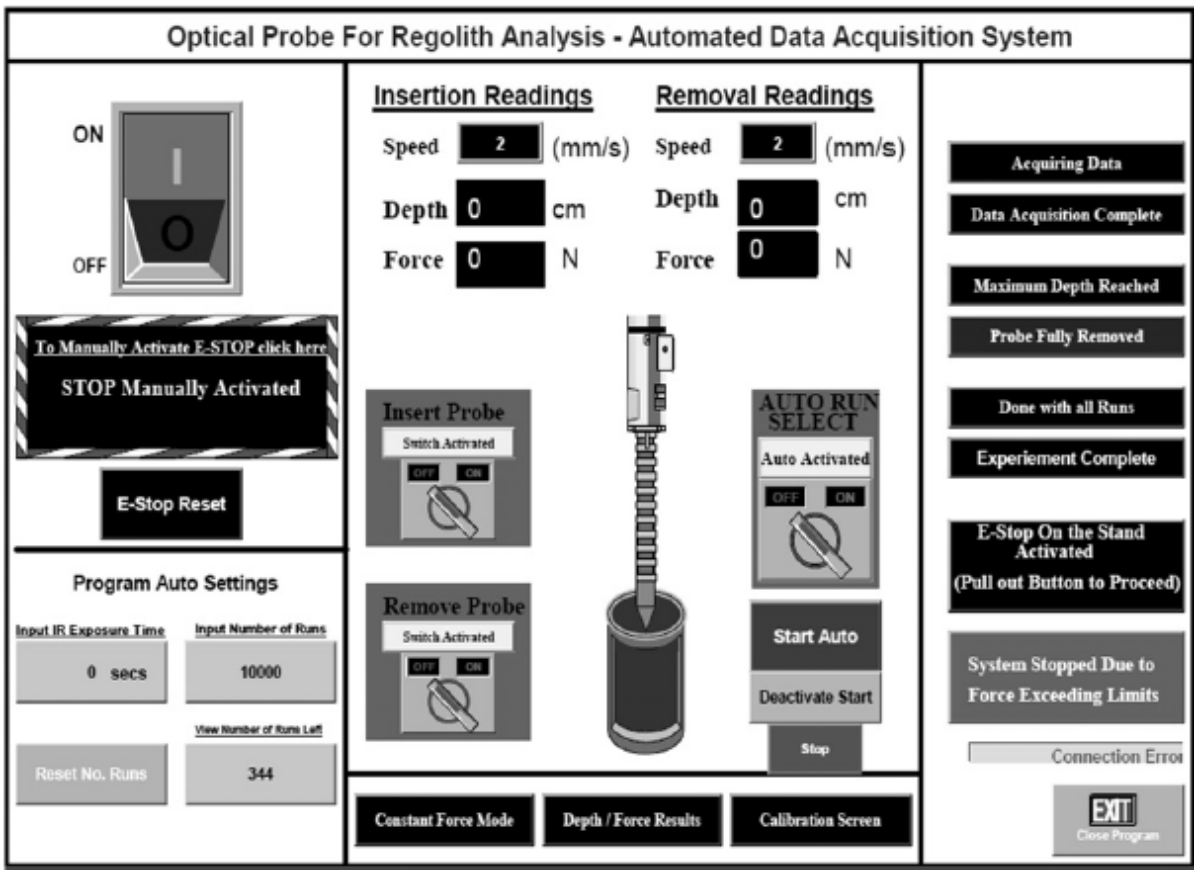

Figure 2.4. Graphical User Interface (GUI) screen

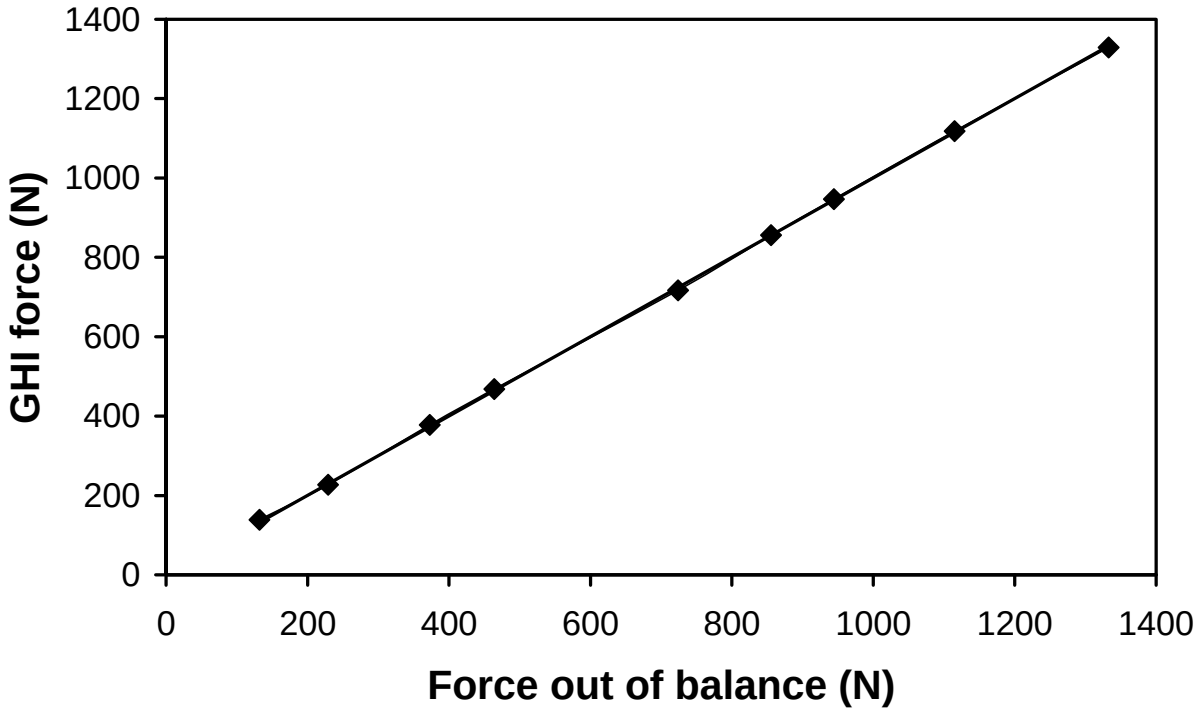

Figure 2. 5. Calibration of the readings out of the load cell (GHI) with the balance reading.

Samples are prepared by filling a 25 cm diameter and 65 cm deep cylindrical bucket with dry playground sand. The particle size distribution of sand was determined by sieving as shown in Figure 2.6. The results show that the sand contains 36 % medium size particles (>0.5 mm) and 64 % fine grained particles (< 0.3 mm). The sand is poured in the bucket in 5 kg layers and the bucket is vigorously shaken in order to homogenize and compact the regolith. The height is measured after each compaction step to be sure that each layer has the same bulk density. Based on the effect of speed of penetration, Penetration experiments were run at a constant speed of 2 mm s^{-1}. All results are presented as measured force as a function of penetration depth.

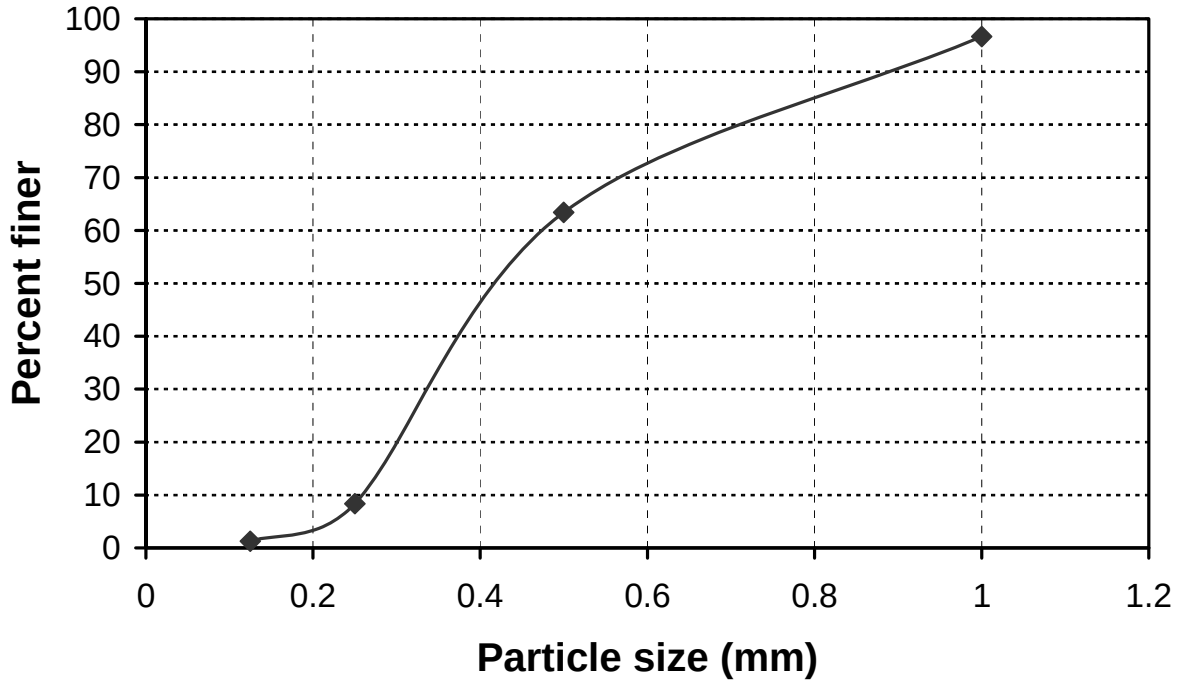

Figure 2.6. Particle size distribution curve for playground sand

2.5. Experimental results

2.5.1. Effect of Compaction

In regolith materials, the required insertion force is generally a strong function of the density and thus of compaction (Murthy, 2002). To test the effect of compaction, a minimum bulk density of about 1550 kg/m^3 (similar to that is indicated on Mars (Matijevic et al., 1997) and a maximum one of about 1700 kg/m^3 (similar to that is indicated on the moon (Mitchell et al., 1974) was chosen. A cylindrical container was filled with sand with a measured bulk density of 1550 kg/m^3. Three insertion and removals were conducted at this bulk density and the average error % of the three runs was 24%. The container was then shaken in order to compact the material to a higher bulk density, followed by three more penetration measurements. This procedure was repeated three times and the bulk density was determined at each step. At a bulk density of 1550 kg/m^3, the 0.9 cm diameter, 60 degree tip angle probe required about 50 N to penetrate to a depth of 50 cm while it took about 1000 N to reach the same depth when the bulk density was 1700 kg/m^3 where the average error % was 13% (Fig. 2.7). A change of about 9% in the bulk density between 1550 kg/m^3 and 1700 kg/m^3 induces a factor of 20 in the penetration force. The effect of compaction did not appear at the beginning of the experiment (the first 10 cm), the force value of all of the four bulk densities are with-in the same range. After 10 cm depth, the effect of compaction appeared according to each bulk density. Penetration forces linearly increased with depth for 1550, 1600 and 1660 kg/m^3 because of pore spaces where sand particles can expand. After 45 cm depth for 1700 kg/m^3, penetration force curve has an exponential increase with depth which is due to the high level of compaction where it is hard for sand particles to dilate and that the probe is getting closer to the bottom of the container. Therefore, compaction has a profound impact on the forces required for probe penetration. The

insertions and withdrawals of the probes themselves did not seem to compact the sand to a measurable degree.

2.5.2 Effect of Penetration Speed

Four different motor speeds were tested (Fig. 2.8): 1, 2, 3 and 4 mm s^{-1} in sand with a bulk density of 1700 kg/m^3 using the same 0.9 cm probe with a tip angle of 60° from the previous experiment. In the first 30 cm, the penetration force data for all speeds overlapped, and reached 380 N at a depth of 30 cm. We did not observe any significant difference in the required forces between each speed. Thus, for the rest of the experiments, we decided to use an insertion speed of 2 mm s^{-1} since the actual penetration rate from a planetary lander or rover will probably be slow.

2.5.3 Effect of Tip Angle

Each probe was made with four tip angles: 30, 60, 90 and 120° since we expected that the tip angle would influence the penetration force to reach a given depth, we found that the required forces were insensitive to tip angle (Fig.2. 9). The average error is about 13% which is about ± 150 N where the four curves are falling under the standard error of measurements and then their difference is not statistically significant.

2.5.4. Effect of Diameter

Five different circular probes were made with different diameters (2.5, 1.9, 1.2 and 0.9 cm) and tested. A 30° tip angle was fixed in each experiment. The results show that the diameter strongly affects the penetration force (Fig. 2.10). Indeed, to reach a depth of 20 cm, a 0.9 cm probe requires about 200 N while the 1.9 cm probe needs about 1000 N. Thus, doubling the diameter (increasing the area by a factor of four) results in an increase of penetration force by a factor of five.

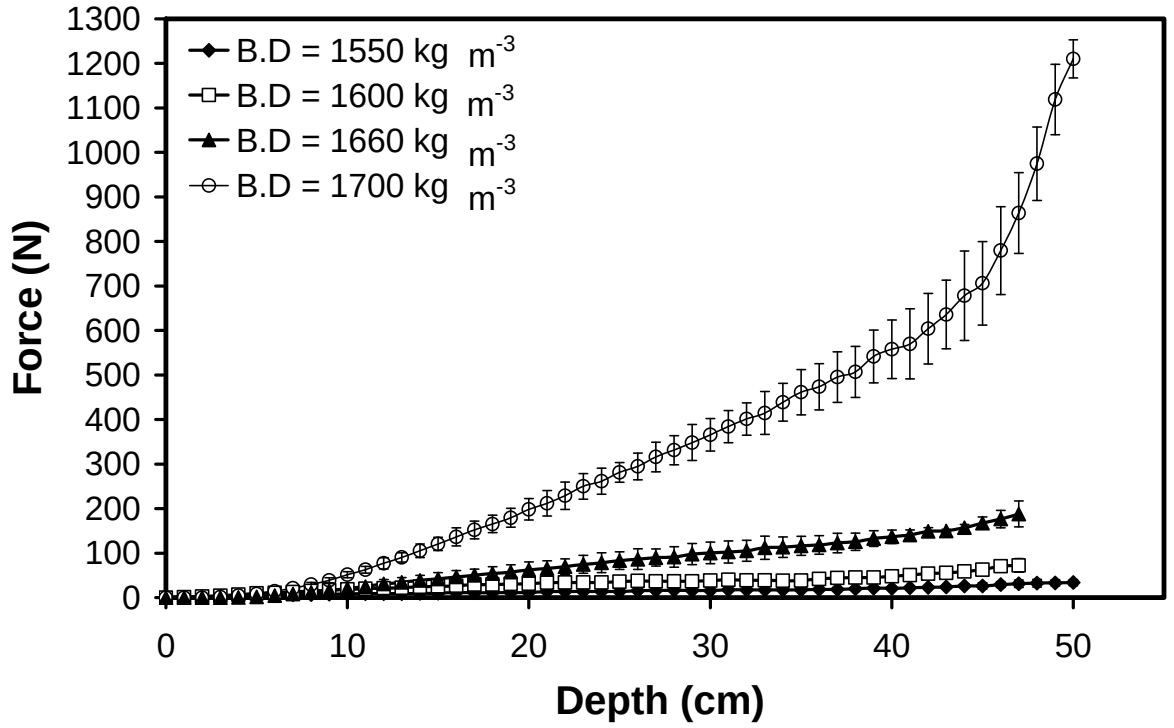

Figure 2.7. Penetration force as a function of depth in sand under different bulk density (D = 0.9 cm, T.A = 60°).

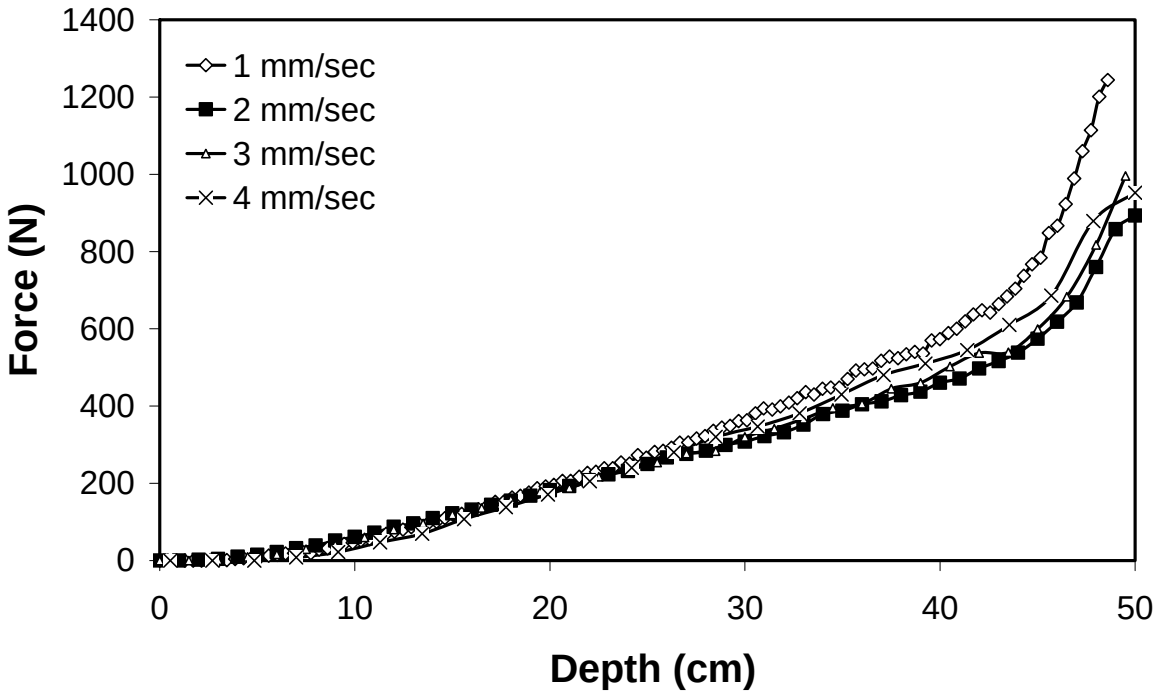

Figure 2.8. Penetration force as a function of depth in sand for different motor speeds. (D = 0.9 cm, T.A = 60°).

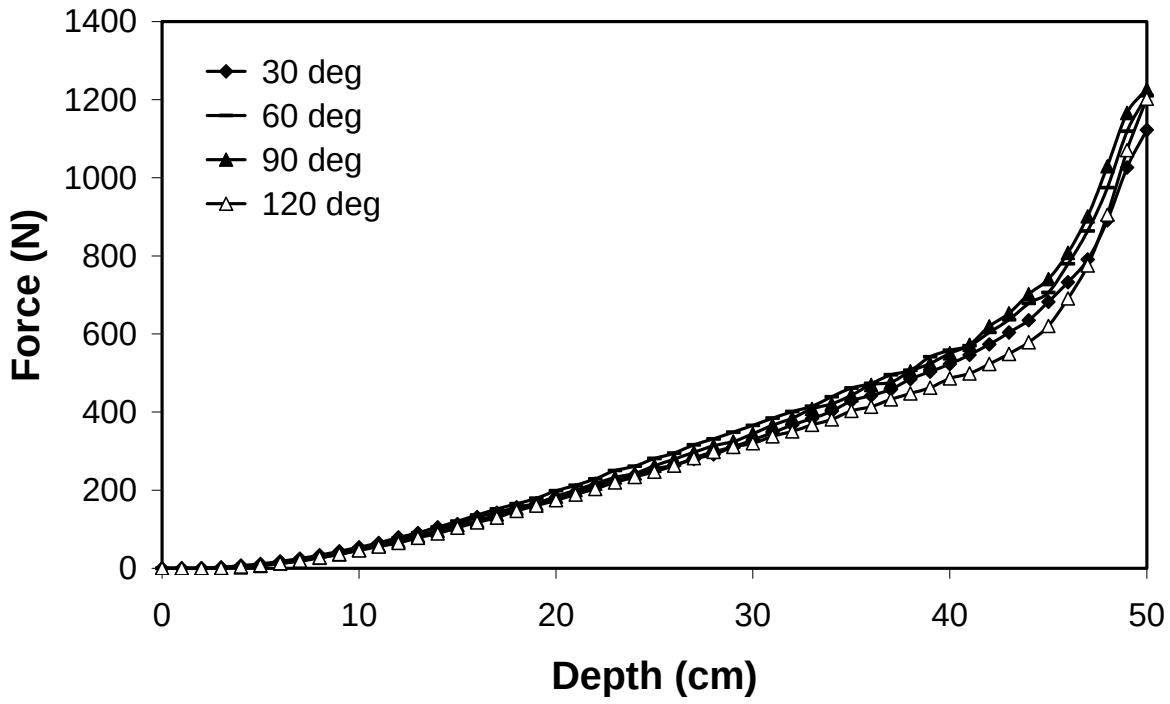

Figure 2.9. Penetration force as a function of depth in sand for different tip angles and the same probes diameter (D = 0.9 cm).

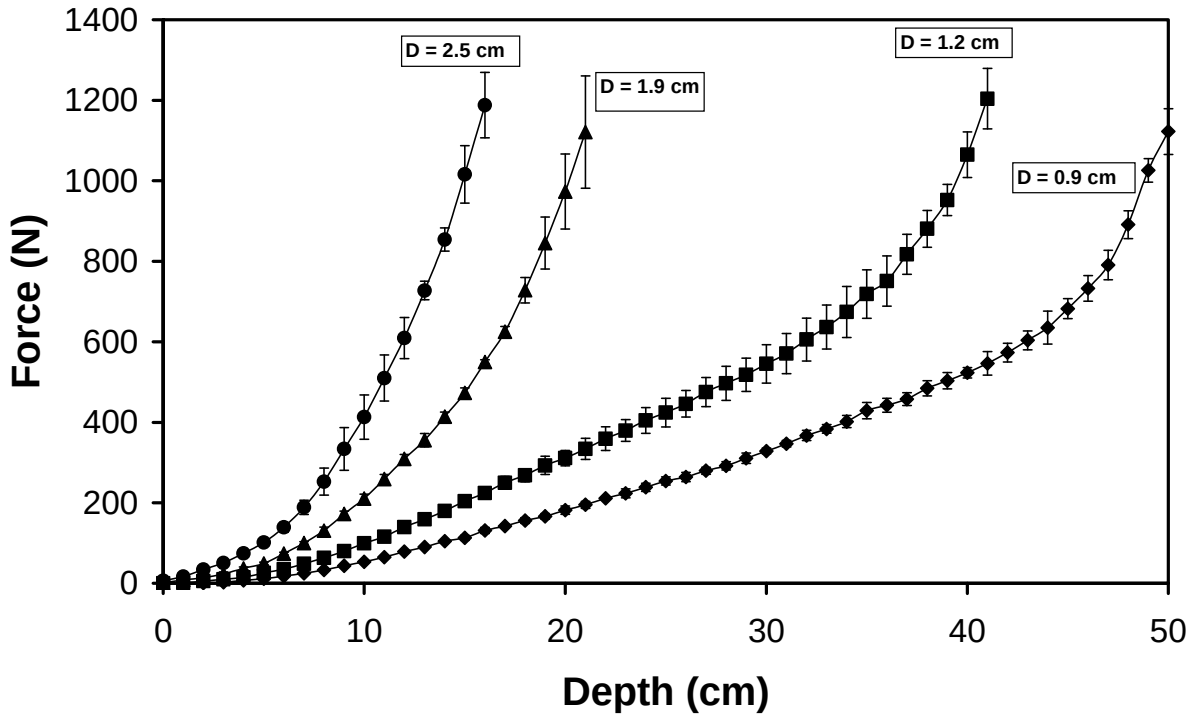

Figure 2.10. Penetration force as a function of depth in sand for different diameter probes (Tip angle is 30°; bulk density is 1700 kg/m^3).

2.6. Discussion

2.6.1 Bearing Capacity Theory

The axial downward movement of the penetrometer through regolith is closely related to the problem of CPT in geotechnical engineering where it uses bearing capacity theory for explanation (Mitchell et al., 1974). The total resistance force (F_T) during probe insertion into the subsurface is the sum of two forces; cone resistance (q_c) and sleeve friction (f_s):

$$F_T = q_C A_C + f_S A_S \quad (1)$$

Where A_c is the area of the cone, A_s is the area of the sleeve. For sands, the cone resistance can be calculated from (Puech et al, 2002):

$$q_C = \gamma \times Z \times Nq\left(1 + \left(K \times \sin\varphi \times \frac{Z}{L}\right)\right) \quad (2)$$

Where γ is the effective unit weight of sand (N m^{-3}), Z is the penetration depth (m), φ is the friction angle of sand (degree), D_r is the relative density, K is the coefficient of lateral pressure at rest (dimensionless), Nq is the bearing capacity factor (dimensionless), L is the lateral extension of the slip lines (m) (lateral distance where sand was moved due to penetration) and B is cone diameter (m).

The friction angle is defined as (Harr, 1977)

$$\varphi = 25 + (0.15 \times D_r) \quad (3)$$

The coefficient of lateral pressure is defined as (Harr, 1977)

$$K = 1 - \sin\varphi \quad (4)$$

Bearing capacity factor Nq is defined as (Puech et al, 2002)

$$Nq = a \times e^{b \tan\varphi} \quad (5)$$

For sand, a = 1.0584 and b = 6.1679 (Puech et al, 2002)

$$Nq = 1.0584 \times e^{6.1679 \tan \varphi}$$

The lateral extension of the slip lines L is defined as (Puech et al, 2002)

$$L = B \times e^{(\frac{\pi}{2} \times \tan \varphi)} \times \tan(\frac{\pi}{4} + \frac{\varphi}{2}) \quad (6)$$

The relative density is an index that quantifies the degree of compaction (packing between loosest and densest state) of coarse-grained soils (Lunne et al., 1997):

$$D_r = \frac{e_{\max} - e}{e_{\max} - e_{\min}} \quad (7)$$

Where e is the void ratio of the sample, $e_{\max}$ is the maximum possible void ratio (loosest condition) and $e_{\min}$ is the minimum void ratio (densest condition) of the sand (Lunne et al., 1997). For sand, the values of e_{max} and e_{min} are 0.71 and 0.34, respectively. The void ratio is the ratio between the volume of void and the volume of solid:

$$e = \frac{V_v}{V_s} \quad (8)$$

From the knowledge of particle density of sand, the volume of solid particles can be calculated from:

$$V_S = \frac{m_s}{\rho_s} \quad (9)$$

Where V_S is the volume of solid particles (m^3), m_s is the mass of sand (kg) and ρ_s is the particle density of sand (kg m^{-3}). The particle density (ρ_s) determination for sand is carried out by filling a beaker with water to a specific volume, pouring a weighted amount of sand into the beaker and measure the change in volume. The resulting sand particle density is ρ_s = 2556 kg m^{-3}. From the volume of solid particles (V_S), the volume of voids (V_v) is calculated by:

$$V_v = V_T - V_S \quad (10)$$

Where V_T is the total volume of regolith.

Using the previous values for e_{max} and e_{min}, and combining with the value of e, we determine D_r. Theoretical friction resistance of the sleeve Fs (Harr, 1977)

$$Fs = \frac{Kp \times \gamma \times Z \times As}{3} \tag{11}$$

Where γ is the effective unit weight of sand (N m^{-3}), Z is the penetration depth (m), As is the area of sleeve (m^2) and Kp is the passive coefficient of lateral stress (Harr, 1977)

$$Kp = \frac{1+\sin\phi}{1-\sin\phi} \tag{12}$$

Then we calculate the total force (F_T, eq. (1)) to insert the probe in the regolith simulant. The results are displayed in Figures 2.11 and 2.12 and compared to the experimental data for two different diameter probes (D = 0.9 cm and D = 1.2 cm). Theoretical results fit very well the experimental data which verifies the validity of the model. We observe a divergence between the model and the experimental data around 45 cm depth. After 45 cm, we are reaching the bottom of the cylinder and there is no place for the regolith to expand which increases the resistance force.

In the model, the relative density of the tested samples and the probes diameter are the most dominant effects which affect the cone resistance. Experimental data are in agreement with the theoretical model regarding these two dominant effects.

2.6.2 Application to other planetary bodies

Gravity plays an important role in the performance of penetrometers whether they are fast or slow. Fast penetrometers may not be able to obtain sufficient kinetic energy from free-fall in the gravity field to achieve the desired degree of penetration. Therefore, there may be a need for

added propulsion specifically to increase the impact velocity. Also, a body with weak gravity would likely lack an atmosphere that could be used to orient the falling penetrometer with respect to the surface. Gravity also affects the mechanical properties of the subsurface material. A low gravity environment such as that found on asteroids and comets reduces the required penetration force because the required force is proportional to the overburden pressure and thus to gravity. Results from Deep Impact mission revealed a low-density material on comet Temple 1 (Kerr, 2005) which would ease the penetration process. On the other hand, an anchor system may be used in order to hold the lander or the rover with the body of the asteroid during penetration. The maximum force for penetration would be the weight of the lander and rover on their targeted planetary surface. Table 2.3 shows the weight for past, present and future vehicles on their planets, which represents the maximum applicable force before tilting the rover. Penetration forces are directly proportional to the lithostatic pressure which is affected by gravity.

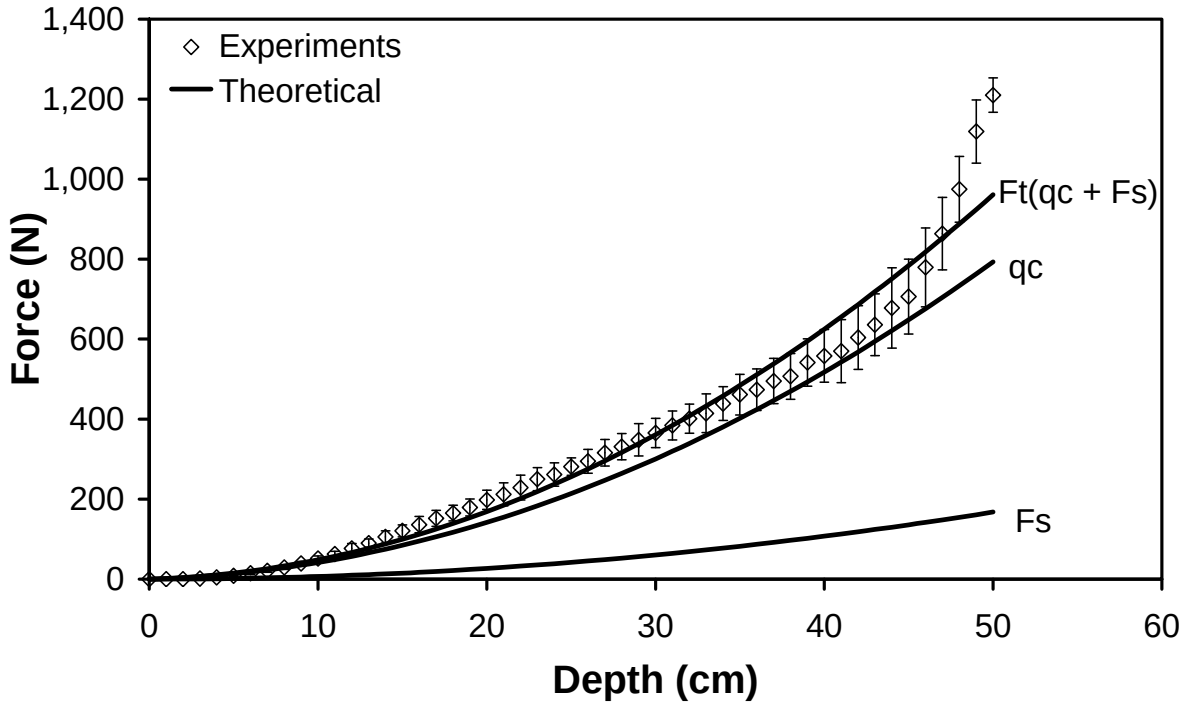

Figure 2.11. Theoretical versus experimental data in sand (D = 0.9cm).

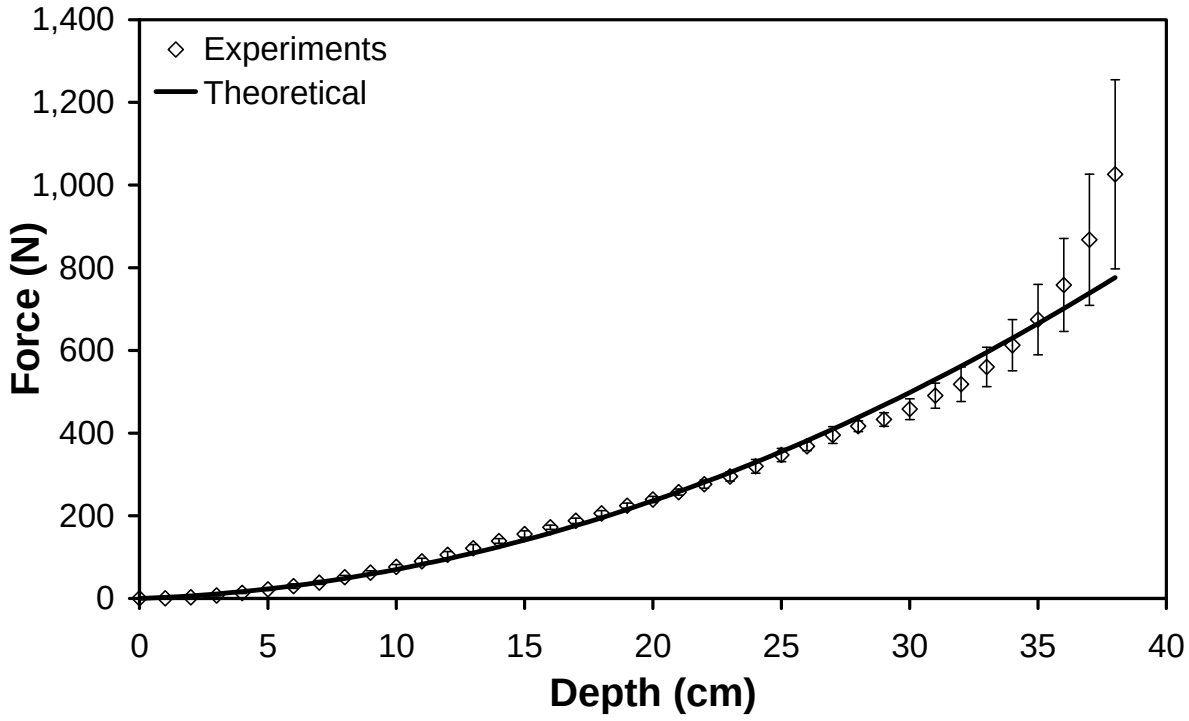

Figure 2.12. Theoretical versus experimental data in sand (D = 1.2cm).

Figure 2.13 shows the theoretical penetration forces as a function of depth which are needed to penetrate Earth, Venus, Mars, Moon and Titan. In this model, we assume that sand covers about the first meter of the subsurface of these planetary bodies and has a bulk density of about 1800 kg/m^3 and the gravity is scaled according to each planetary body. When the gravity of the planetary body decreases, density, porosity, friction angle and relative density will decrease and therefore, force needed for penetration will decreases as well. Figure 2.14, shows the moon theoretical model and the results obtained by Apollo 14, 15 and 16 lunar data. Results from Apollo 14 are in good agreement with the theoretical model while the data of ASR on board Apollo 15 and 16 are less than the theoretical model by about 145 N. The reason is that the subsurface of the Moon is not homogenous all over and its subsurface layers vary in thickness from one place to another.

Figure 2.14 supports our assertion that the driving factor for penetration on other planetary bodies is the gravity. A spacecraft weighing about 200 N on the Moon or Titan is capable of delivering penetration forces for a 1-cm diameter probe to reach a depth of about 0.5 m; a rover weighting about 500 N on Mars would reach the same depth. For the planetary bodies of interest (mostly Mars, Titan and the Moon), the maximum force to penetrate down to 0.5 meters is below 400 N (Fig. 2.13). This means that most landers / rovers would be able to do penetration experiments on their respective planetary bodies. The only exceptions would be the smallest rovers like Sojourner and Beagle-2 (Mars). This also demonstrates that the weight of static landers (Phoenix and Huygens, for example) would be enough to insert a probe in the subsurface during landing.

Table 2.3. Rovers and their weights on the target planetary body.

Vehicle	Planetary Body	Weight (N)
Luna 13	Moon	184
Surveyor	Moon	480
Lunokhood	Moon	1360
Viking	Mars	2210
Sojourner	Mars	39
Beagle 2	Mars	123
Spirit/Opportunity	Mars	683
Mars Science Lab	Mars	3320
Venera 13	Venus	6740
Huygens	Titan	431

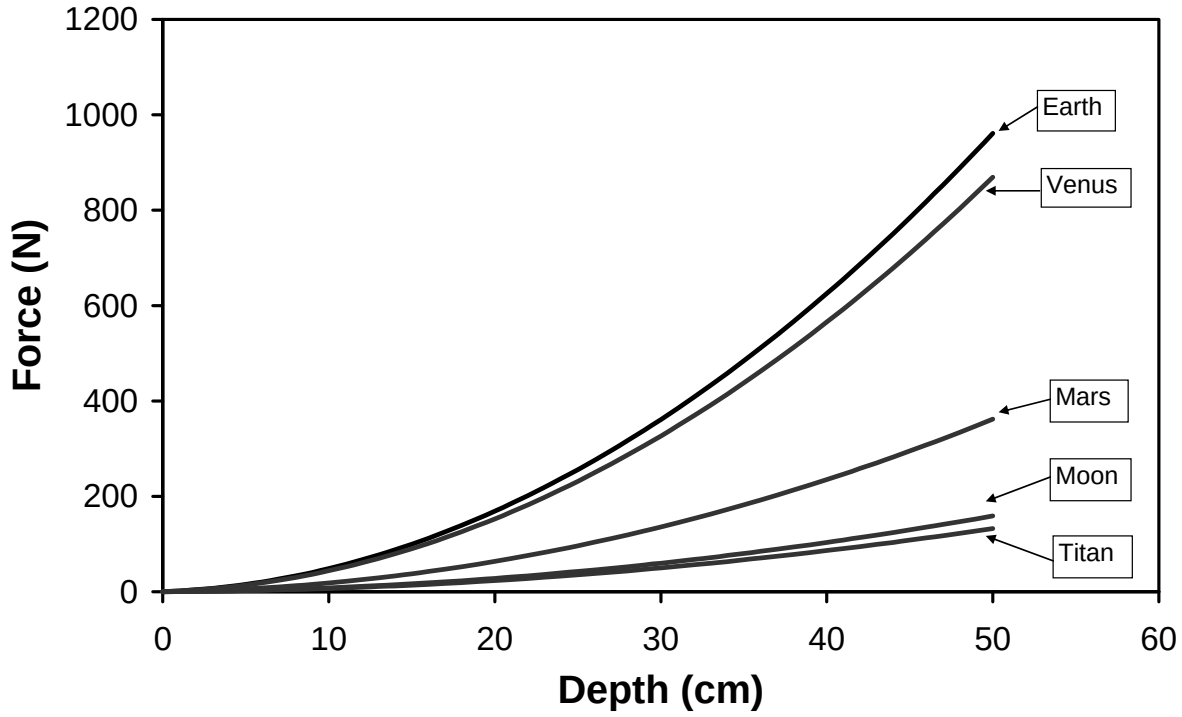

Figure 2.13. Theoretical penetration forces as a function of depth for different planetary bodies under their own gravity.

.

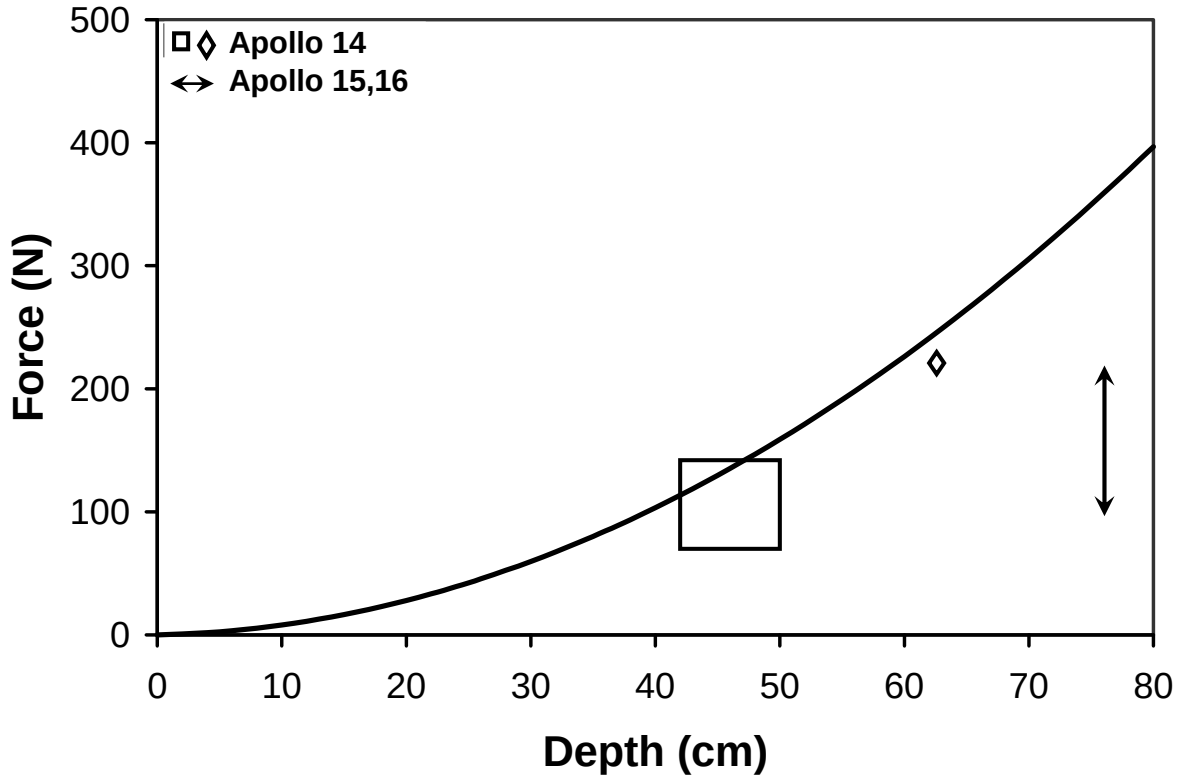

Figure 2.14. Theoretical penetration force as a function of depth for the moon along with Apollo 14, 15 and 16 lunar data. Thick black line is the theoretical calculation.

2.7. Conclusions

This research was conducted to investigate and quantify different factors which affect the insertion process of different probes in sand. To capture most of the effects, probes of different diameter, length, penetration speed and tip angle were used.

It was found that compaction levels play an important role on the required forces for probe penetration. An increase in bulk density from 1550 kg/m^3 to 1700 kg/m^3 resulted in increase in penetration force from 10 N to 200 N at 20 cm depth.

The diameter of the probes is the second most dominant effect. It was found that by increasing the diameter of the probe, the corresponding penetration force increases linearly with depth

No noticeable effect relating the speed and probe tip angles on the corresponding forces of penetration was found. Since there is no significant effect of tip angle, we can add a down looking hemispherical window in place of the tip which can provide spectra of any material the probe is going to touch.

Mars Science Lab (MSL) will be weighting about 3320 N on Mars. A 9 mm probe would be a good choice for OPRA to reach to about 0.5 m down into the subsurface of Mars or the Moon. These conclusions are based on conditions of dry regolith, icy soils are not considered.

2.8. References

Glaser, L. D, J. B. Andrew and K. A. Zacny. A review of penetrometers for subsurface access on comets and asteroids. Meteoritics & Planetary Science 43, 1021-1032, 2008.

Hansen, J. B. A revised and extended formula for bearing capacity. Bulletin No. 28, Danish Geotechnical Institute, Copenhagen, 1970.

Harr, M. E. Mechanics of particulate media, 260, McGraw-Hill. 1977.

Housen, K. R and L. L. Wilkening. Regoliths on Small Bodies in the Solar System. Annual Review of Earth and Planetary Sciences, 10, 355-376, 1982.

Kargl, G., N. I. Kömle, A. J. Ball, and R. D. Lorenz. Penetrometry in the solar system II. Proceedings of the International Workshop held in Graz, Austria, September 25–28, 2006. Vienna: Austrian Academy of Sciences Press, 2006

Kerr R. A. Deep Impact finds a flying snowbank of a comet. Science 309, 1667, 2005.

Kochan, H., H. Hamacher, L. Richter, L. Hirschmann, S. Assanelli, R. Nadalini, S. Pinna , V. V. Gromov, S. Matrossov, E. N. Yudkin, P. Coste, C. Pillinger, and M. Sims. The Mobile Penetrometer (Mole)—A tool for planetary sub-surface investigations. In Penetrometry in the solar system, edited by Kömle N., I., Kargl G., Ball A. J., and Lorenz R. D. Graz, Austria: Space Research Institute, Austrian Academy of Sciences. 212–243, 2001.

Longwell, C. R., and Flint, R. F. Introduction to Physical Geology, 324-345, John Wiley & Sones, Inc., New York and London, 1962.

Lorenz, D. R., M. Bannister, P. M. Daniell, Z. Krysinski, M. R. Leese, R. J. Miller, G. Newton, P. Rabbetts, D. M. Willett and J. C. Zarnecki. An impact penetrometer for a landing spacecraft. Measurement Science and Technology 5, 1033– 1041, 1994.

Lunne, T., P. K. Robertson, J. J. M. Powell. Cone Penetration Testing in Geotechnical Practice, first ed. Blackie Academic and Professional, London, 1997.

Matijevic, J. R., J. Crisp, D. B. Bickler, R. S. Banes, B. K. Cooper, H. J. Eisen, J. Gensler, A. Haldemann, F. Hartman, K. A. Jewett, L. H. Matthies, S. L. Laubach, A. H. Mishkin, J. C. Morrison, T. T. Nguyen, A. R. Sirota, H. W. Stone, S. Stride, L. F. Sword, J. A. Tarsala, A. D. Thompson, M. T. Wallace, R. Welch, E. Wellman, B. H. Wilcox, D. Ferguson, P. Jenkins, J.

Kolecki, G. A. Landis and D. Wilt. Characterization of the Martian Surface Deposits by the Mars Pathfinder Rover, Sojourner. Science 278, 1765, 1997.

Mitchell, J.K., L. G. Bromwell, W.D. Carrier and N.C. Costes and R.F. Scott. Soil mechanics experiment. In; Apollo 14 preliminary science report. *NASA SP*. NASA SP-272, 87-108, 1971

Mitchell, J.K., W.N. Houston, W.D. Carrier and N.C. Costes. Apollo soil mechanics experiment S-200. Final report, NASA Contract NAS 9-11266, Space Science Laboratory Series 15, Issue 7, Uni. California, Berkeley, 1974.

Murthy, V. N. S. Geotechnical Engineering: Principles and Practices of Soil Mechanics and Foundation Engineering (Civil and Environmental Engineering).CRC, 2002.

Puech, A., and P. Foray. Refined model for interpreting shallow penetration CPTs in sands, Offshore Technology Conference, 6 -9 May 2002, Houston, Texas, 2002.

Richter L., P. Coste, V. V. Gromov, H. Kochan, R. Nadalini, T. C. Ng, S. Pinna, H. E. Richter, and K. L. Yung. Development and testing of subsurface sampling devices for the Beagle 2 Lander. Planetary and Space Science 50, 903–913, 2002.

Pilgrim, R., R. Ulrich and M. Leftwich. Subsurface spectroscopic probe for regolith analysis. Poster at 40th LPSC conference, Houston, TX, 1219, 2009.

Stoker, L. Richter , W.H. Smith, L.G. Lemke, P. Hammer, J.B. Dalton, B. Glass and A. Zent. The Mars underground mole (MUM): a subsurface penetration device with insitu infrared reflectance and raman spectroscopic sensing capability. Sixth International Conference on Mars, 3007, 2003.

Terzaghi, K. Theoretical soil mechanics, John Wiley, New York, 1943.

Vesic, B. A. Bearing capacity of deep foundations in sand. High way research record No39, 112-153, 1963.

Zarnecki, J. C., M. R. Leese, J. R. C. Garry, N. Ghafoor and B. Hath. Huygens surface science package. Space Science Reviews 104, 593-611, 2002.

Zarnecki, J. C., M. R. Leese, B. Hathi, A. J. Ball, A. Hagermann, M. C. Towner, R. D. Lorenz, J. A. M. McDonnell, S. F. Green, M. R. Patel, T. J. Ringrose and, H. Svedhem, J. Delderfield, M. Grande, D. J. Parker, P. G. Challenor, and J. E. Geake. A soft solid surface on Titan as revealed by the Huygens surface science package. Nature 438, 792–795, 2005.

CHAPTER 3: PENETRATION TESTING FOR SUBSURFACE REGOLITH PROBES IN MARTIAN ANALOG MATERIAL

3.1. Introduction

Regolith mechanical properties of planetary bodies affect both landing of spacecraft and exploring planetary surfaces. Planetary geotechnical parameters are of high importance for scientists and missions designers. Scientists use these parameters to understand the formation and evolution of planetary profiles while mission designers use this information to decide landing sites and target areas of investigations. Likely, most soil mechanical properties are interrelated. Knowledge of one parameter could lead to estimate the rest of the mechanical parameters. Level of compaction, consolidation and others useful information can be known from geotechnical parameters such as density, porosity, void ratio which are indicative of the nature and condition of the surface and subsurface structure. Determination of these parameters will improve future mission success and will provide required information to further understand the history and evolution of planetary surface and subsurface.

On all the surveyor lunar landers, a strain gauge is attached on its three legs to measure the force of penetration into lunar regolith during landing (Scott and Robertson, 1968). Their landing velocities ranged from 1.4 to 4.2 m s^{-1} and the penetration depth ranged from 2.1 to 10.5 cm. It was concluded that the force of penetration at the surface is zero and it increase with increasing depth at the rate of 1.87 ± 0.33 MPa m^{-1} (Mitchell et al., 1971). The Soil Mechanics Surface Sampler (SMSS) which was carried on surveyors 3, 4 and 7 indicated that the lunar regolith has a bulk density of about 1.5 g cm^{-3}, an angle of friction range from 35 to 37º and the bearing capacity was about 2.1 N cm^{-2} at a depth of about 3 cm (Mitchell et al., 1971). The Apollo

Simple Penetrometer (ASP) on board Apollo 14 was part of the Apollo Lunar Surface Experiment Package (ALSEP) which used to investigate the lunar regolith soil mechanics (Mitchell et al., 1974). ASP was a metal rod 68 cm long and 0.95 cm in diameter with a 30 degree cone angle used in three penetration tests on the Moon by manually pushing it into lunar regolith by astronaut. ASP reached to a depth of 42, 44 and 50 cm and the penetration force was in the range of 70 to 135 N using one hand. A second deployment of ASP reached a depth of 62 cm and required a force of 225 N using both hands (Mitchell et al., 1974). A Self-Recording Penetrometer (SRP) was on board Apollo 15 and 16 missions. This instrument was connected to a recording drum which recorded the force versus depth. At a maximum depth of 76 cm, the Apollo 15 SRP recorded a force of 111 N and the Apollo 16 SRP recorded a maximum force of 215 N (Mitchell et al., 1974). PROP-M (Pribori Ochenki Prokhodimosti-Mars, Martian cross-country capability evaluation instrument) is a tethered walking rover with a mass of 4.5 kg on board Mars 2, 3, 6 and 7 missions to Mars in the period between 1971 to 1973 (Harvey, 2007). PROP-M was designed to make penetrometry and densitometry measurements along its path. The maximum tethered length was 15m; therefore, the rover was programmed to stop and to take measurements every 1.5m (Harvey, 2007). At each measurement point, the penetrometer would be hammered into the regolith and the results would be recorded. Results from Mars 2/3 indicate the surface of Mars had a surface density of 1.2, 1.6 and in some places up to 3.5 g cm^{-3} (Harvey, 2007). Venera 9 and 10 brought valuable data about Venus. The landers equipped with density meter as one of the soil mechanics instruments. Venera 9 and 10 reported a surface density ranging from 2.7 to 2.9 g cm^{-3} (Harvey, 2007). ACC-E is a piezoelectric force sensor (impact penetroemter) which was part of the Surface Science Package (SSP) onboard the Huygens probe which is used to investigate the subsurface of Saturn's moon Titan (Lorenz et al., 1994). ACC-E,

an impact penetrometer, was the first instrument touched down the surface of titan for soil mechanics investigation. The miniature probe (mass of 15 g, 14 mm diameter) has a sensing element of 2mm. The force sensor can measure the force in the range of 0 – 2000 N. The results indicated that the surface had a weak crust and, beneath that, a structure consisted of wet sand and embedded pebbles (Zarnecki et al., 2005). Based on the knowledge of the densities of other extraterrestrial planetary bodies, prediction of the forces of penetration as a function of depth can be accomplished.

The downward movement of the penetrometer through regolith is opposed by two reaction forces: the base or cone resistance, which pushes against the cone and sleeve friction, which acts up on the lateral side of the penetrometer (Vesic, 1963). Penetration into regolith materials is directly proportional to the effective unit weight of the regolith (γ), bearing capacity factor (N_q), depth of penetration (D) and friction angle (φ). The main objective of this research is to estimate the bearing capacity factor (N_q) experimentally based on forces of penetration for Martian analog material (JSC Mars-1). From penetration forces as well as the knowledge of some mechanical properties of JSC Mars-1, one can estimate the bearing capacity factor (N_q) under different levels of compaction. (N_q) varies from one type of material to another due to intrinsic regolith properties. Knowledge of (N_q) will help us approximate the force of penetration under different levels of compaction to simulate the conditions on Mars such as density and gravity.

3.2. Experimental Apparatus

A specific apparatus was designed and built to measure the penetration forces in unconsolidated materials. A general illustration of the setup is shown in Figure 3.1. An automated control system was designed where the whole penetration experiment can be

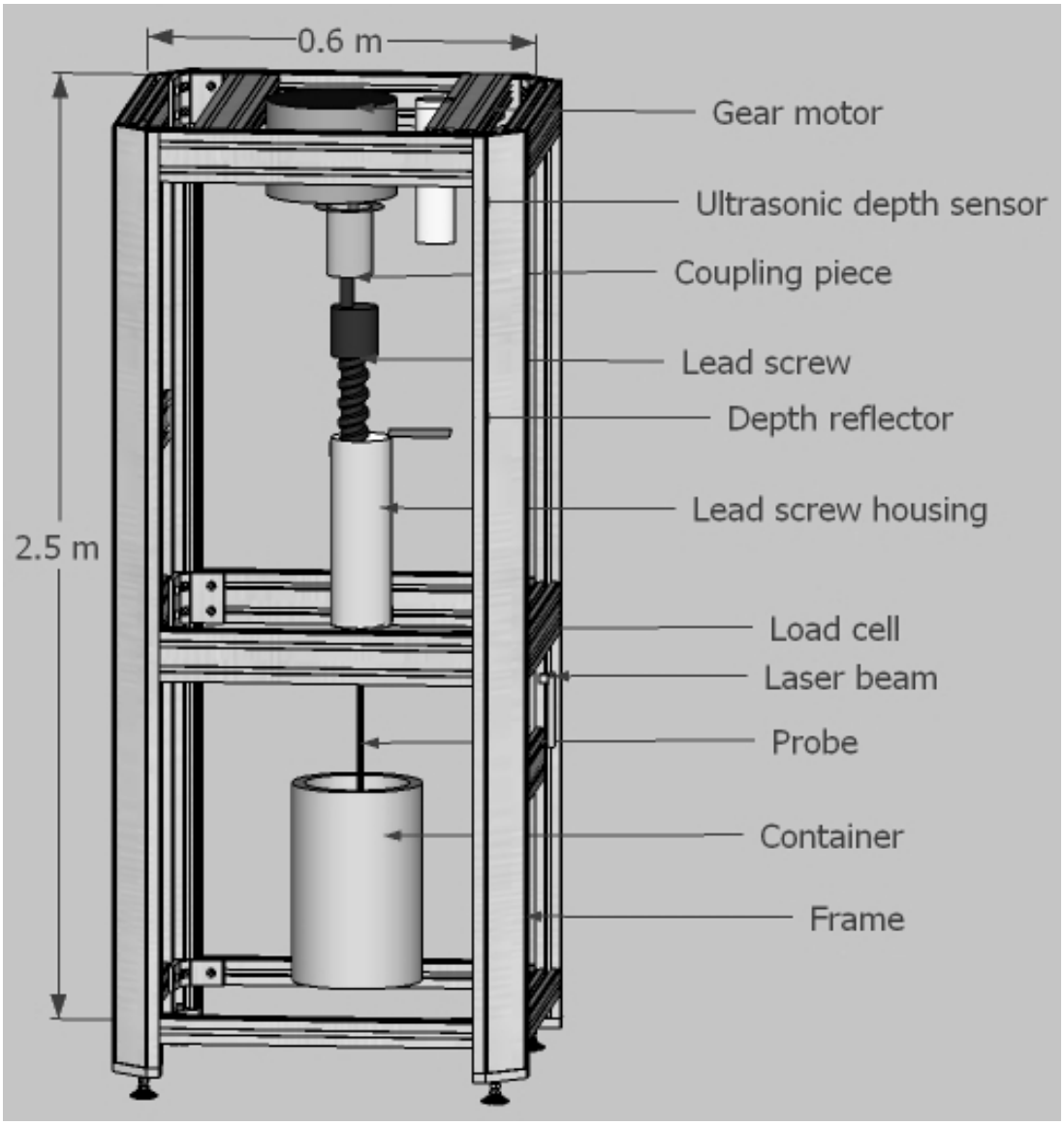

Figure 3.1. The penetration testing apparatus

monitored and controlled through a personal computer. Two parameters are being monitored during penetration testing: the penetration force and penetration depth. The results of the penetration experiment are automatically saved in an Excel file. A complete description of the penetration rig and its automated control system can be found in (ElShafie et al., 2010).

3.3. Experimental Procedures

The particle size distribution of JSC Mars-1 was determined by sieving as shown in Figure 3.2. The results show that JSC Mars-1 contains 17% medium size particles (>0.5 mm) and 83% fine grained particles (<0.3 mm). Penetration experiments were run at a constant speed of 2 mm s^{-1}. Samples are prepared by filling a 16 cm diameter and 24 cm deep cylindrical bucket with 27.5 kg of dry JSC Mars-1. Then, the bucket is shaken in order to homogenize and compact the regolith to the desired height. All possible care was taken to obtain a uniform density throughout the column regolith. Penetration testing is done only once per sample preparation.

To determine the bearing capacity factor N_q from forces of penetration, a cylindrical container was filled with JSC Mars-1 with a measured bulk density of 1120 kg m^{-3}. Insertion and removals were conducted at this bulk density using 1.2 cm diameter probe. JSC Mars-1 poured out of the container and re-poured in for each penetration test. JSC Mars-1 was adjusted to the same bulk density of 1120 kg m^{-3} for two more penetration testing. The average force of the three penetration testing is calculated and N_q factor is determined at each data point. The average of N_q was determined and implemented in a Matlab code to determine the theoretical force of penetration based on the knowledge of bulk density. Table 3.1 shows symbols used through the paper and their corresponding definition. Table 3.2 shows test probes used throughout the research.

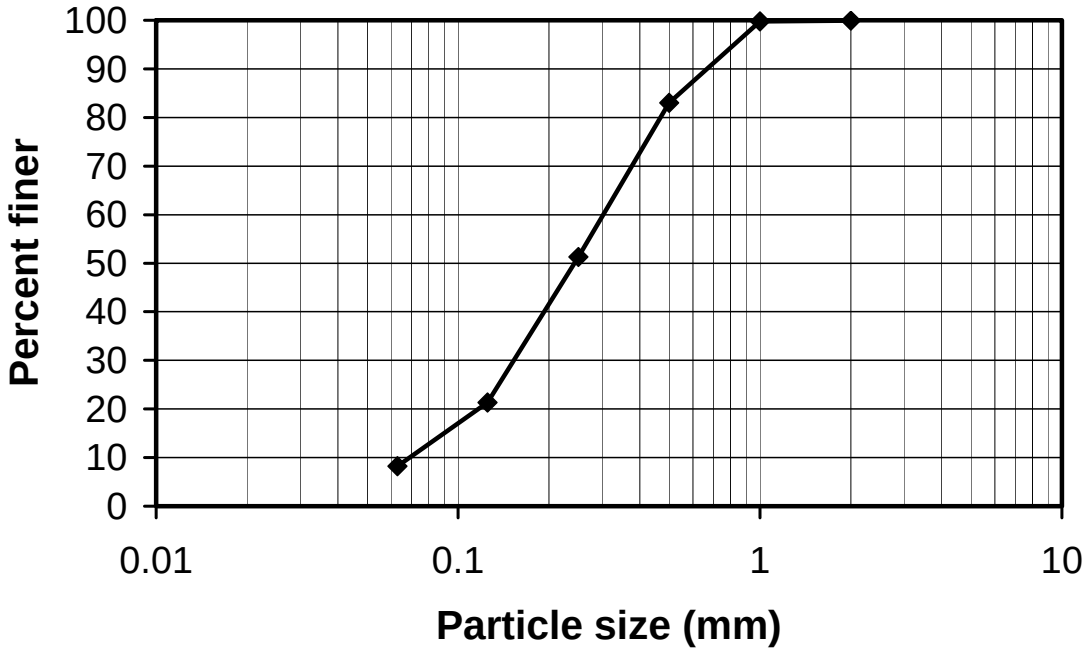

Figure 3.2. Particle size distribution for JSC Mars-1.

Table 3.1. List of symbols used in the paper

Symbol	Def.
A_c	Area of the cone (m^2)
A_s	Area of the sleeve (m^2)
B	Cone diameter (m)
D	Probe diameter (cm)
D_r	Relative density (dimensionless)
e	Void ratio (dimensionless)
e_{max}	Maximum possible void ratio (loosest condition)
e_{min}	Minimum void ratio (densest condition)
f_s	Sleeve friction (N m^{-2})
F_T	Total resistance force (N)
K	Coefficient of lateral pressure at rest (dimensionless)
K_p	Passive coefficient of lateral stress (dimensionless)
L	Lateral extension of the slip lines (m)
m_s	Mass of JSC Mars-1 (kg)
N_q	Bearing capacity factor (dimensionless)
q_c	Cone resistance (N m^{-2})
V_s	Volume of solid particles (m^3)
V_T	Total volume (m^3)
V_v	Volume of voids(m^3)
Z	Penetration depth (m)
γ	Effective unit weight of JSC Mars-1 (N m^{-3})
φ	Friction angle of sand (degree)
ρ_p	Particle density of JSC Mars-1 (kg m^{-3})
ρ_b	Bulk density of JSC Mars-1 (kg m^{-3})

Table 3.2. List of probes and their experimental parameters.

Probe	Diameter (cm)	Length (cm)	Tip Length (cm)	Tip Angle (º)
1	1.2	23	1	30
2	2	23.5	1.5	30

3.4. Experimental results

Penetration force is a strong function of the density of regolith materials (Robertson et al., 1997) and increase with increasing bulk density (ElShafie et al., 2010). Five different levels of compaction were prepared to achieve a bulk density of 1120, 1158, 1167, 1184 and 1241 kg m^{-3}. Figure 3.3 shows the forces of penetration as a function of depth under different bulk densities. Solid line represents the theoretical force of penetration based on the knowledge of the bearing capacity factor N_q and bulk density. Penetration forces increase with increasing the compaction level. Figure 3.3 F shows the penetration force versus depth using a 1.9 cm diameter probe under a bulk density of 1184 kg m^{-3}. The N_q factor used for the theoretical force is the same as determined by 1.2 cm diameter probe (Fig. 3.3 D). Theoretical penetration curve is in agreement with the experimental data which supports the validity of the N_q factor under the same bulk density for different diameter probes.

Penetration energy is determined using two different diameter probes (D = 1.2 and 1.9 cm) under the same level of compaction (B.D = 1184) (Fig. 3.4). Penetration energy is determined by integrating the area under the curve for the experimental penetration forces. To reach to about 20 cm depth, a 1.2 cm probe requires about 90 J while the 1.9 cm probe needs about 180 J. Increasing the area by about a factor of two correspond to doubling the penetration energy.

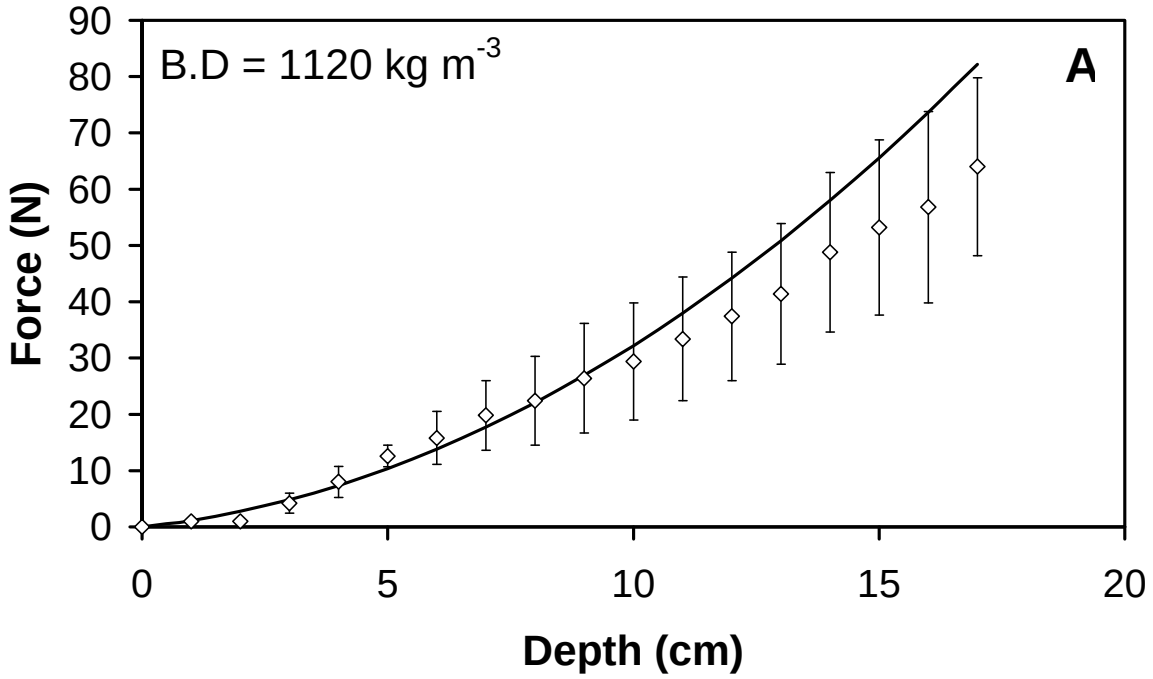
B.D = 1120 kg m-3
A
Force (N)
Depth (cm)
0
10
20
30
40
50
60
70
80
90
0
5
10
15
20

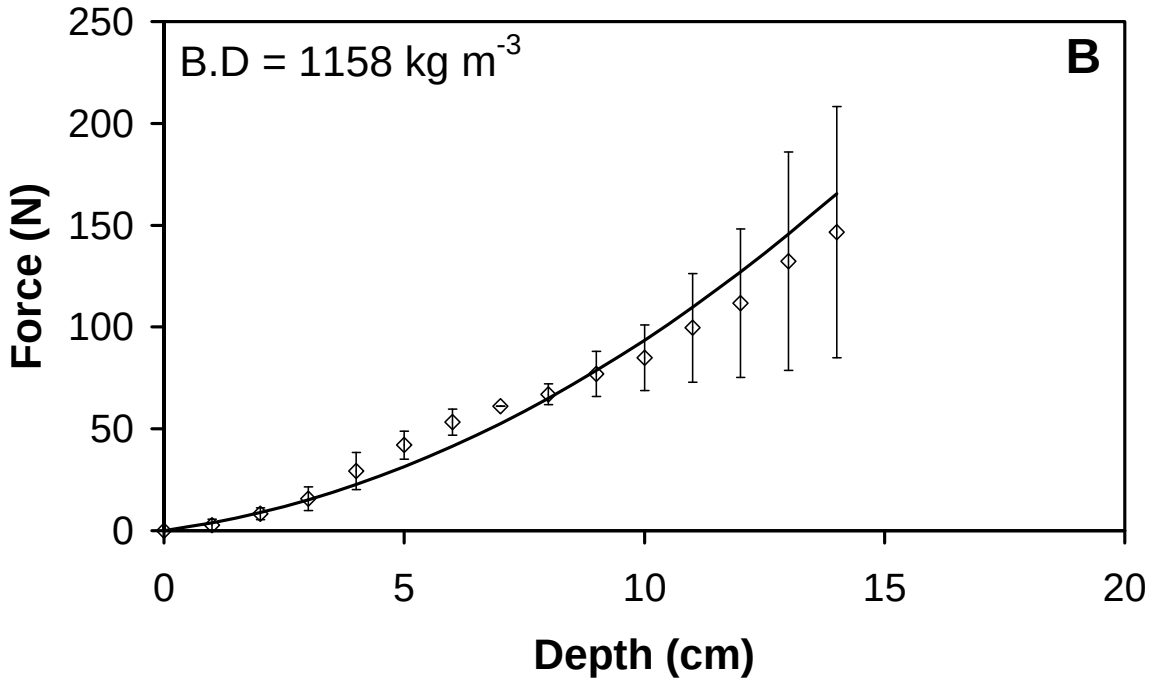
B.D = 1158 kg m-3
B
Force (N)
Depth (cm)
0
50
100
150
200
250
0
5
10
15
20

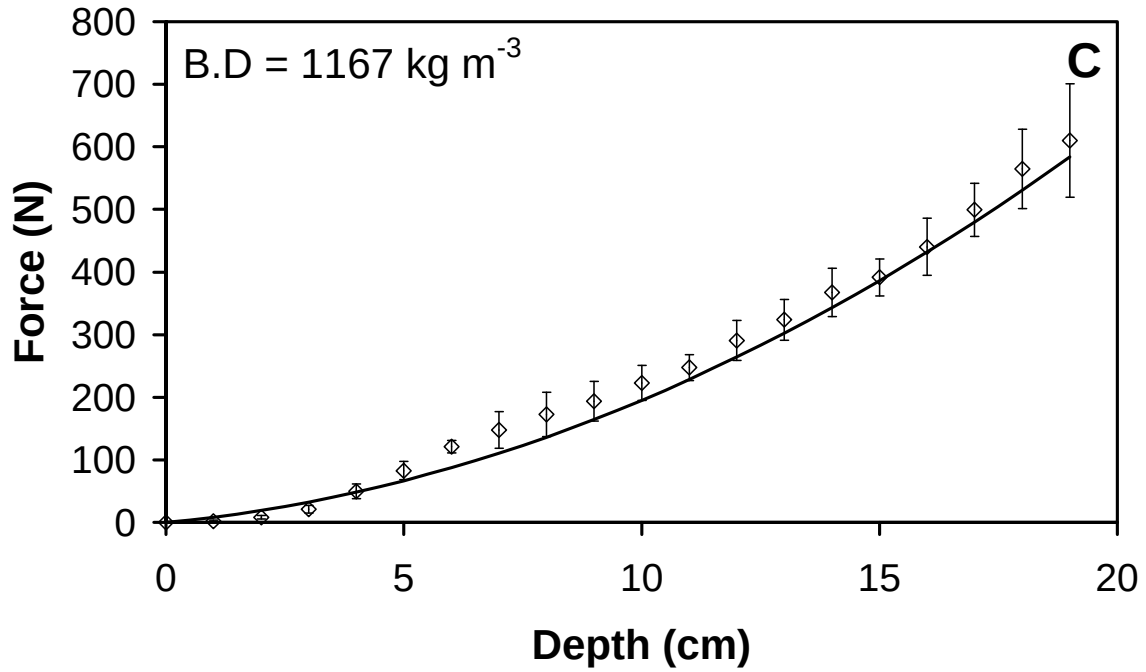
B.D = 1167 kg m-3
C
Force (N)
Depth (cm)
0
100
200
300
400
500
600
700
800
0
5
10
15
20

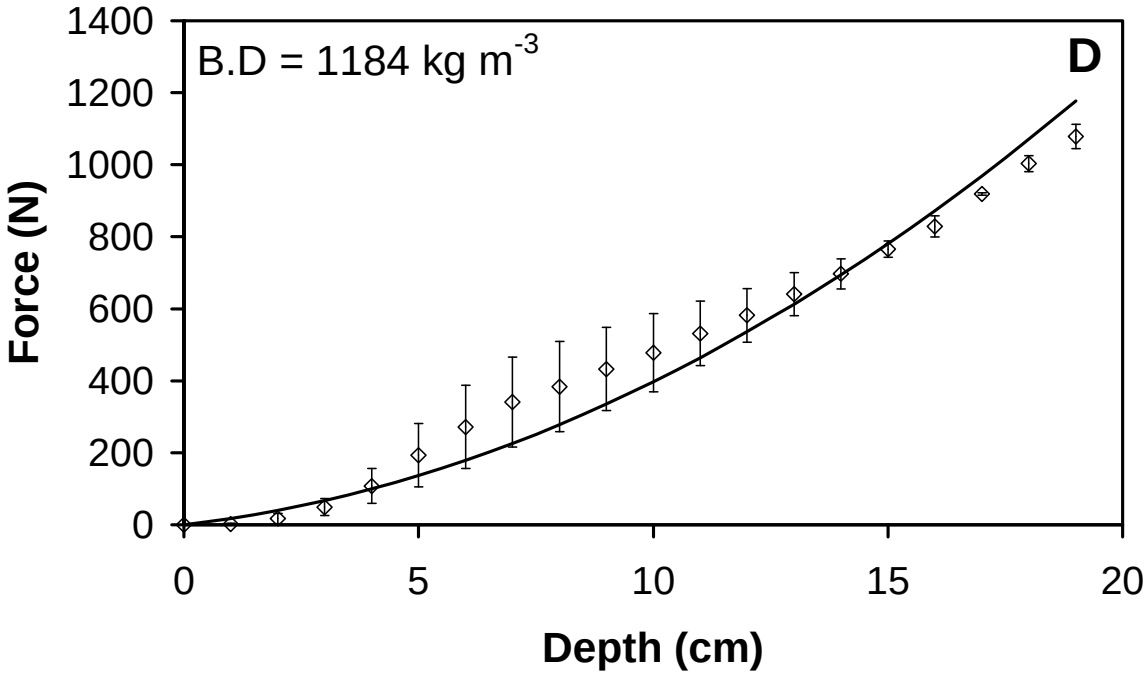
B.D = 1184 kg m-3
D
Force (N)
Depth (cm)
0
200
400
600
800
1000
1200
1400
0
5
10
15
20

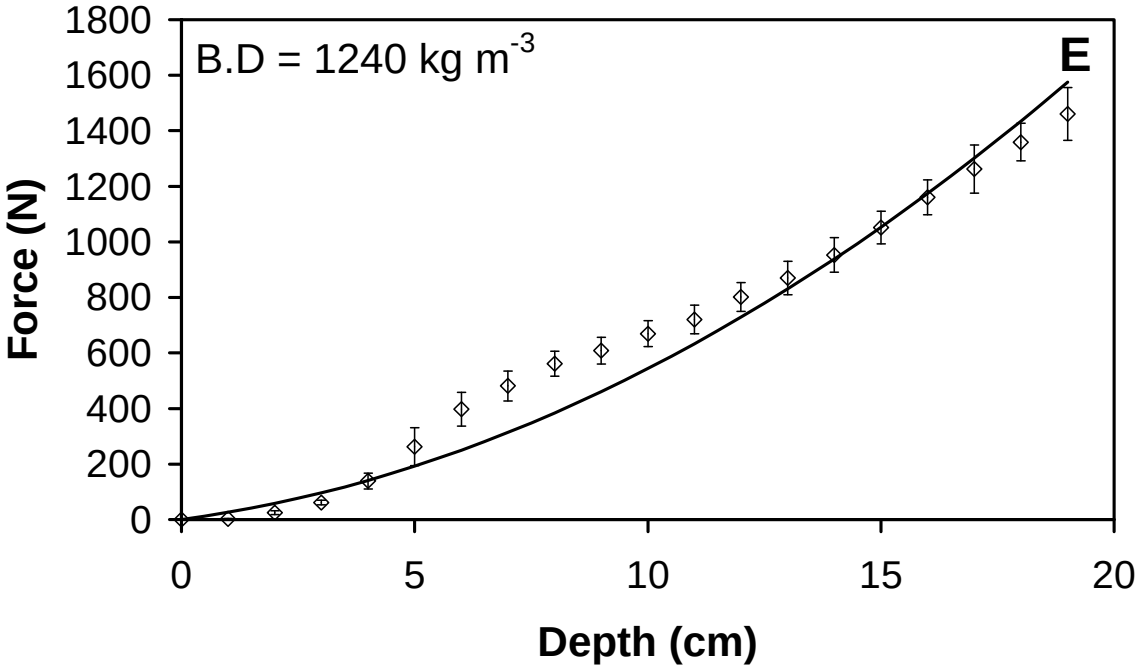

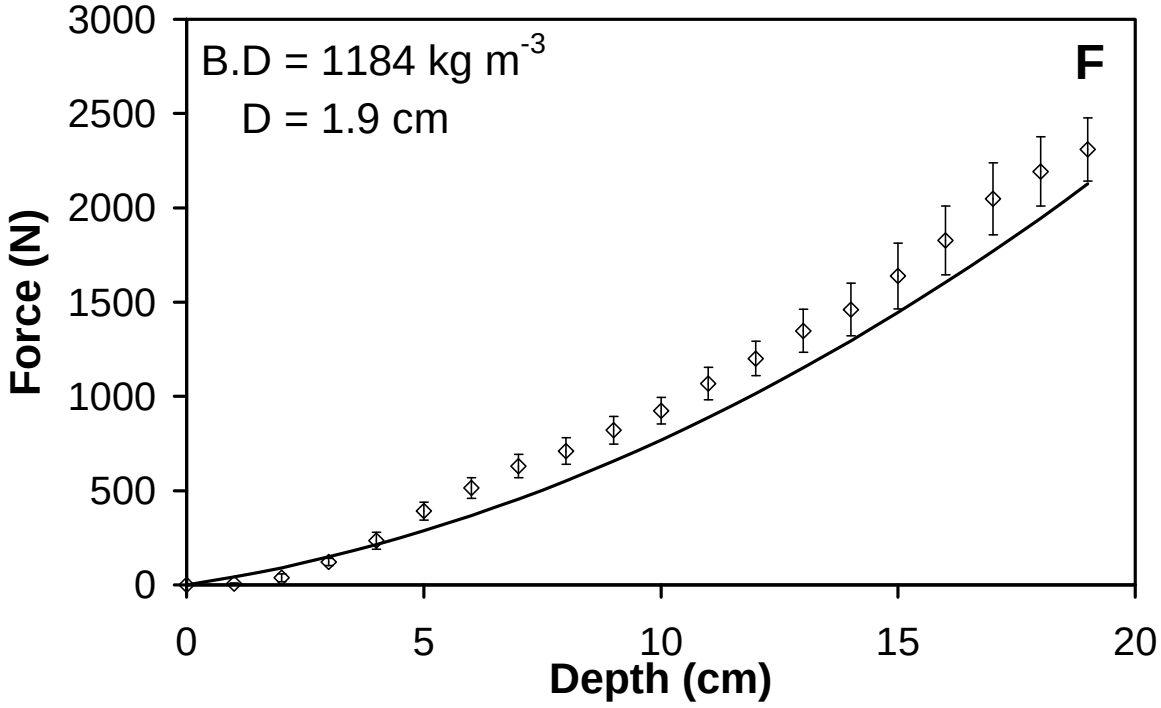

Figure 3.3. Penetration forces as a function of depth for different bulk density (D = 1.2 cm for A, B, C, D, and E, T.A = 60º) (For F, D = 1.9, T.A = 60º).

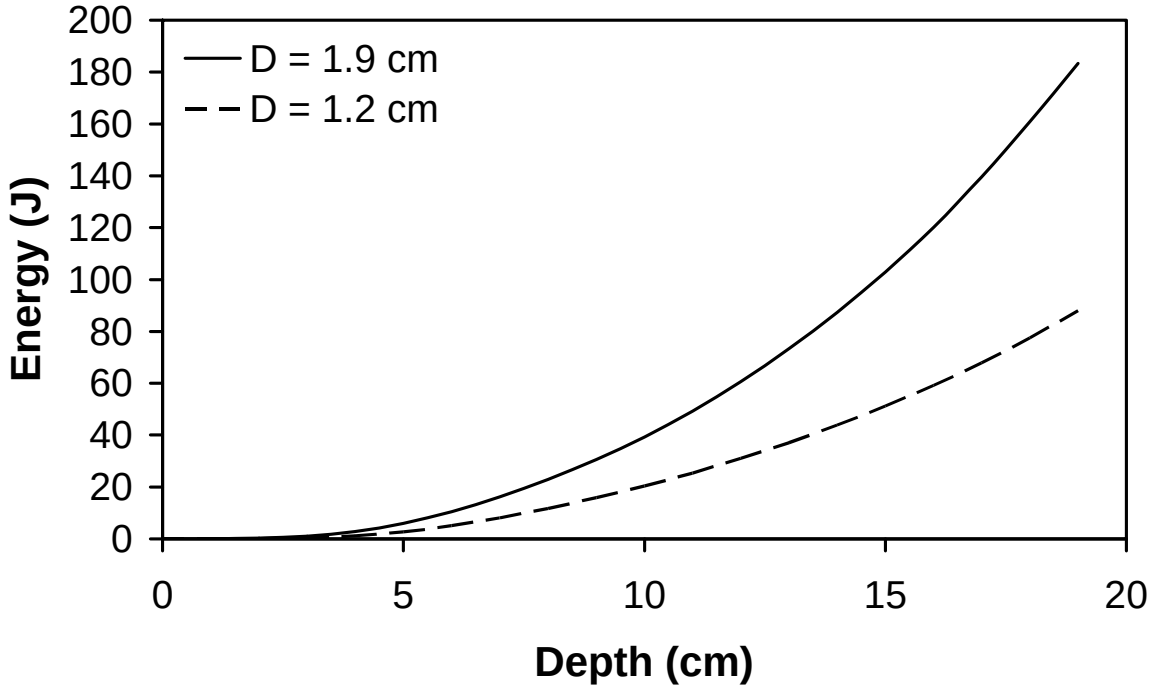

Figure 3.4. Penetration energy as a function of depth for two different diameter probes under the same bulk density (B.D = 1184 kg m^{-3}).

3.5. Discussion

Terzaghi (1943), Vesic (1963), Meyerhof (1963) and Hansen (1970) developed the bearing capacity theory. The bearing capacity factors are affected by the level of compaction as well as regolith friction angle (Vesic, 1963). Estimating the force of penetration using the current bearing capacity factors with JSC Mars-1 regolith material did not show good agreement between the experimental and theoretical values. Therefore, determination of the bearing capacity factor N_q for JSC Mars-1 was essential from forces of penetration.

Bearing capacity theory can be used to explain the movement of the penetrometer through regolith materials. The total penetration force (F_T) during probe insertion into the subsurface is the sum of two forces; the cone resistance (q_c) and the sleeve friction (f_s):

$$F_T = q_C A_C + f_S A_S \tag{1}$$

Where A_c is the area of the cone, A_s is the buried area of the sleeve. The cone resistance can be calculated from (Puech and Foray, 2002):

$$q_C = \gamma \times Z \times N_q \left(1 + \left(K \times \sin\varphi \times \frac{Z}{L}\right)\right) \tag{2}$$

Where γ is the effective unit weight of sand (N m^{-3}), Z is the penetration depth (m), N_q is the bearing capacity factor (dimensionless), K is the coefficient of lateral pressure at rest (dimensionless), φ is the friction angle (degree) and L is the lateral extension of the slip lines (m). The friction angle is defined as (Harr, 1977).

$$\varphi = 25 + (0.15 \times D_r) \tag{3}$$

Where D_r is the relative density. The coefficient of lateral pressure is defined as (Harr, 1977).

$$K = 1 - \sin\varphi \tag{4}$$

Finally, the lateral extension of the slip lines L is defined as (Puech and Foray, 2002):

$$L = B \times e^{(\frac{\pi}{2} \times \tan\varphi)} \times \tan(\frac{\pi}{4} + \frac{\varphi}{2}) \quad (5)$$

Where B is the cone diameter (m). From the knowledge of particle density of JSC Mars-1, the volume of solid particles can be calculated from:

$$V_s = \frac{m_s}{\rho_p} \quad (6)$$

Where V_s is the volume of solid particles (m^3), m_s is the mass of JSC Mars-1 (kg) and ρ_p is the particle density of JSC Mars-1 (kg m^{-3}). The particle density (ρ_s) determination for JSC Mars-1 is carried out by filling a beaker with water to a specific volume, pouring a weighted amount of JSC Mars-1 into the beaker and measure the change in volume. The resulting JSC Mars-1 particle density is ρ_p = 1900 kg m^{-3} and the values of e_{max} and e_{min} are found to be 1.16 and 0.53, respectively. Table 3.3 shows the particle density, bulk density and void ratio for JSC Mars-1 compared with (Allen et al., 1998) and (Perko et al., 2006).

Based on Figure 3.3, a relation between bearing capacity factor N_q and bulk density can be extrapolated for JSC Mars-1 regolith material. Figure 3.5 shows the average of the bearing capacity factor N_q and bulk density for JSC Mars-1. The bearing capacity factor N_q varies under each level of compaction which increases with increasing the bulk density of the prepared samples. The error in the caption of the bulk density measurement is about 1% which smaller than the symbol.

Table 3.3. JSC Mars-1 regolith properties.

Author	ρ_p (kg m^{-3})	ρ_b (kg m^{-3})		E	
		A	B	e_{max}	e_{min}
[14]	1910	870	1070	1.19	0.78
[15]	1920	900	1160	1.13	0.65
*	1900	879	1240	1.16	0.53

* This paper

A uncompacted regolith

B compacted regolith

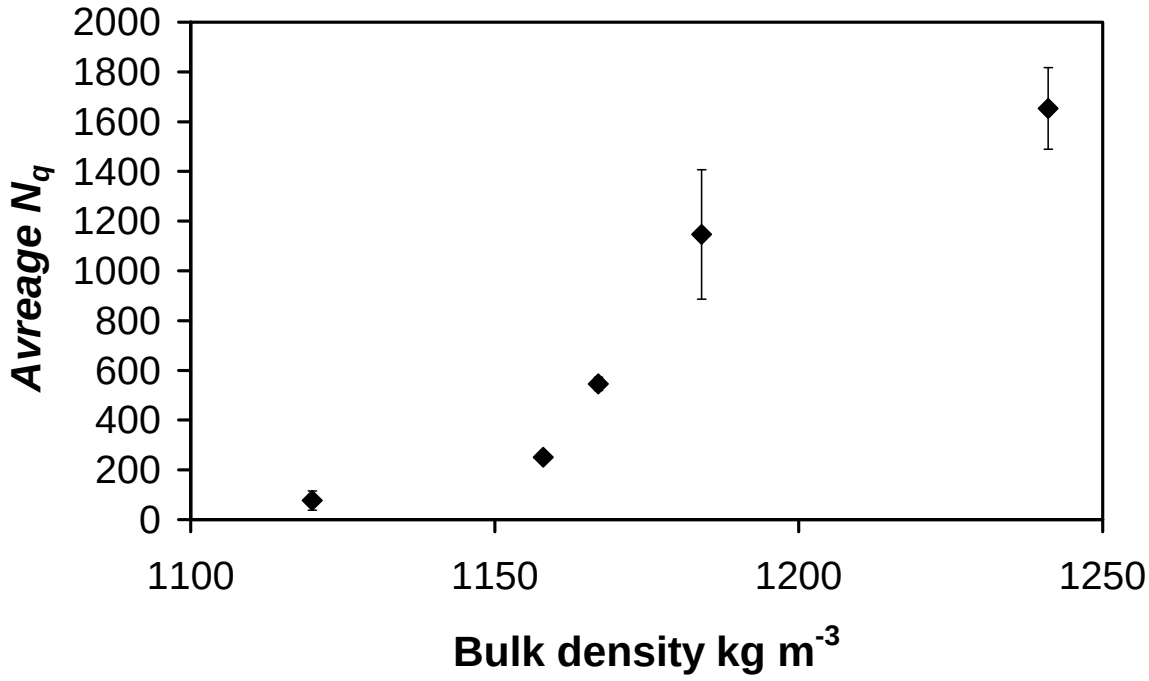

Figure 3.7. Average bearing capacity factor N_q as a function of bulk density.

Determination of the force of penetration is highly important for trafficability of lander/rover and feasibility of subsurface investigations. Viking lander 1 estimated Mars regolith bulk density of 1000 – 1600 kg m^{-3} while Viking lander 2 estimated a bulk density of 1100, 1480 and 2600 kg m^{-3} (Moore et al., 1977). Sojourner, the Mars Pathfinder rover investigated Mars regolith material. The rover used its wheels to do a number of turns and to determine some regolith mechanical properties. The rover applied different turns and reached to different depths. The maximum depth reached by the rover wheels is 6 cm with 1.5 turn. The regolith bulk density is estimated to be 1520 kg m^{-3} (Rover team, 1997). Based on the knowledge of bearing capacity factor N_q and the corresponding bulk density, Figure 3.6 shows the penetration force as a function of depth under Martian gravity for two different bulk densities (B.D = 1160 and 1250 kg m^{-3}).

Regarding the penetration power, Spirit and Opportunity each can generate a peak of about 150 W of solar power. Over an average sol with fairly clean panels, they can produce about 600 W-hrs of power, which is equal to 2.2 MJ. MSL will produce 125 W continuously from its radio-isotropic thermal generator, giving up to 3000 W-hrs/sol or 10.8 MJ. The energy of penetration under Martian gravity is shown in Figure 3.7. Our measurements in compacted JSC Mars-1 simulant (B.D = 1250 kg m^{-3}) with probe diameter of 1.2 cm indicate a requirement of 45 J to achieve about 20 cm. The peak rate of required power for probe insertion will be only about 1.2 W (600 N time's 0.002 m s^{-1}).

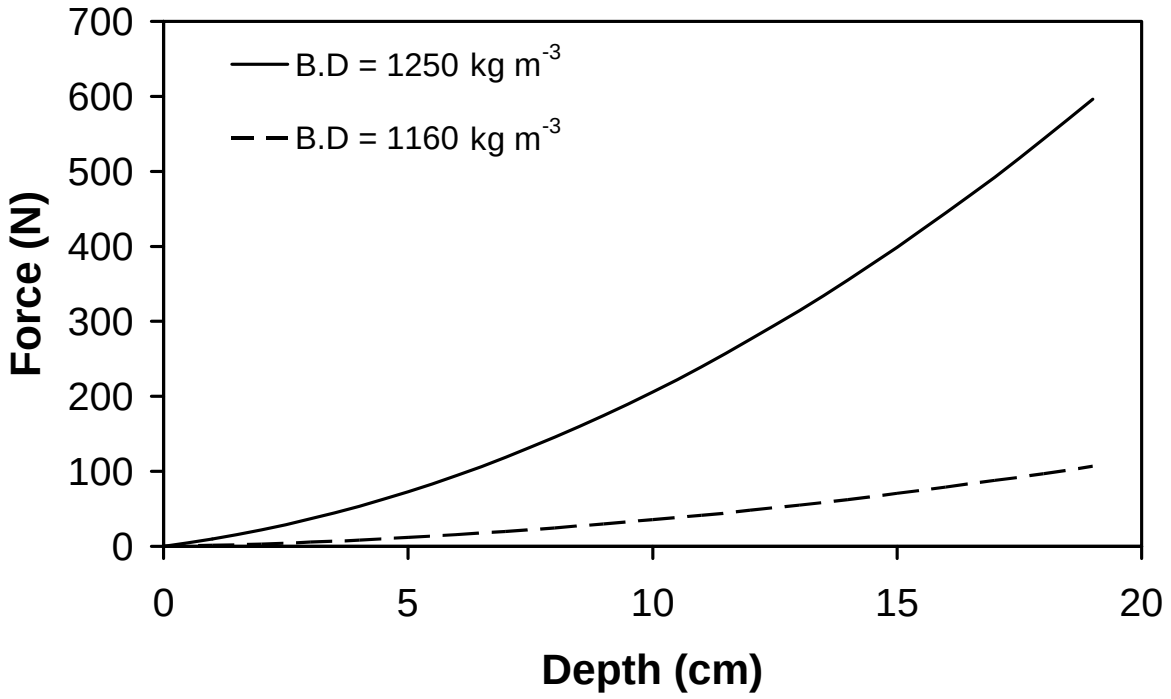

Figure 3.6. Penetration testing under martian gravity under bulk density of 1160 and 1250 kg m^{-3}.

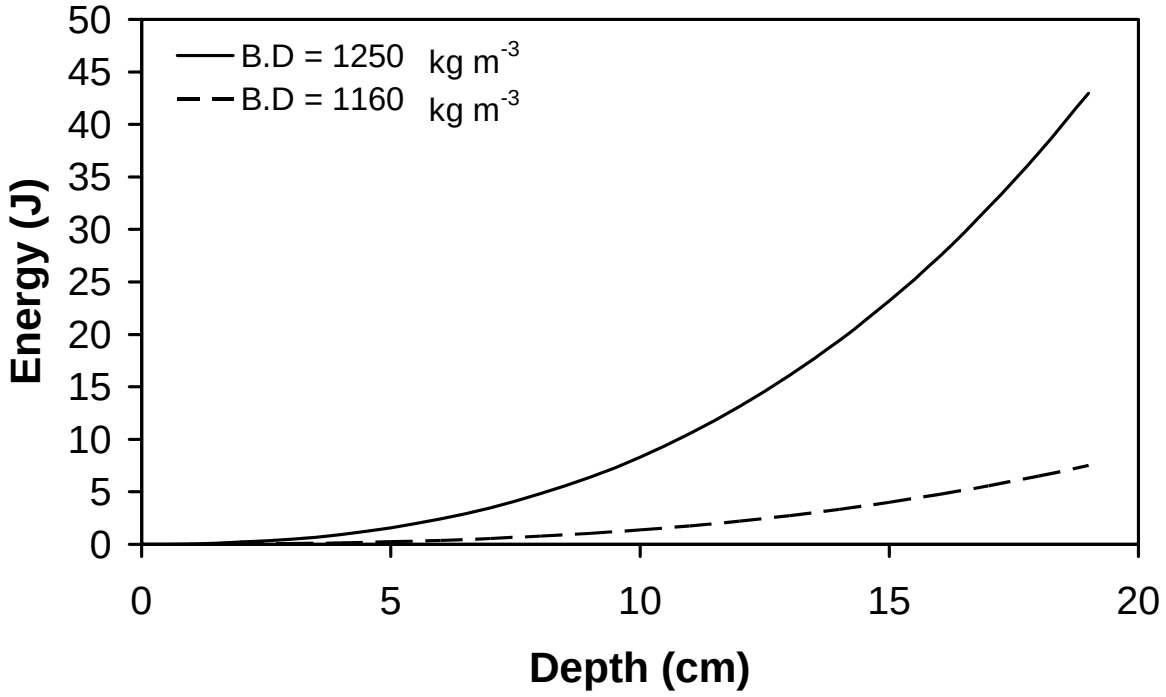

Figure 3.7. Energy of penetration as a function of depth based on penetration forces under Martian gravity for bulk density of 1160 and 1250 kg m^{-3}.

3.6. Conclusions

Bearing capacity equation is used to estimate the force of penetration of regolith materials. Using bearing capacity factor N_q from previous theories did not show agreement between experimental data and theoretical model. Therefore, there was a need to determine this factor in order to best estimate the force of penetration on extraterrestrial planetary bodies. Different penetration forces under different levels of compaction were carried out in order to determine the bearing capacity factor directly from experimental data. The results of this investigation showed that the bearing capacity factor N_q vary under each level of compaction which increase with increasing the bulk density of the prepared samples. Knowledge of regolith mechanical properties determined from previous mission such as bulk density on Mars were used and applied in a theoretical model for estimating the force of penetration under Martian conditions. Under Martian gravity and a bulk density of 1250 kg m^{-3}, 600 N of force are enough to drive a 1.2 cm diameter probe to about 20 cm of the subsurface on Mars with about 1.2 W of power. Estimating the force of penetration would enhance future landing and subsurface planetary investigation which is a success to the whole mission.

3.7. References

Allen, C. C., R. V. Morris, K. M. Jager, DC Golden, D. J. Lindstrom, M. M. Lindstrom, and J. P. Lockwood. 1998. Martian regolith simulant JSC mars-1. *Lunar and Planetary Science XXIX*.

ElShafie, A., VF Chevrier, R. Ulrich, and L. Roe. 2010. Penetration testing for the optical probe for regolith analysis (OPRA). *Advances in Space Research* 46 (3): 327-36.

Hansen, J. B. 1970. A revised and extended formula for bearing capacity.

Harr, M. E. 1977. *Mechanics of particulate media: A probabilistic approach*. Vol. 230McGraw-Hill New York.

HARVEY, B. 2007. Russian planetary exploration: History, development, legacy & prospects (praxis books/Space exploration). *Recherche* 67 : 02.

Lorenz, RD, M. Bannister, PM Daniell, Z. Krysinski, MR Leese, RJ Miller, G. Newton, P. Rabbetts, DM Willett, and JC Zarnecki. 1994. An impact penetrometer for a landing spacecraft. *Measurement Science and Technology* 5 : 1033.

Meyerhof, G. G. 1963. Some recent research on the bearing capacity of foundations. *Canadian Geotechnical Journal* 1 (1): 16-26.

Mitchell, JK, LG Bromwell, WD Carrier III, NC Costes, and RF Scott. 1971. Soil mechanics experiment, apollo 15 preliminary science report. *NASA Spec.Publ.SP-272*: 87-108.

Mitchell, JK, WN Houston, WD Carrier III, and NC Costes. 1974. Apollo soil mechanics experiment S-200. final report, NASA contract NAS 9-11266, space sciences laboratory series 15, issue 7. *Univ.of California, Berkeley*.

Moore, H. J., R. E. Hutton, R. F. Scott, C. R. Spitzer, and R. W. Shorthill. 1977. Surface materials of the viking landing sites. *Journal of Geophysical Research* 82 (28): 4497-523.

Perko, H. A., J. D. Nelson, and J. R. Green. 2006. Mars soil mechanical properties and suitability of mars soil simulants. *Journal of Aerospace Engineering* 19 : 169.

Puech, A., and P. Foray. 2002. Refined model for interpreting shallow penetration CPTs in sands. Paper presented at Offshore Technology Conference.

Robertson, P. K., J. J. M. Powell, and J. J. M. Powell. 1997. *Cone penetration testing in geotechnical practice*Taylor & Francis Group.

Scott, RF, and FI Roberson. 1969. Soil mechanics surface sampler. *Journal of Geophysical Research* 74 (25): 6175-214.

Team, R. 1997. Characterization of the Martian surface deposits by the mars pathfinder rover, sojourner. *Science* 278 (5344): 1765-8.

Terzaghi, K. 1943. Theoretical soil mechanics.

Vesic, AB. 1963. Bearing capacity of deep foundations in sand. *Highway Research Record*.

Zarnecki, J. C., M. R. Leese, B. Hathi, A. J. Ball, A. Hagermann, M. C. Towner, R. D. Lorenz, J. A. M. McDonnell, S. F. Green, and M. R. Patel. 2005. A soft solid surface on titan as revealed by the huygens surface science package. *Nature* 438 (7069): 792-5.

CHAPTER 4: APPLICATION OF PLANETARY ANALOG MECHANICAL PROPERTIES TO SUBSURFACE GEOLOGICAL INVESTIGATIONS

4.1. Introduction

Determination of the mechanical and physical properties of planetary analogs is of high importance for scientists and missions designers. Scientists use these parameters to understand the formation and evolution of planetary surfaces, layering and geomorphological features while mission designers decide landing sites and target areas. Most soil mechanical properties are interrelated, so the knowledge of one parameter can lead to estimating the others: level of compaction, consolidation and others useful information can be determined from mechanical parameters such as density, porosity, void ratio which are thus indicative of the physical and chemical properties of the surface and subsurface. Therefore, Studying the mechanical properties of planetary analog materials will improve future mission success and will enhance landing site selection, rover landing and its trafficability; and the feasibility for accessing the subsurface using drills and penetrometers.

Mars soil mechanical properties also affect geomorphological processes such as gullies and crater formation, erosion (Schultz, 2002; Sullivan et al., 2011) landslides and lithology of the subsurface layers (Lucas and Mangeney, 2007; Perko et al., 2006). Regolith mechanical properties are important because they control the stability of water ice (and other potential volatiles like CO_2) in the Martian subsurface. Indeed, significant deposits of water ice have been recently observed in the shallow subsurface of regions where they are thermodynamically unstable (Bandfield, 2007; Byrne et al., 2009). This is due to slow diffusion of water vapor through the regolith, which acts like a kinetic barrier (Schorghofer and Aharonson, 2005;

Schorghofer, 2007). However, the diffusion coefficient of water vapor through a regolith layer is mainly dependent on porosity and tortuosity, both parameters being strongly affected by compaction (Bryson et al., 2008; Chevrier et al., 2007; Chevrier et al., 2008; Hudson et al., 2007). Therefore, understanding the mechanical properties of regolith analogs can indirectly help models of water ice stability, by providing additional constraints on the diffusive properties of the soil.

Successful investigations of the subsurface using penetrometers have been used on the Moon and will be used for future Mars missions. The success of Apollo Simple Penetrometer (ASP), the Self-Recording Penetrometer (SRP) and the drill activities on the Moon in conducting core samples and interpretation of its data are based on a detailed investigation of the mechanical properties of the Moon soil simulant (Rowe and Selig, 1962; Mitchell, 1964; Christensen et al., 1967). Changes in the penetration forces have been used as indicators for the inhomogeneities of the subsurface profile (Roscoe, 1970; Costes et al., 1970; Houston and Namiq, 1971), which in turn give information on the nature of the regolith.

The downward movement of the penetrometer through regolith is opposed by two reaction forces: the base or cone resistance, which pushes against the cone and sleeve friction, which acts up on the lateral side of the penetrometer (Vesic, 1963). Penetration into regolith materials is dependant on the effective unit weight of the regolith, bearing capacity, depth of penetration and angle of internal friction. Angles of internal friction have been estimated from different missions and using different techniques, such as trench analysis through dumping the regolith and calculating the angle of repose or using the rover wheels as a shear device (Viking landers (Shorthill et al., 1976, Moore et al., 1977, Moore and Clow, 1982), Mars Exploration Rovers (Sullivan et al., 2011), Phoenix lander (Arvidson et al., 2009, Bonitz et al., 2008, Shaw et al.,

2009) and Mars Pathfinder (Rover team et al., 1997, Moore et al., 1999)). These estimates enhanced our knowledge of the regolith geological context but the measurements techniques are not relevant for friction angle since the angle of repose describe the uncompacted condition of the regolith and not the compacted state which is often the case with natural regolith. Therefore, laboratory measurements are necessary to understand how compaction affects the friction angle.

Previous experiments on sand (Terzaghi, 1943; Hansen, 1970) showed good agreement between the measured penetration forces and theoretical calculations (ElShafie et al., 2010); however, no agreement was observed when we used Martian analogs. This discrepancy is due to the bearing capacity factor which is a function of the angle of internal friction and probably depends on nature of the regolith analog. Perko et al., 2006 conducted some mechanical measurements for different regolith analogs for the purpose of geomorphological modeling. Unfortunately, for the measurements of the angle of internal friction for JSC Mars-1, only two data points were presented which are not sufficient to build a complete relationship between the penetration force, the bearing capacity factor and the angle of internal friction.

Therefore, the main objective of this paper is to measure the mechanical properties of planetary analogs (palagonite JSC Mars-1, an unaltered basaltic soil from Mojave desert and a composite analogue JSC Mars-2), and determine the effect of the angle of internal friction on the bearing capacity factor. This will help us build a theoretical framework from which important mechanical properties can be determined by in situ penetration measurements on future missions. We chose JSC Mars-1, JSC Mars-2 simulate and Mojave soil because they simulate several properties of the Martian regolith (porosity, density and particle size distribution, Evans and Adams, 1979; Allen et al., 1998; Yen et al., 2005; Peters et al., 2008).

4.2. Experimental Apparatus

A specific apparatus was designed and built to measure the penetration forces in unconsolidated materials. A complete description of the penetration test rig and its automated control system can be found in (ElShafie et al., 2010). A general illustration of the setup is shown in Figure 4.1. An automated control system was designed where the whole penetration experiment can be monitored and controlled through a personal computer. Two parameters are being monitored during penetration testing: the penetration force and penetration depth. The results of the penetration experiment are automatically saved in an Excel file.

4.3. Martian regolith analogues

In order to better design and test future instrumentation that are going to be used on future missions to Mars or any other planetary body, regolith simulants that adequately represent various dust, soil and rock properties that exist on these bodies are required. JSC Mars-1 is a common palagonitie soil (Allen et al., 1998), previously used in various studies. Mojave Mars simulant (MMS) is a basaltic sand (Peters et al., 2008) which contrary to JSC Mars-1, is not altered. JSC Mars-2, is a synthetic simulant composed of 45% basalt, 45% montmorillonnite, and 10% hematite (Famale et al., 1982). These basaltic in nature regolith materials proved to be good spectral and mineralogical analogs for Mars (Evans and Adams, 1979; Singer, 1982; Morris et al., 2000; Goetz et al., 2005; Yen et al., 2005; Morris et al., 2006a, 2006b; Peters et al., 2008) and therefore, were chosen for this research.

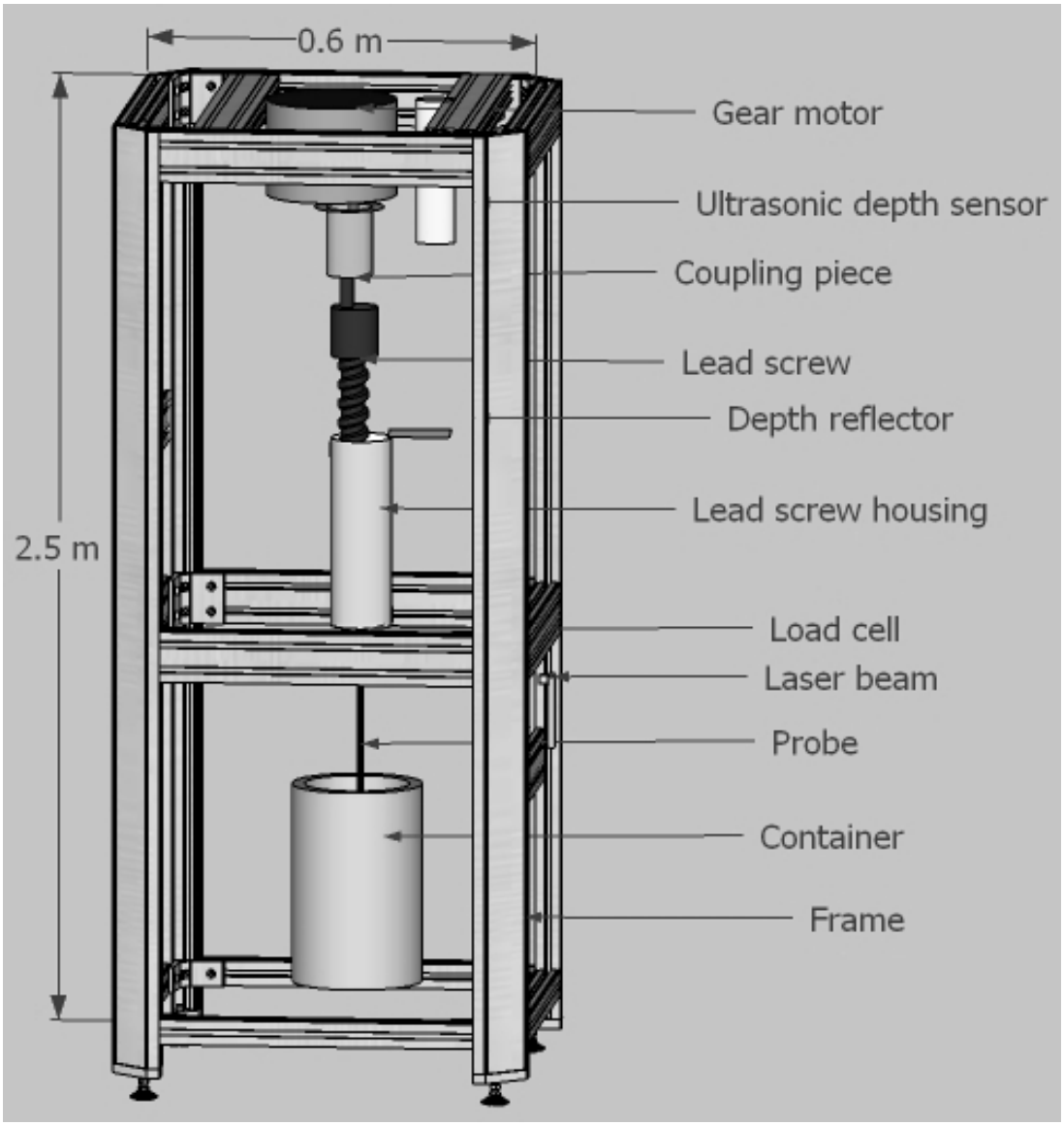

Figure 4.1. The penetration testing apparatus.

4.4. Experimental Results

Penetration forces are a strong function of the bulk density of regolith materials (Lune et al., 1997; ElShafie et al., 2010). Penetration testing was performed in the three different analogs and for various bulk densities. However, JSC Mars-2 appeared to be almost impossible to compact and therefore, we could not determine any of its mechanical properties (friction angle) except the penetration force as a function of depth at bulk density of 1180 kg m^{-3} using 1.2 cm diameter probe for reference (Fig. 4.2). At this density (1180 kg m^{-3}), a force about 140 N was required to penetrate down to 20 cm while it took about 250 N to reach to the same depth at density of 1700 kg m^{-3} in sand (ElShafie et al., 2010).

Four different compaction levels were prepared to achieve a bulk density of 1120, 1167, 1184 and 1241 kg m^{-3} in JSC Mars-1 and 1330, 1365, 1474 and 1504 kg m^{-3} in Mojave soil. Penetration testing was carried out at the assigned bulk densities for both analogs. For Mojave soil, the penetration force was observed to increase with bulk density. At about 12 cm depth, the penetration forces were 40, 65, 150 and 225 N for bulk densities of 1330, 1365, 1474 and 1504 kg m^{-3}, respectively (Fig. 4. 3). At 12 cm depth in JSC Mars-1, the penetration forces were 50, 300, 600 and 900 N for bulk densities of 1120, 1167, 1184 and 1241 kg m^{-3}, respectively (Fig. 4.4).

4.5. Determination of the bearing capacity factor N_q

The bearing capacity factor N_q was determined from penetration forces in Martian analog regolith materials. A cylindrical container was filled with the desired regolith material and the bulk density was measured. Insertion and removals of a 1.2 cm diameter probe was conducted at a constant penetration speed of 2 mm s^{-1}. The regolith material was removed from the container

and re-poured in for two more penetration test at the same bulk density by weighting specific mass and achieving the desired heigh. The average force versus depth of the three penetration tests was determined and N_q factor was then calculated at each data point. The average N_q factor was determined and implemented in a MatLab code to determine the average theoretical force versus depth profile based on the knowledge of the regolith mechanical properties (bulk density, porosity, void ratio and friction angle). Symbols used through out the paper and their corresponding definition are shown in Table 4.1.

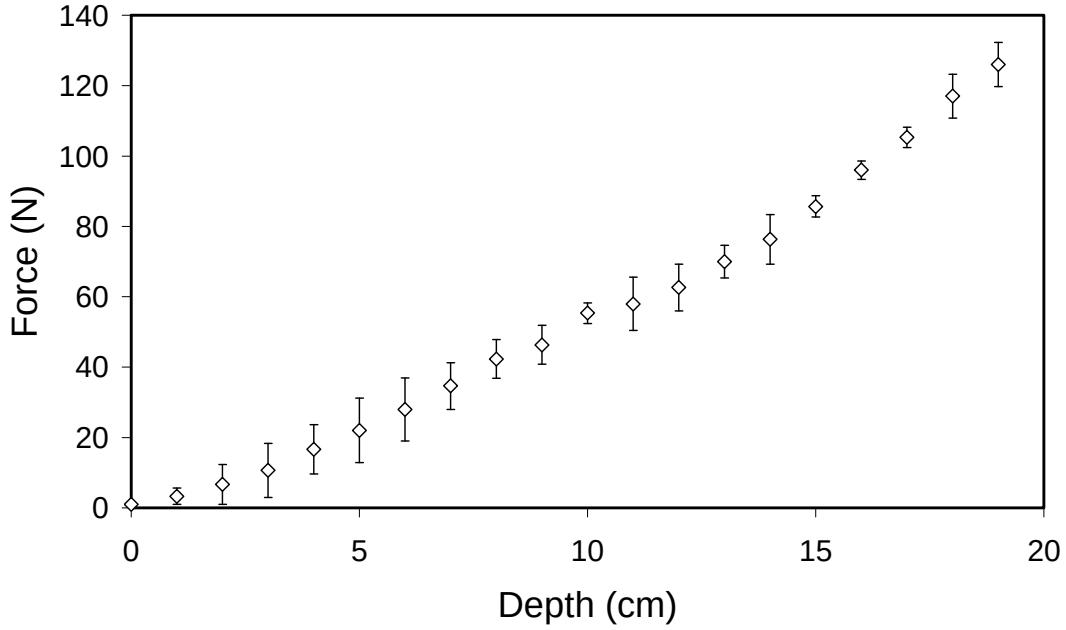

Figure 4.2. Penetration force as a function of depth in JSC Mars-2 (B.D = 1180 kg m^{-3}, D = 1.2 cm).

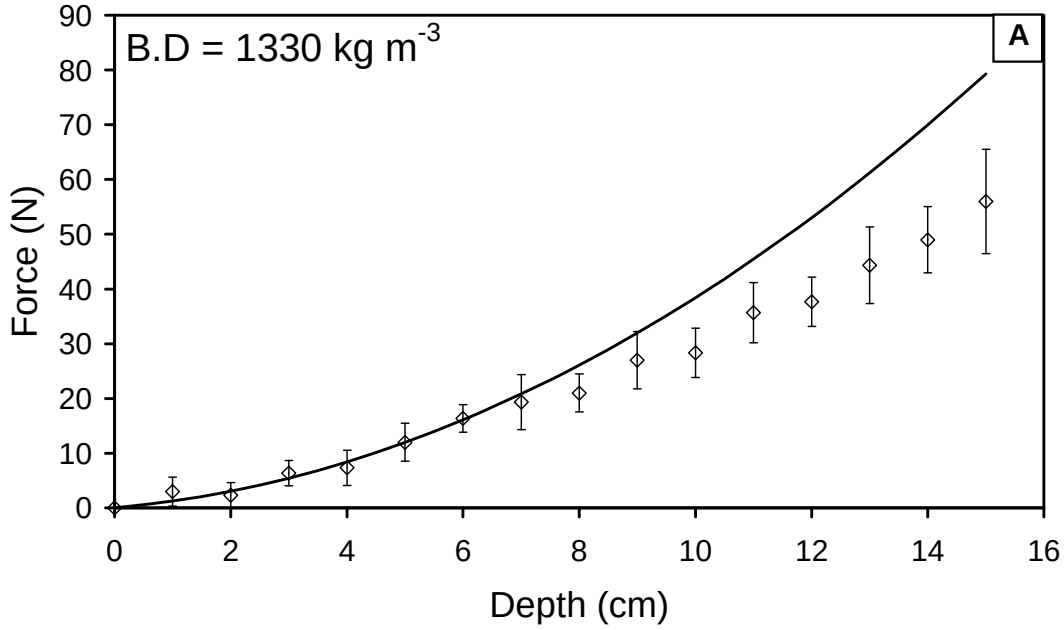
B.D = 1330 kg m-3
A
Force (N)
Depth (cm)
0
10
20
30
40
50
60
70
80
90
0
2
4
6
8
10
12
14
16

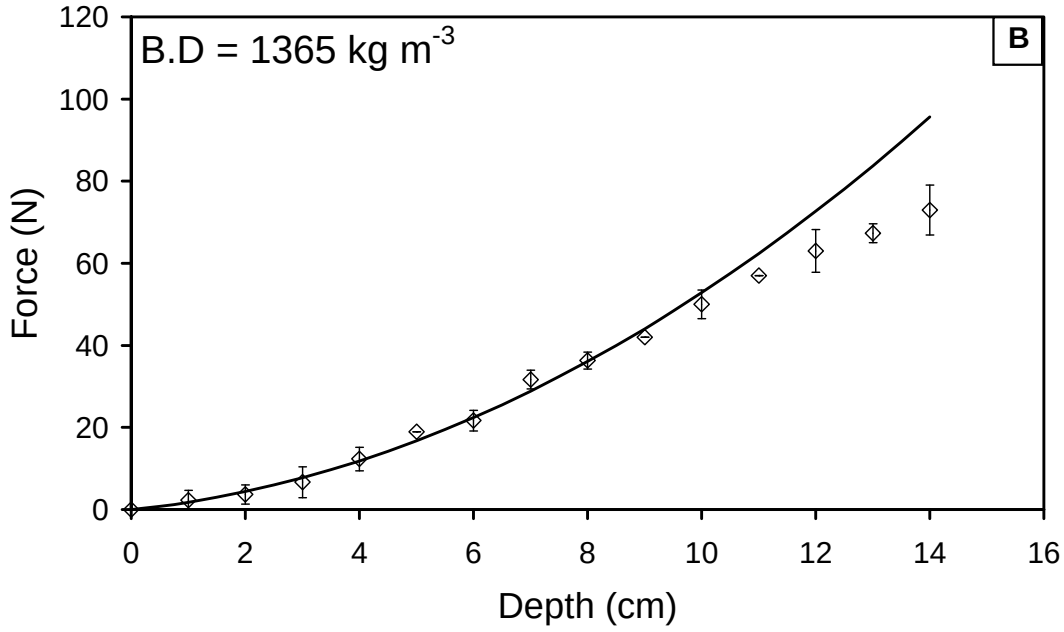
B.D = 1365 kg m-3
B
Force (N)
Depth (cm)
0
20
40
60
80
100
120
0
2
4
6
8
10
12
14
16

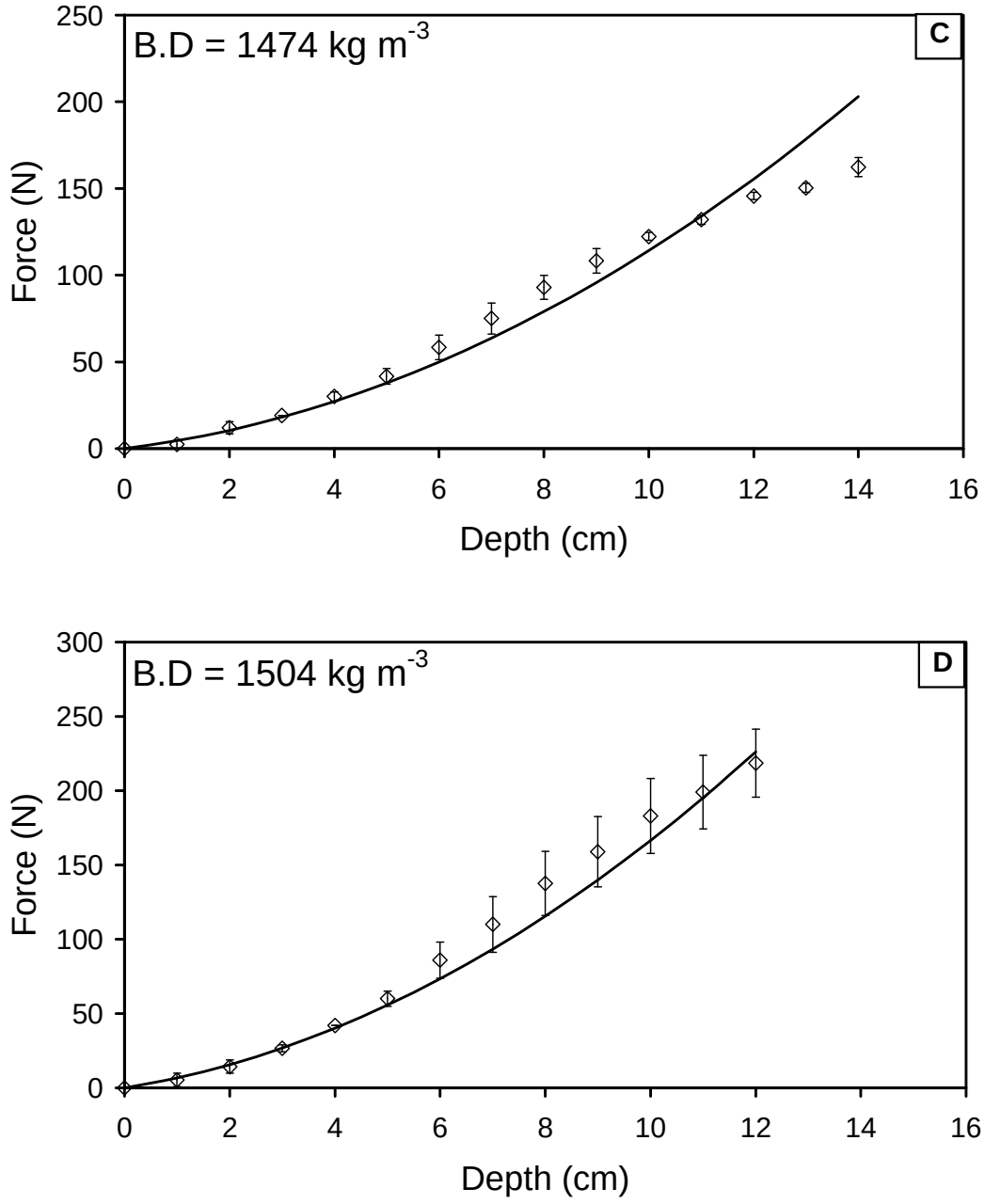

Figure 4.3. Experimental and theoretical forces versus depth under different bulk densities for Mojave soil.

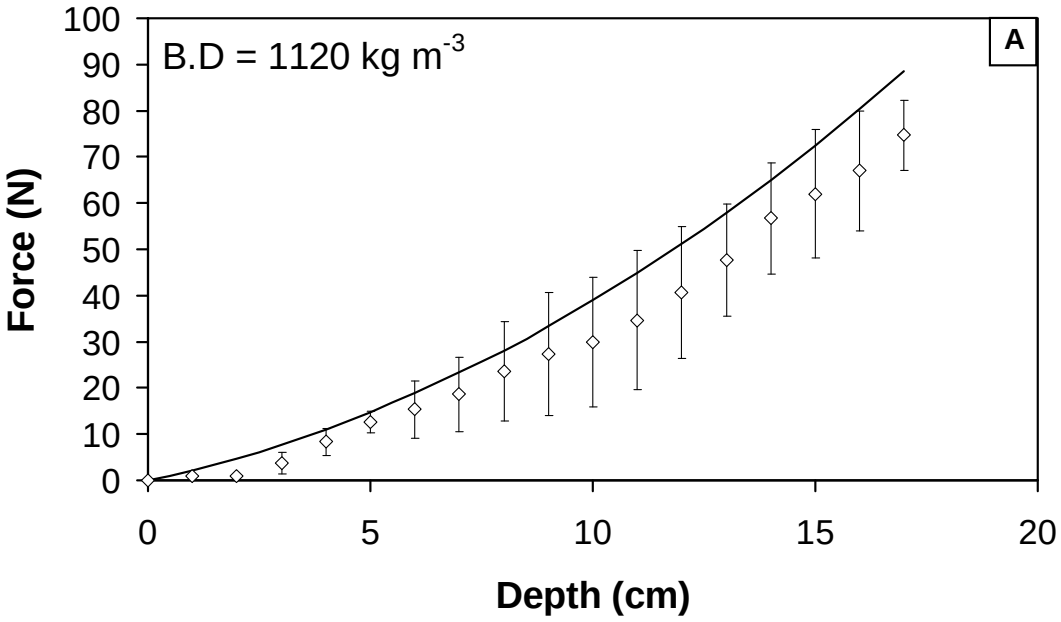
A
B.D = 1120 kg m-3
Force (N)
Depth (cm)
0
10
20
30
40
50
60
70
80
90
100
0
5
10
15
20

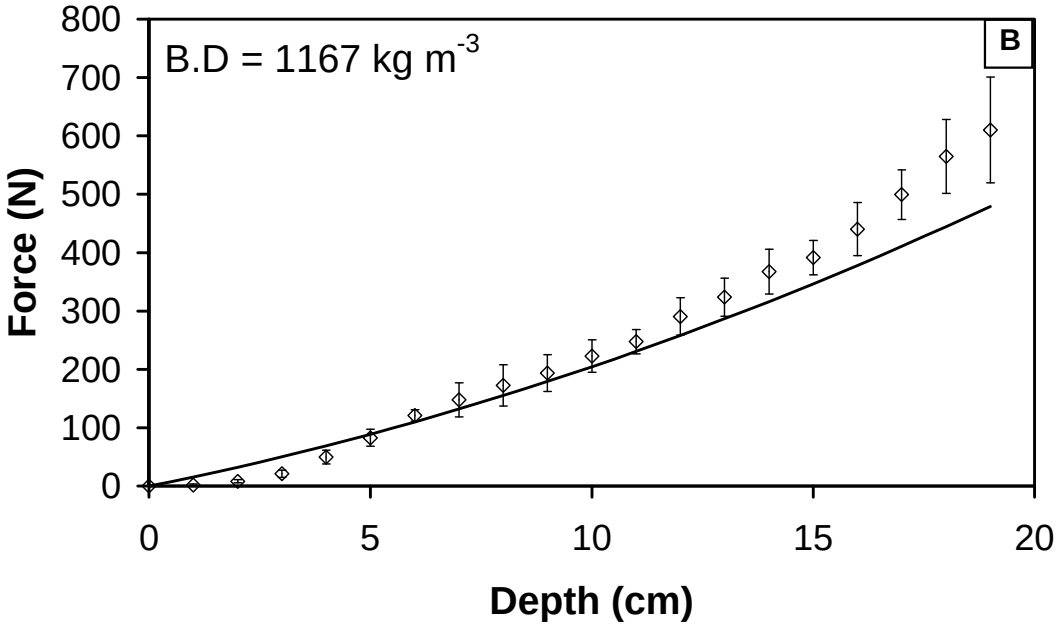
B
B.D = 1167 kg m-3
Force (N)
Depth (cm)
0
100
200
300
400
500
600
700
800
0
5
10
15
20

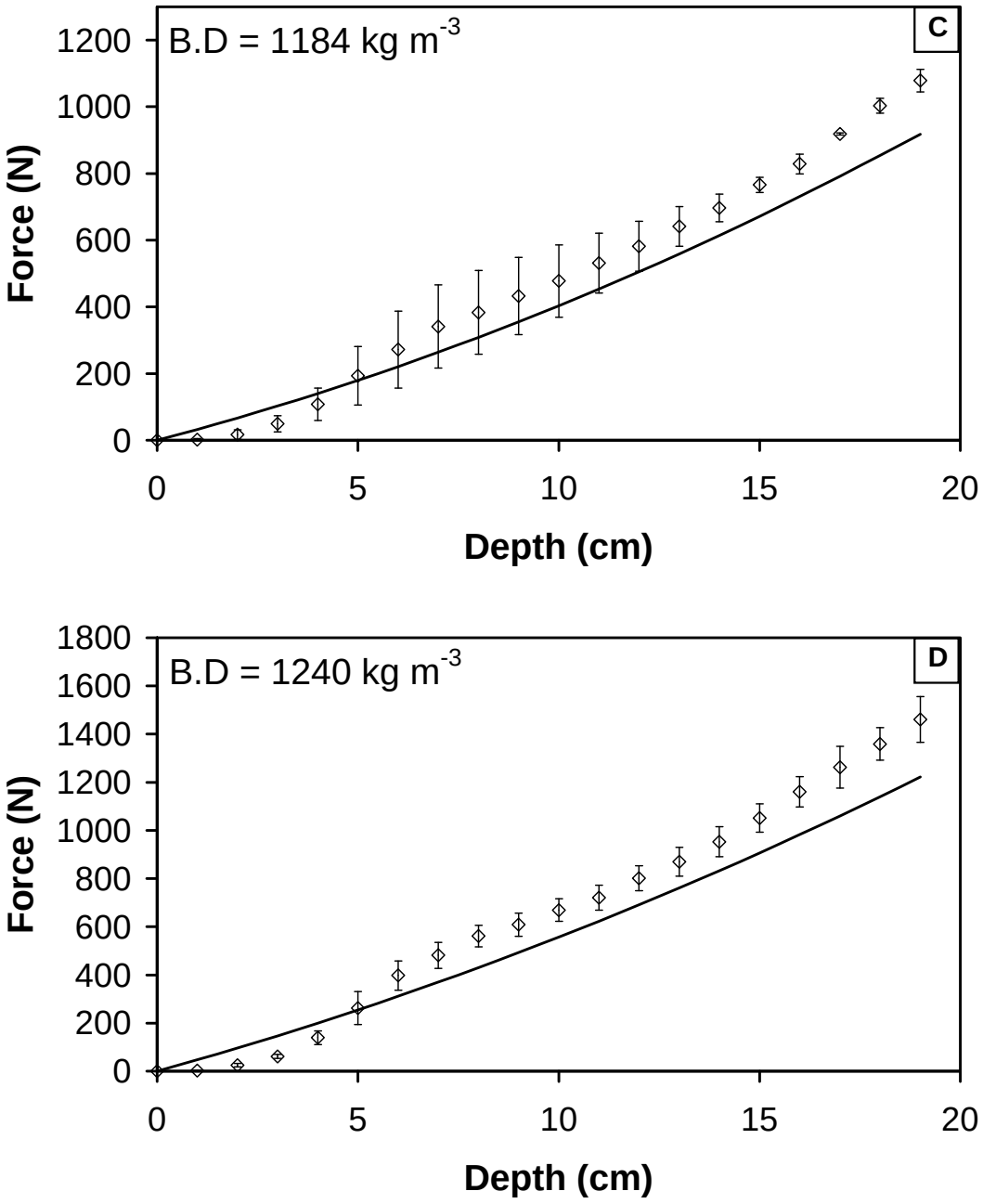

Figure 4.4. Experimental and theoretical forces versus depth under different bulk densities for JSC Mars-1.

Table 4.1. List of symbols used in the paper.

Symbol	Def.
A_c	Area of the cone (m^2)
A_s	Area of the sleeve (m^2)
B	Cone diameter (m)
D	Probe diameter (cm)
D_r	Relative density (dimensionless)
e	Void ratio (dimensionless)
e_{max}	Maximum possible void ratio (loosest condition)
e_{min}	Minimum void ratio (densest condition)
f_s	Sleeve friction ($N\ m^{-2}$)
F_T	Total resistance force (N)
K	Coefficient of lateral pressure at rest (dimensionless)
K_p	Passive coefficient of lateral stress (dimensionless)
L	Lateral extension of the slip lines (m)
N_q	Bearing capacity factor (dimensionless)
q_c	Cone resistance ($N\ m^{-2}$)
V_s	Volume of solid particles (m^3)
V_T	Total volume (m^3)
V_v	Volume of voids(m^3)
Z	Penetration depth (m)
γ	Effective unit weight ($N\ m^{-3}$)
φ	Friction angle (degree)

4.6. Discussion

The bearing capacity theory has been used to explain the downward movement of penetrometers through regolith materials (Terzaghi, 1943; Hansen, 1970). The total penetration force (F_T) during probe insertion into the subsurface is the sum of two forces; the cone resistance (q_c) and the sleeve friction (f_s):

$$\boldsymbol{F_T = q_C A_C + f_S A_S} \quad (1)$$

Where A_c is the area of the cone, A_s is the buried area of the sleeve. The bearing capacity factor N_q can be calculated from (Puech and Foray, 2002):

$$N_q = \frac{q_c}{\gamma \times Z \times \left(1 + \left(K \times \sin\varphi \times \frac{Z}{L}\right)\right)} \quad (2)$$

Where γ is the effective unit weight of the regolith (N m^{-3}), Z is the penetration depth (m), K is the coefficient of lateral pressure at rest (dimensionless), φ is the friction angle (degree) which is function of the relative density (Dr) and L is the lateral extension of the slip lines (m). The coefficient of lateral pressure is defined as (Harr, 1977)

$$K = 1 - \sin\varphi \quad (3)$$

The lateral extension of the slip lines L is defined as (Puech and Foray, 2002):

$$L = B \times \exp\left(\tfrac{\pi}{2} \times \tan\varphi\right) \times \tan\left(\frac{\pi}{4} + \frac{\varphi}{2}\right) \quad (4)$$

Where B is the cone diameter (m). The relative density (Dr) is an index that quantifies the degree of compaction (packing between loosest and densest state) of coarse-grained soils (Lunne et al., 1997):

$$D_r = \frac{e_{\max} - e}{e_{\max} - e_{\min}} \quad (5)$$

Where e is the void ratio of the sample. e_{max} is the maximum possible void ratio (loosest condition) and e_{min} is the minimum void ratio (densest condition) of the sand (Lunne et al., 1997). The void ratio is the ratio between the volume of void (V_V) and the volume of solid (V_s):

$$e = \frac{V_v}{V_s} \tag{6}$$

From the knowledge of particle density, the volume of solid particles can be calculated from:

$$V_s = \frac{m_s}{\rho_s} \tag{7}$$

Where V_s is the volume of solid particles (m^3), m_s is the mass of sand (kg) and ρ_s is the particle density ($kg.m^{-3}$). The particle density (ρ_s) is determined using the specific gravity measurements. Most of the previous bearing capacity investigations were carried out on sand, because of its extensive Earth's applications (Terzaghi, 1943 and Vesic, 1963). Using the current tabulated bearing capacity values to predict the forces of penetration in Martian analogs, under friction angle of 44 and 45°, the bearing capacity factor N_q is (173.3 and 115.3) respectively (Terzaghi, 1943 and Vesic, 1963). The predicted penetration forces at 20 cm deep in JSC Mars-1 (1120 kg m^{-3}) are (113 and 70 N), respectively, compared to a measured value of 1400 N. Therefore, calculated penetration forces using the current bearing capacity factors based on sand friction angles for JSC Mars-1 and Mojave do not show good agreement with the measured experimental values. Therefore, determination of the bearing capacity factor N_q, friction angle, specific gravity and void ratios for JSC Mars-1 and Mojave was essential for correct prediction of penetration forces.

4.7. Friction angle measurements

Direct shear tests were performed on JSC Mars-1 and Mojave soil in order to determine the angle of internal friction (using the standard method ASTM D-3080). For sample preparation, the mass and volume of each prepared sample was measured and soil density was determined. The regolith sample was placed in a shear box which has two movable parts. The contact between the top and lower parts of the shear box is approximately the height of the sample. A confining stress is applied vertically on the top part of the box and the lower part of the shear box is pulled laterally until the regolith sample fails. The applied load and strain induced is recorded at specific intervals to determine the stress-strain curve at specific confining stress. The procedure was repeated three times for each applied stress under the same density. From the slope of shear stress-stress curve, the angle of internal friction (φ) of the soil samples was determined by a best fit linear regression (Fig 4.5, 4.6). The angle of internal friction of the studied regolith analogs is found to increase with increasing relative density. For the Mojave soil (Fig. 4.7 A), the angle of friction varied from 32 to 41.3° for bulk density between 1300 and 1500 kg m^{-3} and from 39.4 to 54.7° for bulk density between 900 and 1120 kg m^{-3} for JSC Mars-1(Fig. 4.7 B).

4.8. Specific gravity, maximum and minimum void ratios measurements

Specific gravity (G_s) measurements for JSC Mars-1 and Mojave soil were measured according to the standard method ASTM D854 – 02. A weighted amount of regolith was poured into a pycnometer (a bottle which can be precisely filled to a specific volume). A specified amount of water was added to the regolith and then shaked. The mass of the pycnometer, water and regolith was then determined. Air filling the voids was extracted with a pump for about 20

minutes. The final mass of the pycnometer, water and regolith after air extraction was determined and the specific gravity was calculated (equation 8).

$$G_s = \frac{w_0}{w_0 + (w_a - w_b)} \tag{8}$$

Where W_0 is the mass of dry regolith, W_a is the mass of bottle filled with water to a specific volume and W_b the total mass (water + regolith + pycnometer). Specific gravity of Mojave soil and JSC Mars-1 was found to be 2.47 and 2.69 , respectively (Table 4.2).

The void ratio is defined as the ratio between the volume of voids and the volume of solid particles in porous materials. The maximum and minimum void ratios are values for materials in their loosest and densest state. Based on the knowledge of specific gravities of JSC Mars-1 and Mojave soil, a weighted amount of regolith was poured into a stud with a known volume using a funnel in order to be sure that the material is in its loosest state. The volume of solids was determined and the maximum void ratio (e_{max}) was calculated. For Mojave soil and JSC Mars-1 e_{max} was found to be 1.54 and 1.78 at bulk densities of 1059 and 887 kg m^{-3}, respectively. For the minimum void ratio (e_{min}) measurements, the regolith samples were prepared into five layers. After loading each layer into a mould, compaction was achieved by applying several blows from a standard weighted hammer at a specified height using a modified proctor (43.2 cm height with 25 blows/layer, ASTM D1557). The volume of solids was then determined and the minimum void ratio calculated. For Mojave soil and JSC Mars-1, e_{min} was found to be 0.562 and 0.863 at bulk densities of 1720 and 1325 kg m^{-3}, respectively (Table 4.2).

After determination of the angle of internal friction, specific gravity and void ratios for JSC Mars-1 and Mojave, we implemented all of these input parameters into a MatLab code and loaded our penetration forces data for both analogs in order to determine the bearing capacity

factor N_q (equation 2). We determined the bearing capacity factor N_q and it was used to determine the theoretical force of penetration (Fig 4.3 and 4.4).

We observed a positive correlation between the bearing capacity factor N_q and the angle of internal friction for Mojave soil and JSC Mars-1 (Fig. 4.8). The bearing capacity factor (N_q) showed an exponential dependency with the angle of internal friction for Mojave soil, N_q increased from 64 to 338 with increasing φ from 32 to 41.3° respectively. For JSC Mars-1, we fitted the results using an exponential and linear fit. Exponential fit was used since nearly all the previous tested soils on Earth showed an exponential trend and friction angles does not exceed 50°. However, JSC Mars-1 showed higher friction angles where N_q increased from 161 to 3347 with increasing φ from 39.4 to 54.7° respectively for JSC Mars-1 and we found that a linear fit suited the results with R^2 of 0.95 (Fig. 4.8).

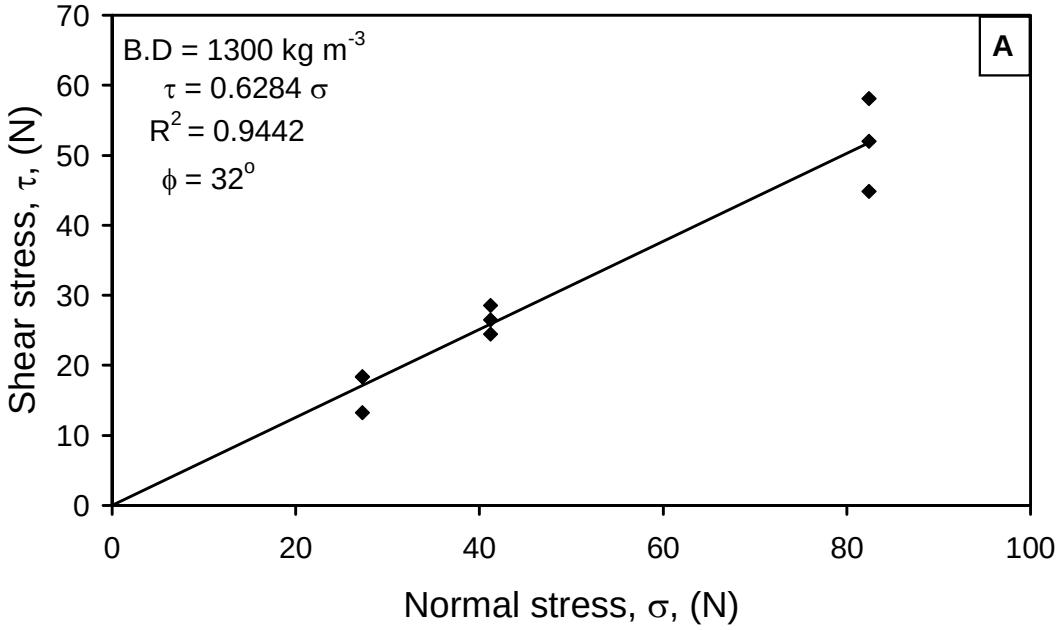
B.D = 1300 kg m-3
τ = 0.6284 σ
R2 = 0.9442
ϕ = 32o
A
Shear stress, τ, (N)
Normal stress, σ, (N)
0
10
20
30
40
50
60
70
0
20
40
60
80
100

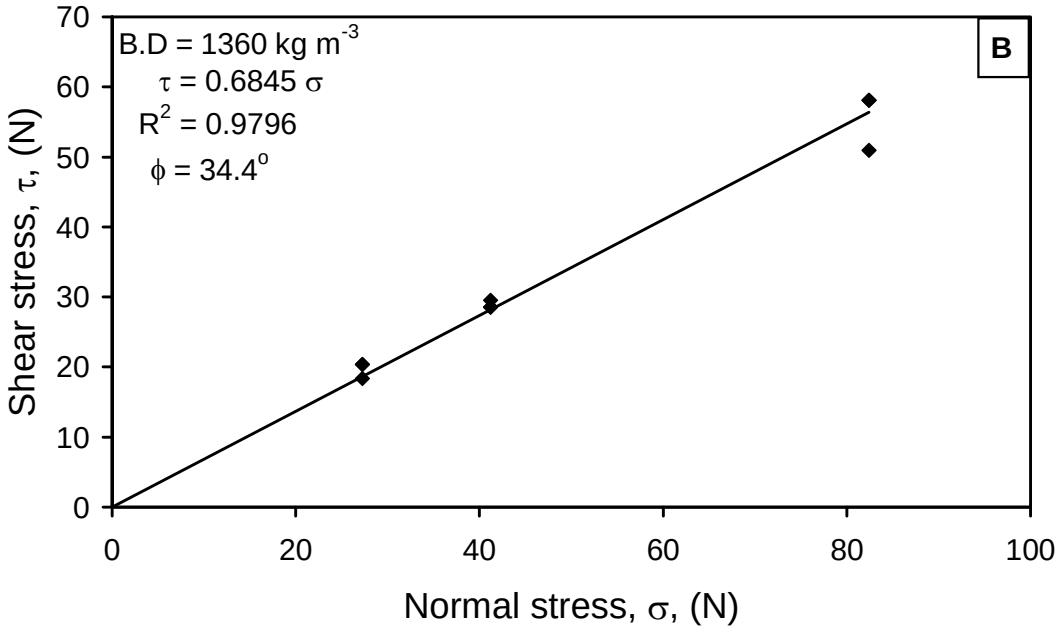
B.D = 1360 kg m-3
τ = 0.6845 σ
R2 = 0.9796
ϕ = 34.4o
B
Shear stress, τ, (N)
Normal stress, σ, (N)
0
10
20
30
40
50
60
70
0
20
40
60
80
100

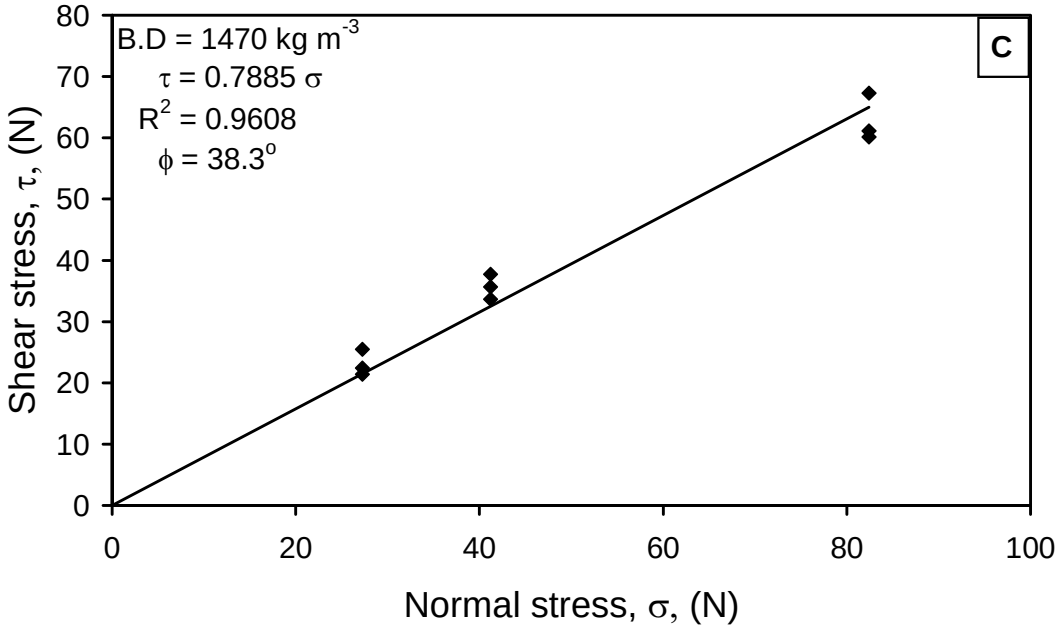

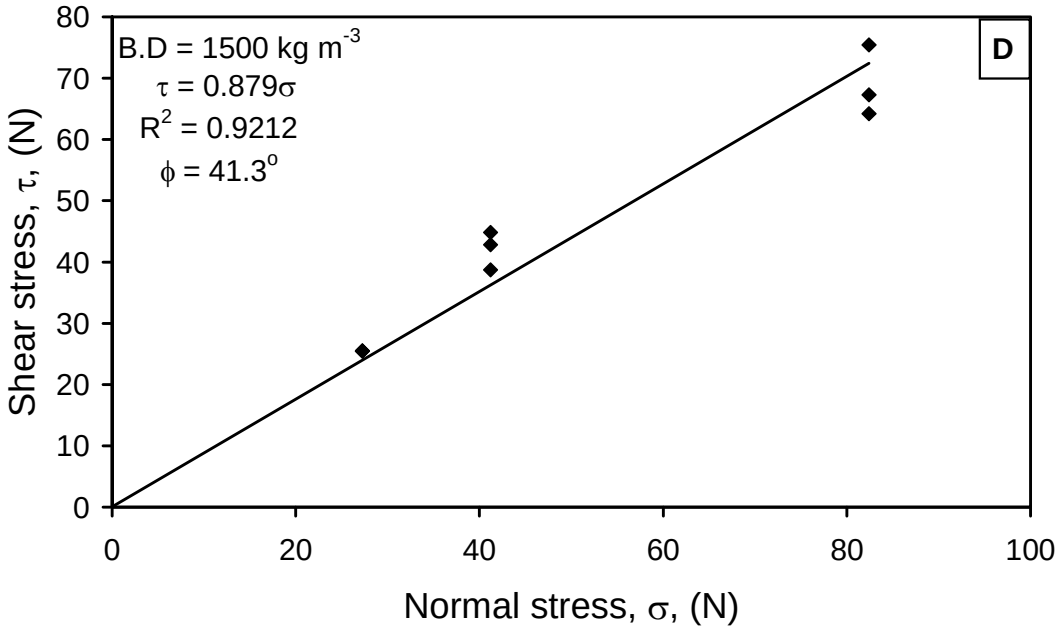

Figure 4.5. Shear stress versus normal stress under different bulk densities for Mojave soil (A to D).

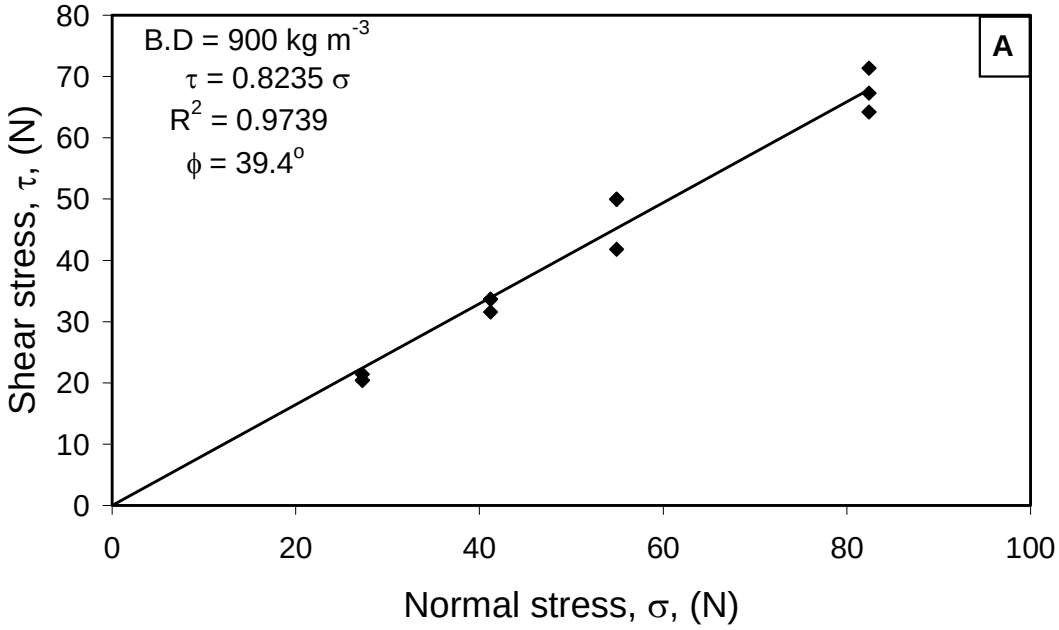
B.D = 900 kg m-3
τ = 0.8235 σ
R2 = 0.9739
ϕ = 39.4o
A
Shear stress, τ, (N)
Normal stress, σ, (N)
0
10
20
30
40
50
60
70
80
0
20
40
60
80
100

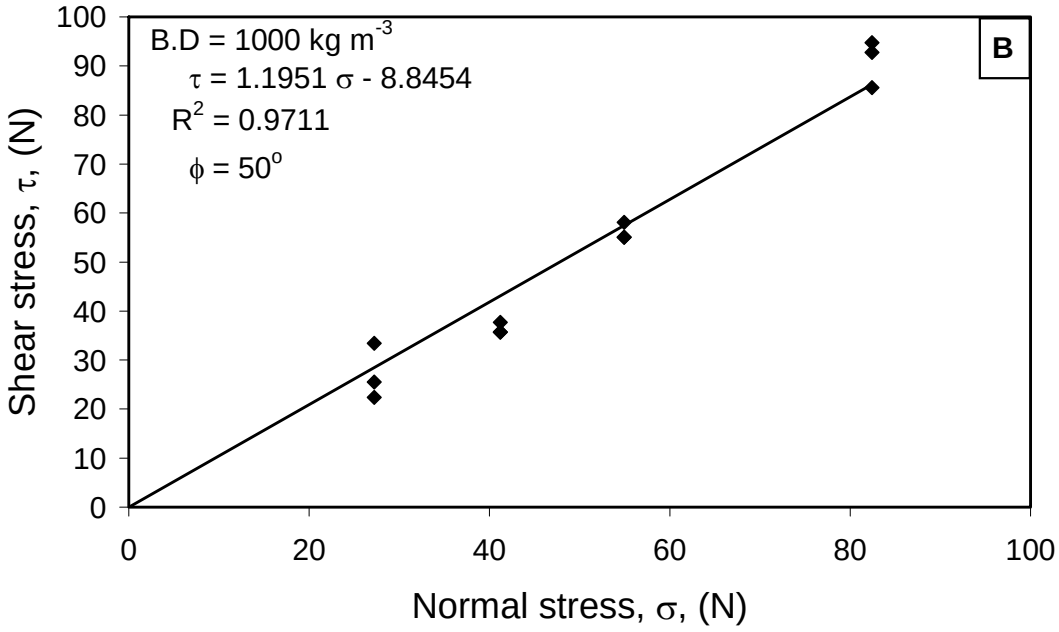
B.D = 1000 kg m-3
τ = 1.1951 σ - 8.8454
R2 = 0.9711
ϕ = 50o
B
Shear stress, τ, (N)
Normal stress, σ, (N)
0
10
20
30
40
50
60
70
80
90
100
0
20
40
60
80
100

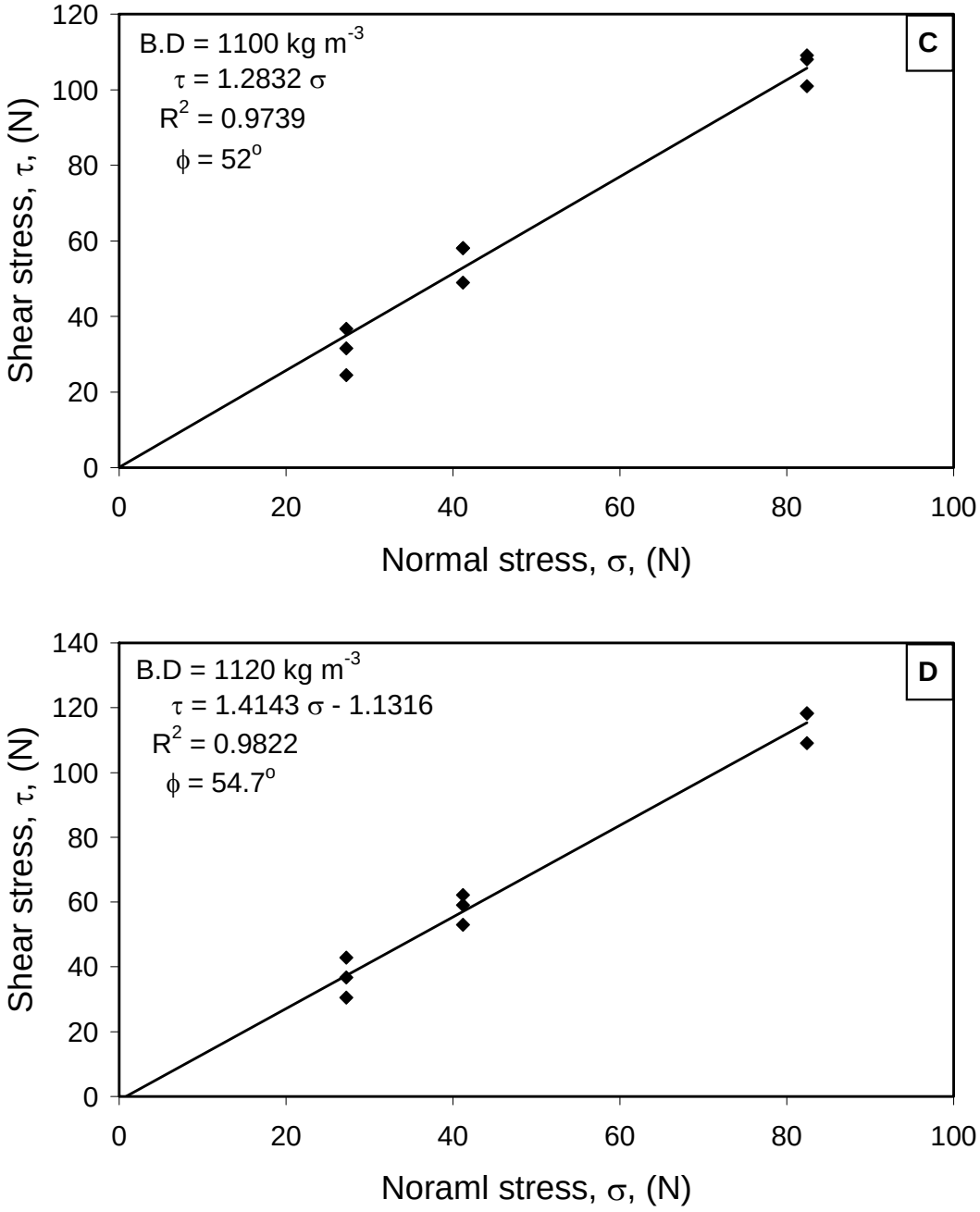

Figure 4.6. Shear stress versus normal stress under different bulk densities for JSC Mars-1 (A to D).

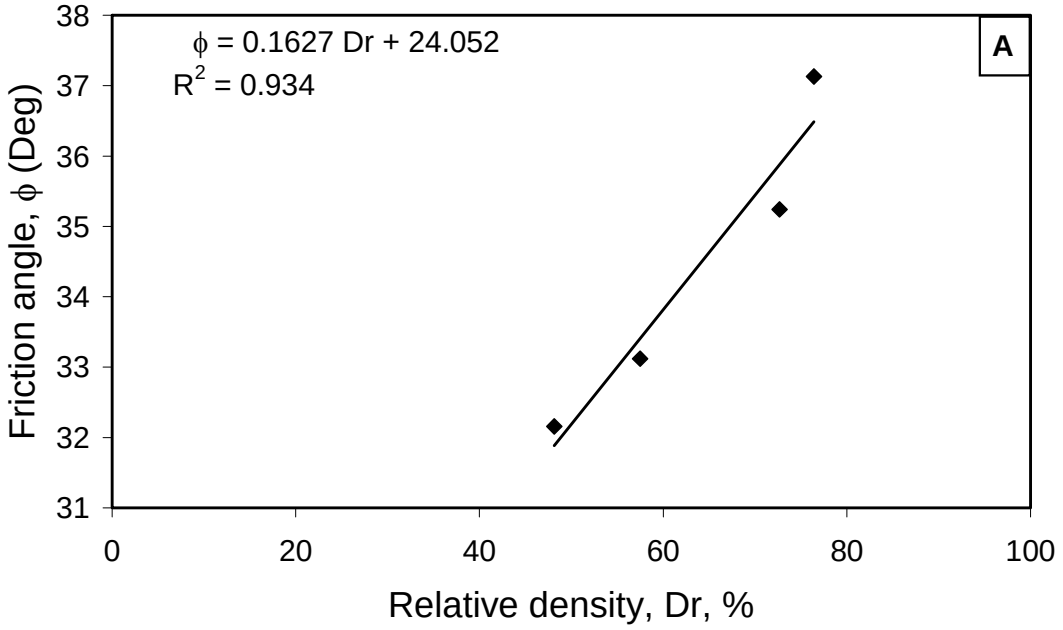

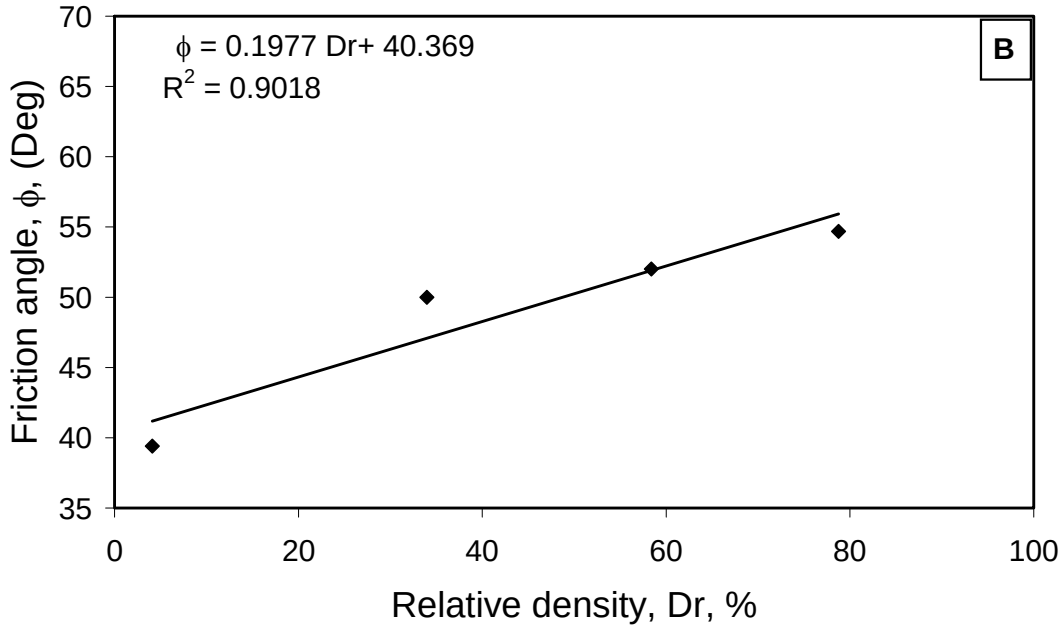

Figure 4.7. The angle of internal friction as a function of relative density for Mojave soil (A) and JSC Mars-1 (B).

Table 4.2. Specific gravity, maximum and minimum void ratios values for JSC Mars-1 and Mojave soil.

Type of regolith	G_s	e_{max}	e_{min}
JSC Mars-1	2.47	1.78, $\rho = 887$ kg m^{-3}	0.863, $\rho = 1325$ kg m^{-3}
Mojave soil	2.69	1.54, $\rho = 1059$ kg m^{-3}	0.562, $\rho = 1720$ kg m^{-3}

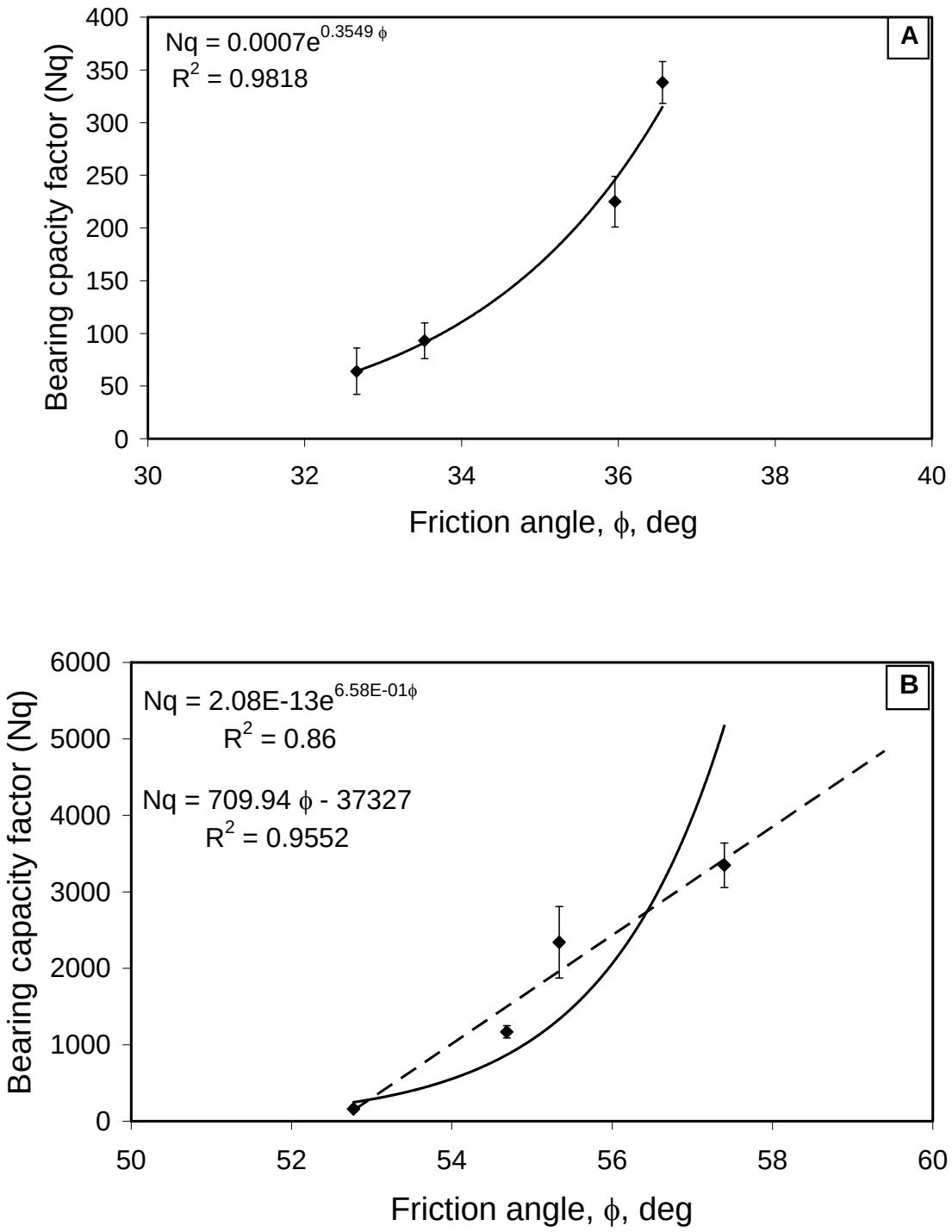

Figure 4.8. Bearing capacity factor N_q versus angle of internal friction for Mojave soil (A) and JSC Mars-1 (B).

The variations in the friction angle, void ratios and specific gravity between Mojave soil and JSC Mars-1 are due to the difference in the particle size distribution between both analogs. The particle size distribution of JSC Mars-1 was determined by sieving while the particle size distribution of Mojave soil was determined from (Peters et al., 2008) (Fig. 4.9). As shown in Figure 4.9, JSC Mars-1 and Mojave soil are in two different particle size categories. JSC Mars-1 contains 17% medium size particles (>0.5 mm) and 83% fine grained particles (<0.3 mm) which cover the range from 2 to 0.063 mm while Mojave soil dominates the range from 0.15 to < 0.001 mm. Due to the wide range in particle sizes and shape structure of JSC Mars-1 (resulting from alteration), small dust particles can fill in the voids when the regolith under compaction which leads to a higher friction angle than Mojave soil which explains the difference in friction angles, void ratios and specific gravities.

Due to the difference in the particle size distribution between JSC Mars-1, Mojave soil simulant and JSC Mars-2, variation in the penetration forces was noticeable. At the maximum achieved compaction of JSC Mars-1 (1240 kg m^{-3}), it required about 1000 N to reach to 15 cm depth and going from the lowest compacted to the most compacted state (1120 to 1240 kg m^{-3}), forces were from 60, 600, 800 and 1000 N. However, Mojave soil showed a different penetration resistance force category, from the lowest prepared sample density (1330 kg m^{-3}) to the maximum compaction (1504 kg m^{-3}) of Mojave soil, forces of penetration required were from 60, 80, 160 and 240 N. While, it required about 80 N to reach to the same depth in JSC Mars-2 at density of 1180 kg m^{-3}. Therefore, less force was required to penetrate in JSC Mars-2, Mojave soil and then JSC Mars-1. Based on this correlation, prediction force of the penetrated regolith can be indicative of its density and internal structure.

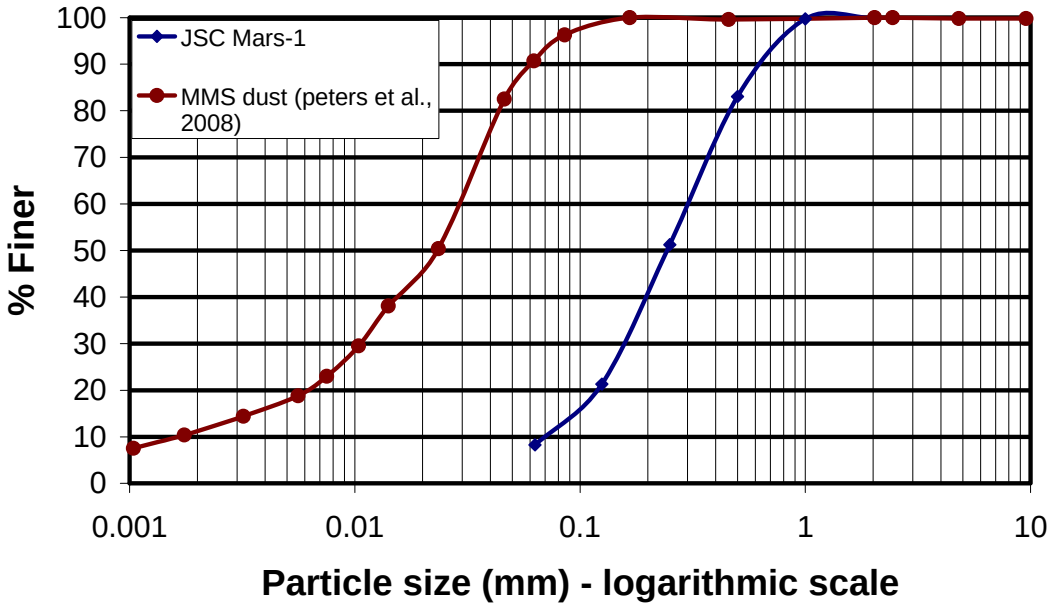

Figure 4.9. Particle size distribution for JSC Mars-1 and Mojave soil simulant (Peters et al., 2008).

4.9. Implications for Martian investigation

Using the Viking Landers surface sampler, drift and crusty to cloddy materials showed friction angles of 14° – 21° and 28° – 39° while, a friction angle of 27° – 33° was estimated for blocky materials based on trench analysis (Moore and Clow, 1982). Using the Sojourner wheels as a shear device on the Mars Pathfinder mission, friction angle of the Martian surface was estimated from the correlation of the electric current in the wheel motor during digging and trenching experiment. Drift and mixed materials showed low (28.2°) to moderate (34° – 38°) friction angles while cloddy materials showed higher values (33.3° – 42.4°) assuming the angle of internal friction is equal to the angle of repose (Rover team, 1997). The angle of internal friction was estimated by the Phoenix lander based on the assumption of the slope of dump piles equal to the angle of internal friction and was estimated to be 38° ± 5° (Shaw et al., 2009). The Mars Exploration Rovers Spirit and Opportunity investigated the mechanical properties of the Martian regolith using rover wheel trenches and wheel scuffs where an estimation of the friction angle ranged from 30° – 37° (Sullivan et al., 2011).

Our friction angle measurements of JSC Mars-1 and Mojave soil are high, 39.4 to 54.7° at bulk density of 900 to 1120 kg m^{-3} for JSC Mars-1 and 32 to 41.3° at bulk density of 1300 and 1500 kg m^{-3} for Mojave soil, compared to that estimated by previous missions (Table 4.3).

Indirect measurements of the friction angle (angle of repose) obtained from different missions are good based on the used tools and techniques, however, variation in the friction angle measurements between this research and estimates from other missions can be accounted for the non compacted state of the regolith measured technique (angle of repose, slope of dump piles) by these missions. This implies the uncertainty of the used techniques. Therefore, these

measurements can not be used for predicting the feasibility for in situ exploration of the subsurface or correlating to the variation in the subsurface density or porosity.

Based on the friction angle measurements and knowledge of the bearing capacity factor N_q, we can predict the penetration forces under Martian gravity. Figure 4.9 shows the penetration force as a function of depth under Martian gravity for JSC Mars-1 and Mojave soil at bulk densities of (B.D = 1330 and 1500 kg m^{-3} for Mojave, B.D = 1150 and 1240 kg m^{-3} for JSC Mars-1). To reach to about 20 cm depth under the Martian gravity, a force of 50 N and 170 N is required to penetrate in a Mojave type soil at a bulk density of 1330 and 1500 kg m^{-3} and, a force of about 100 N and 700 N is required on penetrate in JSC Mars-1 at bulk densities of 1150 and 1240 kg m^{-3}, respectively.

Regarding the penetration power, Spirit and Opportunity each can generate a peak of about 150 W of solar power. Over an average sol with fairly clean panels, they can produce about 600 W-hrs of power, which is equal to 2.2 MJ. MSL will produce 125 W continuously from its radio-isotropic thermal generator, giving up to 3000 W-hrs/sol or 10.8 MJ. The energy of penetration under Martian gravity is shown in Figure 4.10. Our measurements in Mojave soil and JSC Mars-1 (B.D = 1330 and 1500 kg m^{-3} for Mojave, B.D = 1150 and 1240 kg m^{-3} for JSC Mars-1) with probe diameter of 1.2 cm indicate a requirement of 3 to 14 J to achieve about 20 cm in Mojave soil and from about 5 to 55 J was required to reach to the same depth in JSC Mars-1. The peak rate of required power for probe insertion will be 0.34 W (170 N time's 0.002 m s^{-1}) for Mojave soil and only about 1.4 W (600 N time's 0.002 m s^{-1}) for JSC Mars-1.

Table 4.3. Friciton angle and bulk density at different Martian landing sites compared to this study.

Mission	Friction angle (Deg)	Bulk density (Kg m^{-3})	References
Viking Lander-1 drift	14-21	1150	(Moore and Clow, 1982)
Viking Lander-1 blocky	28-39	1600	(Moore and Clow, 1982)
Viking Lander-1 crusty	27-33	1400	(Moore and Clow, 1982)
Pathfinder drift & mixed	26 - 28	1066 - 1269	(Rover team, 1997)
Pathfinder moderate	34 - 38	1285 - 1518	(Rover team, 1997)
Pathfinder cloddy	40 - 41	1422 - 1636	(Rover team, 1997)
Phoenix lander	38 ± 5	1235	(Shaw et al., 2009)
Mars Exploration Rover	30 - 37	1630	(Sullivan et al., 2011)
JSC Mars-1	39.4 - 54.7	900 - 1120	(This investigation)
Mojave soil	32 - 41.3	1300 - 1500	(This investigation)

4.10. Conclusions

The successful exploration of planetary bodies depends on our understanding and prediction of the performance of landers, rovers, and any other subsurface investigating instruments with the regolith of on the surface and the subsurface. Regolith mechanical properties and the bearing capacity factors are the primary factors in the estimation of the penetrability, stability, trafficability on the surface of these planetary bodies. Mechanical properties of planetary analog materials (JSC Mars-1 and Mojave soil) have been investigated to determine the angle of internal friction, specific gravity, and minimum and maximum void ratios. This information have been used along with the results of the penetration testing in both regolith analogs to determine the bearing capacity factor (N_q) which is a crucial factor for the predications of penetration forces. Prediction of the penetration forces under the Martian gravity using a 1.2 cm diameter penetrometer was estimated using the bulk densities of 1150 – 1240 kg m^{-3} in JSC Mars-1 and 1330 – 1500 kg m^{-3} in Mojave soil; 100 – 700 N and 50 – 170 N was the estimated force to reach to about 20 cm in JSC Mars-1 and Mojave, respectively. The forces of penetration varied due to the variation in the intrinsic properties of regolith analogs, mainly the angle of internal friction.

Due to the variation in regolith materials due to particle size distribution, density, penetration forces can be used to differentiate between different layers and to characterize the subsurface regolith with minimum penetration. From lowest to highest possible compaction levels, penetration force in JSC Mars-1 was categorized in the range of (60 to 1000 N) while Mojave soil forces ranged from (60 - 240 N). Therefore, differentiation between JSC Mars-1 and Mojave soil was observable and appeared in the resulting penetration forces. On the other hand, JSC Mars-2 did not require much force for penetration which could make it easy to penetrate to

great depth on the surface of Mars. The same procedure can be used for future Mars subsurface investigation and analysis.

Prediction of the penetration forces for Mars can place a threshold to the weight of the lander or the rover. Spirit and Opportunity rovers each weighted about 683 N on the surface of Mars while MSL is weighting about 3320 N. If Spirit and Opportunity had such a penetrometer on board, they would not penetrate more than 15 cm in a regolith similar to JSC Mars-1 but can penetrate to more than 20 cm in Mojave type materials. MSL on the other side will have enough weight to penetrate to great depth. Penetration forces should not exceed the weight of the lander or the rover on the surface of the planetary body, otherwise, the whole lander or rover will lose its contact with the surface and place the whole mission in danger. The results of this investigation will improve future subsurface investigations of the Martian surface in terms of mission design, landing site selection and will be helpful the interpretation of physical, mechanical and geomorphological investigations as well.

4.11. References

Allen, C. C., K. M. Jager, R. V. Morris, D. J. Lindstrom, M. M. Lindstrom, and J. P. Lockwood. 1998. JSC Mars - 1: A martian soil simulant.

Arvidson, RE, RG Bonitz, ML Robinson, JL Carsten, RA Volpe, A. Trebi-Ollennu, MT Mellon, PC Chu, KR Davis, and JJ Wilson. 2009. Results from the mars phoenix lander robotic arm experiment. *J.Geophys.Res* 114 .

Bandfield, J. L. 2007. High-resolution subsurface water-ice distributions on mars. *NATURE-LONDON*- 447 (7140): 64.

Bonitz, R. G., L. Shiraishi, M. Robinson, R. E. Arvidson, PC Chu, JJ Wilson, KR Davis, G. Paulsen, AG Kusack, and D. Archer. 2008. NASA mars 2007 phoenix lander robotic arm and icy soil acquisition device. *J.Geophys.Res* 113 .

Bryson, K. L., V. Chevrier, D. W. G. Sears, and R. Ulrich. 2008. Stability of ice on mars and the water vapor diurnal cycle: Experimental study of the sublimation of ice through a fine-grained basaltic regolith. *Icarus* 196 (2): 446-58.

Byrne, S., C. M. Dundas, M. R. Kennedy, M. T. Mellon, A. S. McEwen, S. C. Cull, I. J. Daubar, D. E. Shean, K. D. Seelos, and S. L. Murchie. 2009. Distribution of mid-latitude ground ice on mars from new impact craters. *Science* 325 (5948): 1674.

Chevrier, V., D. R. Ostrowski, and D. W. G. Sears. 2008. Experimental study of the sublimation of ice through an unconsolidated clay layer: Implications for the stability of ice on mars and the possible diurnal variations in atmospheric water. *Icarus* 196 (2): 459-76.

Chevrier, V., D. W. G. Sears, J. D. Chittenden, L. A. Roe, R. Ulrich, K. Bryson, L. Billingsley, and J. Hanley. 2007. Sublimation rate of ice under simulated mars conditions and the effect of layers of mock regolith JSC mars-1. *Geophysical Research Letters* 34 (2): L02203.

Christensen, E. M., SA Batterson, HE Benson, C. E. Chandler, RH Jones, R. F. Scott, EN Shipley, F. B. Sperling, and GH Sutton. 1967. Lunar surface mechanical Properties—Surveyor 1. *Journal of Geophysical Research* 72 (2): 801-13.

Costes, NC, WD Carrier, JK Mitchell, and RF Scott. 1970. Apollo 11 soil mechanics investigation. *Science* 167 (3918): 739.

ElShafie, A., VF Chevrier, R. Ulrich, and L. Roe. 2010. Penetration testing for the optical probe for regolith analysis (OPRA). *Advances in Space Research* 46 (3): 327-36.

Evans, D. L., and J. B. Adams. 1979. Comparison of viking lander multispectral images and laboratory reflectance spectra of terrestrial samples. Paper presented at Lunar and Planetary Science Conference Proceedings.

Goetz, W., P. Bertelsen, C. S. Binau, H. P. Gunnlaugsson, S. F. Hviid, K. M. Kinch, D. E. Madsen, M. B. Madsen, M. Olsen, and R. Gellert. 2005. Indication of drier periods on mars from the chemistry and mineralogy of atmospheric dust. *Nature* 436 (7047): 62-5.

Hansen, J. B. A revised and extended formula for bearing capacity. Bulletin No. 28, Danish Geotechnical Institute, Copenhagen, 1970.

Harr, M. E. 1977. *Mechanics of particulate media: A probabilistic approach*McGraw-Hill.

Houston, WN, and LI Namiq. 1971. Penetration resistance of lunar soils. *Journal of Terramechanics* 8 (1): 59-69.

Hudson, T. L., O. Aharonson, N. Schorghofer, C. B. Farmer, M. H. Hecht, and N. T. Bridges. 2007. Water vapor diffusion in mars subsurface environments. *Journal of Geophysical Research E* 112 : Art. No. E05016.

Lucas, A., and A. Mangeney. 2007. Mobility and topographic effects for large valles marineris landslides on mars. *Geophysical Research Letters* 34 (10): 10201.

Lunne, T., PK Robertson, and JJM Powell. 1997. Cone penetration testing. *Geotechnical Practice*.

Mitchell, JK. Current lunar soil research'. 1964. *Proceedings of the American Society of Civil Engineers, Journal of Soil Mechanics and Foundation Engineering Division* 90 : 53.

Moore, H. J., D. B. Bickler, J. A. Crisp, H. J. Eisen, J. A. Gensler, A. F. C. Haldemann, J. R. Matijevic, L. K. Reid, and F. Pavlics. 1999. Soil-like deposits observed by sojourner, the pathfinder rover. *Journal of Geophysical Research* 104 (E4): 8729-46.

Moore, H. J., R. E. Hutton, R. F. Scott, C. R. Spitzer, and R. W. Shorthill. 1977. Surface materials of the viking landing sites. *Journal of Geophysical Research* 82 (28): 4497-523.

Moore, HJ, GD Clow, and RE Hutton. 1982. A summary of viking sample-trench analyses for angles of internal friction and cohesions. *Journal of Geophysical Research* 87 (B12): 10043,10,050.

Morris, R. V., DC Golden, J. F. Bell III, H. V. Lauer Jr, and J. B. Adams. 1993. Pigmenting agents in martian soils: Inferences from spectral, mössbauer, and magnetic properties of nanophase and other iron oxides in hawaiian palagonitic soil PN-9. *Geochimica Et Cosmochimica Acta* 57 (19): 4597-609.

Morris, RV, G. Klingelhöfer, C. Schröder, DS Rodionov, A. Yen, DW Ming, PA de Souza Jr, I. Fleischer, T. Wdowiak, and R. Gellert. 2006. Mössbauer mineralogy of rock, soil, and dust at gusev crater, mars: Spirit's journey through weakly altered olivine basalt on the plains and

pervasively altered basalt in the columbia hills. *Journal of Geophysical Research* 111 (E2): E02S13.

Morris, RV, G. Klingelhöfer, C. Schröder, DS Rodionov, A. Yen, DW Ming, PA de Souza Jr, T. Wdowiak, I. Fleischer, and R. Gellert. 2006. Mössbauer mineralogy of rock, soil, and dust at meridiani planum, mars: Opportunity's journey across sulfate-rich outcrop, basaltic sand and dust, and hematite lag deposits. *Journal of Geophysical Research* 111 (E12): E12S15.

Perko, H. A., J. D. Nelson, and J. R. Green. 2006. Mars soil mechanical properties and suitability of mars soil simulants. *Journal of Aerospace Engineering* 19 : 169.

Peters, G. H., W. Abbey, G. H. Bearman, G. S. Mungas, J. A. Smith, R. C. Anderson, S. Douglas, and L. W. Beegle. 2008. Mojave mars simulant--characterization of a new geologic mars analog. *Icarus* 197 (2): 470-9.

Puech, A., and P. Foray. 2002. Refined model for interpreting shallow penetration CPTs in sands. Paper presented at Offshore Technology Conference.

Robertson, P. K., J. J. M. Powell, and J. J. M. Powell. 1997. *Cone penetration testing in geotechnical practice.* Taylor & Francis Group.

Roscoe, KH. 1970. The influence of strains in soil mechanics. *Geotechnique* 20 (2): 129-70.

Rover team. 1997. Characterization of the martian surface deposits by the mars pathfinder rover, sojourner. *Science* 278 (5344): 1765.

Rowe, RD, and ET Selig. 1962. Penetration studies of simulated lunar dust.

Schorghofer, N. 2007. Dynamics of ice ages on mars. *Nature* 449 (7159): 192-4.

Schorghofer, N., and O. Aharonson. 2005. Stability and exchange of subsurface ice on mars. *J.Geophys.Res* 110 : 1–16.

Schultz, R. 2002. Stability of rock slopes in valles marineris, mars. *Geophysical Research Letters* 29 (19): 38-1.

Shaw, A., R. E. Arvidson, R. Bonitz, J. Carsten, HU Keller, M. T. Lemmon, M. T. Mellon, M. Robinson, and A. Trebi-Ollennu. 2009. Phoenix soil physical properties investigation. *Journal of Geophysical Research* 114 (E1): E00E05.

Shorthill, R. W., H. J. Moore, R. F. Scott, R. E. Hutton, S. Liebes, and C. R. Spotzer. 1976. The" soil" of mars (viking 1). *Science* 194 (4260): 91.

Singer, R. B. 1982. Spectral evidence for the mineralogy of high-albedo soils and dust on mars. *Journal of Geophysical Research* 87 (B12): 10159,10,168.

Sullivan, R., R. Anderson, J. Biesiadecki, T. Bond, and H. Stewart. 2011. Cohesions, friction angles, and other physical properties of martian regolith from mars exploration rover wheel trenches and wheel scuffs. *Journal of Geophysical Research* 116 (E2): E02006.

Terzaghi, K. Theoretical soil mechanics, John Wiley, New York, 1943.

Vesic, B. A. Bearing capacity of deep foundations in sand. High way research record No39, 112-153, 1963.

Yen, A. S., R. Gellert, C. Schroder, R. V. Morris, J. F. Bell III, A. T. Knudson, B. C. Clark, D. W. Ming, J. A. Crisp, and R. E. Arvidson. 2005. An integrated view of the chemistry and mineralogy of martian soils. *Nature*.

CHAPTER 5: INTERPRETATION OF GEOMORPHOLOGICAL SHAPE FORMATIONS SUPPORTED BY MECHANCAL AND ELECTRICAL REGOLITH PROPERTIES

5.1. Introduction

Processes responsible for the formation of gullies, slope streaks, linear and landslides remain speculative (Sullivan et al., 2001, Dickson et al., 2006; Thomas et al., 2003; Lucchitta et al., 1979). Gullies have been proposed to form as a result of aquifer outflow from near surface water (Malin and Edgett 2000; Heldmann et al.,2005) or brought up by cryovolcanic activity (Gaidos, 2001), melting of surface or subsurface ice at high obliquity (Costard et al., 2002; Gilmore and Phillips, 2002; Mangold et al., 2003), debris flow (Iverson, 1997), brines (Andersen et al., 2002; Knauth and Burt 2002; Chevirier and Altheide, 2008), granular flow (Treiman 2003; Shinbort et al., 2004) or during seasonal snowmelt (Reiss and Jaumann, 2002; Kossacki and Markiewicz,2004; Williams et al., 2009; Dixon and Head 2009).

Internal angle of friction which is one of the most important parameters for understanding the movement of the granular material as it contributes to the strength of the formations. It has been theoretically estimated for interpretation and modelling of Martian geomorphological features (Parsons et al., 2008; Lucas and Mangeney, 2007; Mangold and Costard, 2003; Miyamoto et al., 2004). Friction angle is not a material property; however, it is a property that depends on other mechanical input parameters such as void ratio and density (Rowe, 1962; Bolton, 1986). Therefore, understanding the of gully formations, dynamics of Martian landslides, slope streaks and slope stability through interpretation of optical imagery or modelling is based on our knowledge of the mechanical properties of the regolith in which surface forms develop.

Dielectric constant is a measure of how much energy is stored and re-radiated by the material; therefore, calculating the two way travel time of electromagnetic wave can help estimating the dielectric constant which used for radargram inversion (Strangway and Olheft, 1977). Mars Advanced Radar for Subsurface and Ionosphere Sounding (MARSIS) and Shallow Subsurface Radar (SHARAD) sounding radars are currently probing the Martian surface and subsurface to detect subsurface water (Picardi, et al. (2005); Seu, et al. (2007). One of the key elements for quantitative radar data analysis is the comprehensive understanding of how radar waves interact with the nature and structure of the planetary surfaces and subsurfaces. This can be achieved through knowledge of the dielectric constant of the investigated material (Heggy et al., 2003; Heggy et al., 2004; Grimm et al., 2006).

For better interpretation and analysis of geomorphological features observed by radar and optical remote sensing instruments, knowledge of the mechanical properties of the surface and the subsurface is mandatory. Correlating between data sets obtained from different instruments would enhance our current and future modelling and interpretation. Therefore, the objective of this research is to examine the relationship between mechanical and electrical regolith properties, and geomorphological formation which will enhance previous, current and future modelling interpretation and analysis of optical imagery and radar data.

5.2. Experimental method

5.2.1. Flume Experiment

In order to investigate the relationship between shape form and mechanical and electrical regolith properties, flume experiments were conducted using the flume apparatus (Coleman et al., 2009). During our flume experiments, we assumed that liquid water is stable; though, we did

not account for the influence of low atmospheric pressure. Regardless of scaling effect, we concentrated on the relative importance of the investigated parameters and their effect on geomorphological features. Therefore, we conducted our gully experiments in a flume 1 x 0.8 x 0.15 m^3 which has the ability to be adjusted to the desired slope angle (Fig. 5.1). Different degrees of density were examined with a homogenous distribution layers, therefore, a specific sampler test structure was built (0.7 x 0.45 x 0.04 m^3) with a top movable plate (Fig. 5.1). Before loading the regolith, the top movable plate is clamped to the lower test structure. Regolith is poured into the sampler and compacted to the desired density. Density samples covered the range from 974 to 1130 kg m^{-3}. Sliding the top movable plate took place to remove the excess of regolith, to fill the gaps and to have a one homogenous sample test. Once the sample is prepared, it is placed into the flume with the adjusted slope and connected to the water supply. Our experiments were carried out at slope of 10° and water flows of 10 GPH for 25 sec. Gully total length measured from the top of the alcove to the end of the apron using a meter stick with millimetre precision. After finishing the experimental test, regolith emptied from the sampler and new dry fresh regolith was used for subsequent tests.

5.2.2. Mechanical measurements

Regolith mechanical properties are primary factors affect geomorphological and radar interpretation and modelling. Direct shear tests were performed on JSC Mars-1 regolith simulant in order to determine the angle of internal friction (using the standard method ASTM D-3080). For sample preparation, the mass and volume of each prepared sample was measured and soil bulk density was determined. Regolith sample placed in a shear box which has two movable parts. The contact between the top and lower parts of the shear box is approximately the height

of the sample. A confining stress (2.7, 4.2 and 8.4 Kg) is applied vertically on the top part of the box and the lower part of the shear box is pulled laterally until the regolith sample fails. The applied load and strain induced is recorded at specific intervals to determine the stress-strain curve at specific confining stress. The procedure was repeated three times for each applied stress under the same density. From the slope of shear stress-stress curve, the angle of internal friction (φ) of the soil samples was determined by a best fit linear regression.

5.2.3. Electrical measurements

Using a hydraulic press, JSC Mars-1 samples were compacted into pellets where the mass and height was measured and the density was determined. Electrical measurements of the thin samples < 3mm in thickness were carried out at room temperature using a dielectric material test fixture attached to an Impedance/Material Analyzer. The analyzer is connected to a central command unit to extract data and calculate, in real-time, the real and imaginary part of the complex dielectric constant. The samples were placed between the parallel plates of a guarded capacitive cell to reduce edge errors. Sweeping over the frequency range of observation, the real and imaginary parts of the relative complex permittivity were calculated from the capacitance and admittance knowing the thickness of the sample. Values of relative permittivity were measured over the entire frequency range (10 MHz to 1 GHz).

5.3. Results

In order to test the effect of mechanical and electrical properties of regolith analogs on gully shape formations, we set the slope angle (10°), flow rate (10 GPH) and flow time (25 sec) to be the same along the whole gully experiments. Gully shape formation is observed to vary due

to the mechanical and electrical properties of regolith analogs. Regolith bulk density is found to be the most sensitive factor affecting gully morphology.

Over the range of prepared bulk density from 974 to 1130 kg m^{-3}, gully total length is affected by the density of the prepared samples. A linear increase in the formation total length is observed as a function of change in bulk density (Fig. 5.2 A). Total gully length increased from ~25 cm at the lowest bulk density level (~970 kg m^{-3}) to ~50 cm for the highest bulk density (~1130 kg m^{-3}) for JSC Mars-1. Low density imply greater void ratios, therefore, there is more space for the water to flow in all possible ways which produces short formations. However, at high bulk density (low void ratio) water could not push against the regolith. Therefore, it went up into the surface and form longer formations. R^2 calculated for the regression line is ~ 0.92.

The movement of water through regolith is affected by different levels of bulk densities which are controlled by the angle of internal friction. Small angle of internal friction indicates low void ratio and porosity and both of these parameters increase along the increase of the angle of internal friction. To investigate such assumption, we correlated the angle of internal friction to regolith bulk density (Fig. 5.2 B). The angle of internal friction of JSC Mars-1 is found to be a function of bulk density. Increasing the angle of internal friction corresponded to an increase in regolith bulk density. Going from 900 to 1120 kg m^{-3} in JSC Mars-1 bulk density, an increase of 39.4 to 54.7° in angle of internal friction is observed (Fig. 5.2 B). Therefore, shorter and longer formations correspond to a small and big angle of internal friction respectively.

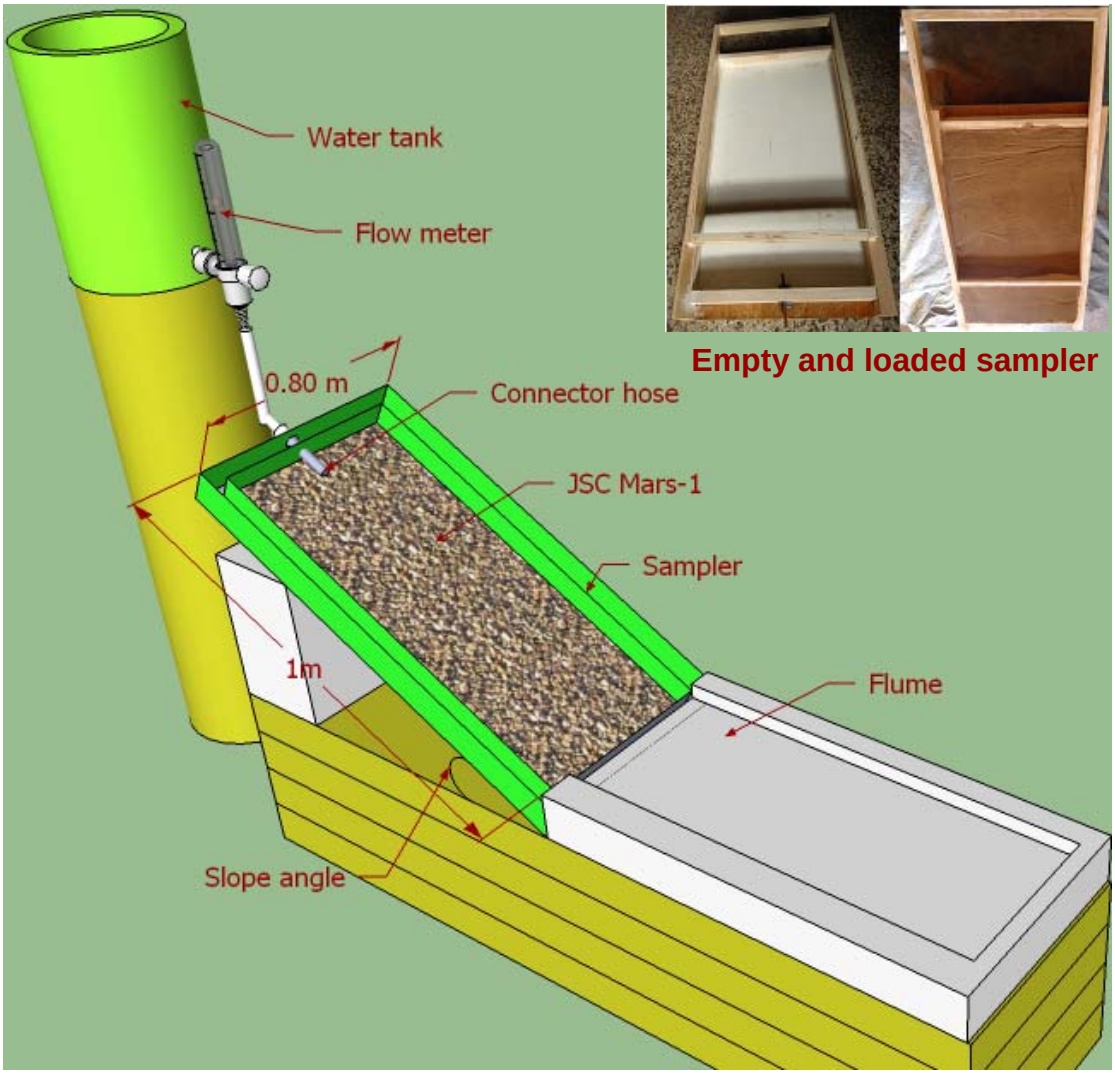

Figure 5.1. Gully simulation flume and test sampler.

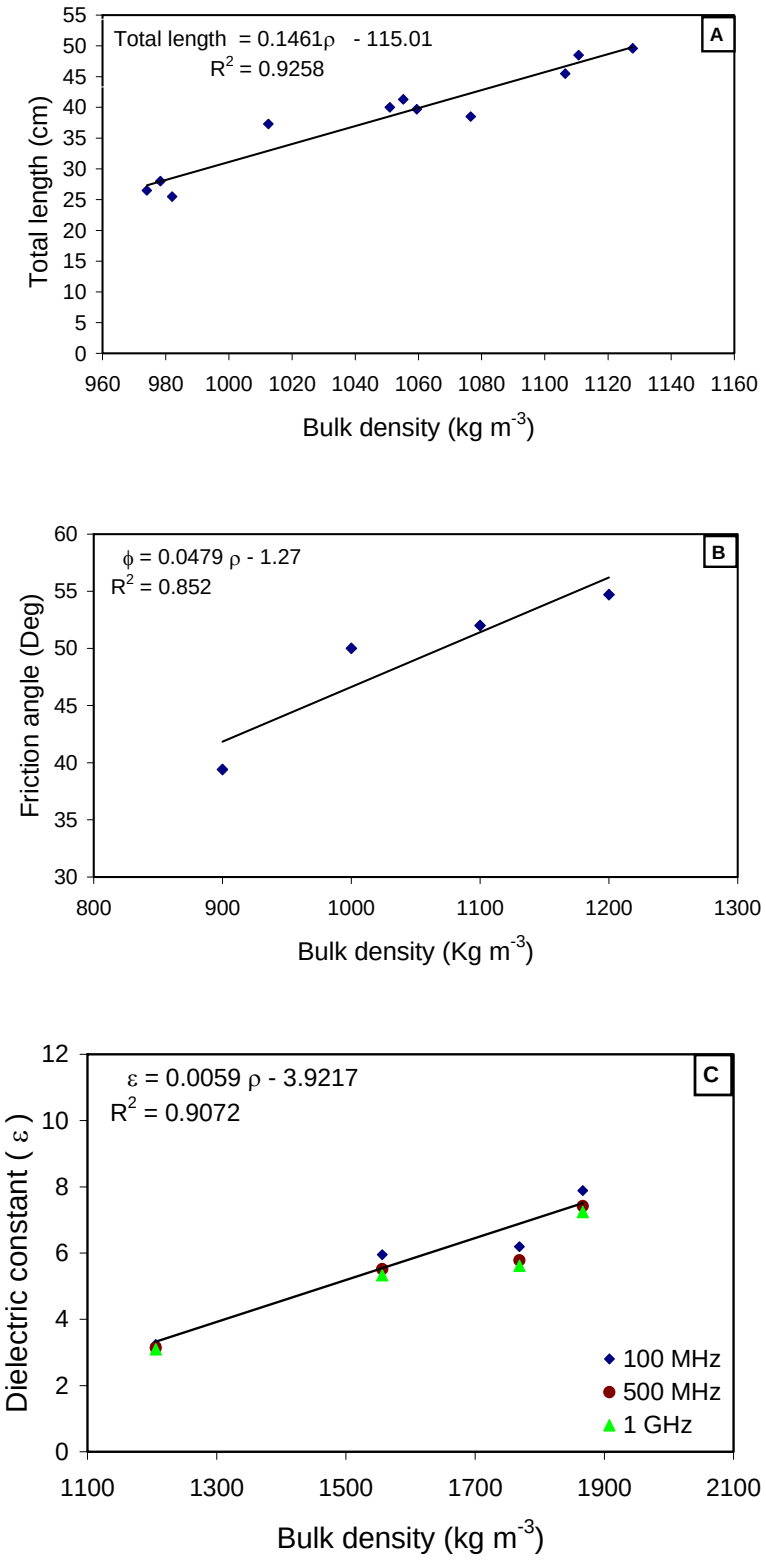

Figure 5.2. Total length, friction angle and dielectric constant as a function of different bulk density for JSC Mars-1.

In an attempt to correlate the gully formation to electrical properties of regolith analogs, the dielectric constant of JSC Mars-1 is measured at different levels of prepared bulk densities. Regolith dielectric constant is found to decrease with increasing detection frequency range and to increase with increasing density of regolith samples (Fig. 5.2 C). The dielectric constant increased from ~ 3 to ~ 8 with an increase in bulk density from 1200 to 1860 kg m^{-3}. From regression line, the calculated R^2 is 0.90. Therefore, short and long gully formations indicate low and high dielectric constant value.

5.4. Discussion

Stability of slopes on Earth is affected by regolith strength which related to the angle of internal friction. If stress increased due to loading exceeding the angle of internal friction, failure will occur and the resulted formation is observed to be similar to gullies found on Mars. Therefore, the shape of the resulted gully is affected by the mechanical properties of the formation.

Gullies on Mars are hypothesized to be formed by action of liquid water (Mellon and Phillips, 2001; Christensen, 2003). Surveying gullies by radar can test such hypotheses since the dielectric constant of liquid water is about one order of magnitude higher than that of most silicates and crustal rocks (Ulaby et al., 1986). (Nunes et al., 2010) surveyed 65 different locations within the two Martian mid‐latitudes using SHARAD radar looking for strong subsurface reflections which can be indicative of the presence of subsurface water. No strong reflections are found within the surveyed areas which may weaken the water hypotheses but still not disproving it.

Liquid water may exist; however, its detection was not possible due to uncertainty of the dielectric constant of Martian surface and subsurface materials, surface scattering and surface irregularities all caused radar reflections to be below SHARAD threshold detection range. In order to better interpret the radar data, pre-existed information about the dielectric constant of the investigated material must be assessed. Currently, such information is not available; therefore, correlating the dielectric constant to shape formation and mechanical properties of regolith will enhance radar inversion.

Since friction angle and dielectric constant of the regolith is found to be function of the density of the prepared samples, where they increase with increasing the density. We used their relations with bulk density to correlate with formation total length. We correlated between the calculated friction angle, dielectric constant and the formation total length (Fig. 5.3 A and B). Based on this correlation, regolith friction angle ranged from ~45 to ~52° and regolith dielectric constant ranged from ~1.8 to ~2.5 along an increase in gully total length from 25 to 50 cm. This correlation can enhance radar dielectric inversion which may solve ambiguities which appeared in SHARAD data (Nunes et al., 2010).

5.5. Conclusions

Simulations of gully formations are conducted in order to understand which factors affect gully shapes. Testing the effect of the mechanical and electrical properties of regolith analogs along with gully formations showed that both properties play an important role in controlling gully morphology. This work confirms that gully total length, regolith dielectric constant and angle of internal friction are found to be function of the density of the formation. An increase in the subsurface density will correspond to an increase in formation total length, regolith angle of

internal friction and dielectric constant. Our experiments suggest that the morphology of the gullies observed on the surface of Mars can be interpreted using orbital cameras and/or radar will be possible as well as estimation of the electrical and mechanical properties of the subsurface, which will enhance previous, current and future Martian gully investigation.

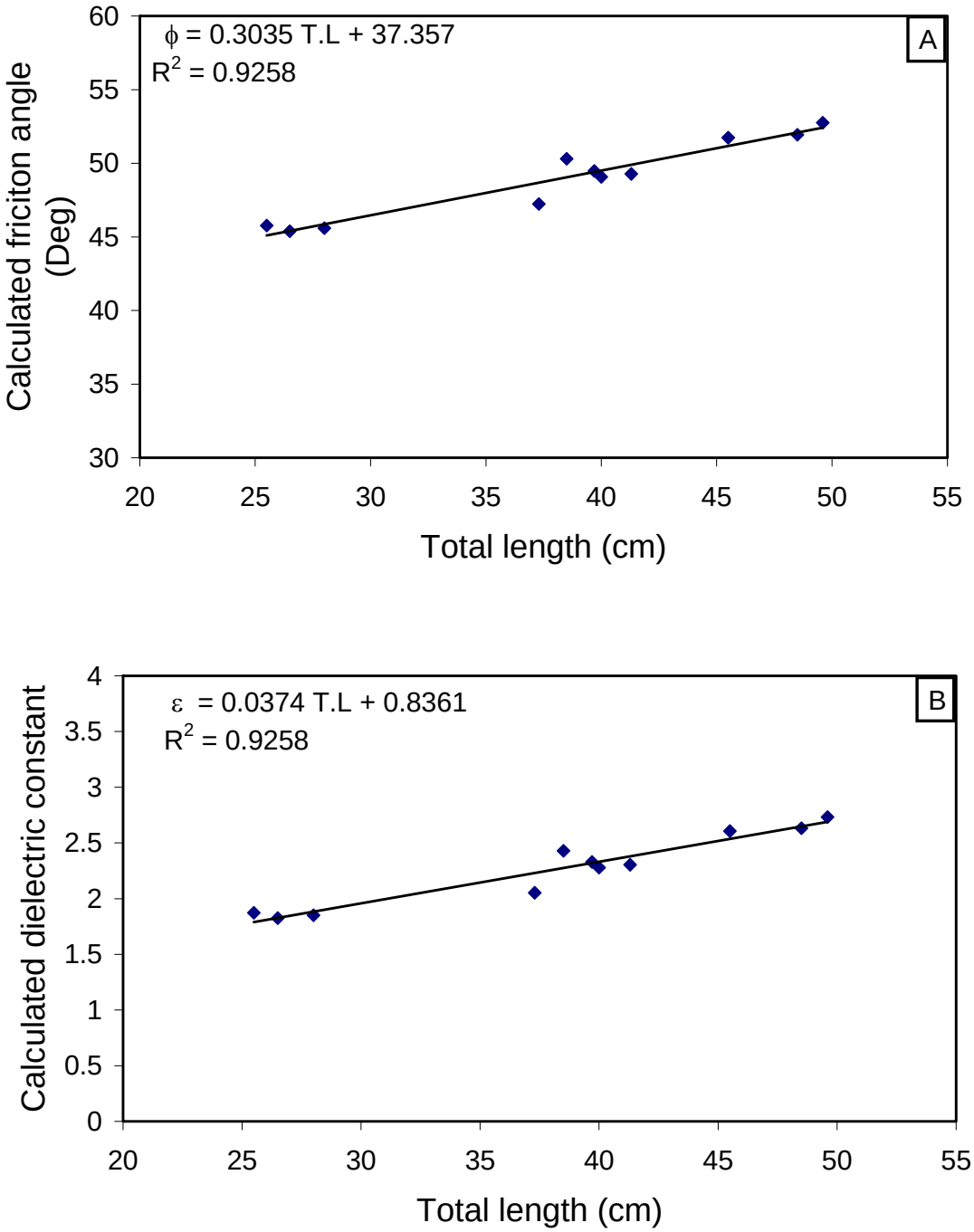

Figure 5.3. Calculated friction angle (A) and dielectric constant (B) as a function of total length for JSC Mars-1.

5.6. References

Andersen, D. T., W. H. Pollard, C. P. McKay, and J. Heldmann. 2002. Cold springs in permafrost on earth and mars. *J.Geophys.Res* 107 (10.1029).

Bolton, MD. 1986. The strength and dilatancy of sands. *Geotechnique* 36 (1): 65-78.

Chevrier, V. F., and T. S. Altheide. 2008. Low temperature aqueous ferric sulfate solutions on the surface of mars. *Geophysical Research Letters* 35 (22): L22101.

Coleman, KA, JC Dixon, KL Howe, LA Roe, and V. Chevrier. 2009. Experimental simulation of martian gully forms. *Planetary and Space Science* 57 (5-6): 711-6.

Costard, F., F. Forget, N. Mangold, and JP Peulvast. 2002. Formation of recent martian debris flows by melting of near-surface ground ice at high obliquity. *Science* 295 (5552): 110.

Dickson, J. L., and J. W. Head. 2009. The formation and evolution of youthful gullies on mars: Gullies as the late-stage phase of mars' most recent ice age. *Icarus* 204 (1): 63-86.

Dickson, J. L., J. W. Head, M. A. Kreslavsky, and D. R. Marchant. 2006. Linear lobate debris aprons, piedmont-like lobes, and crater fill in the acheron fossae graben region, mars: Evidence for debris-covered glacier formation and flow. Paper presented at 37th Annual Lunar and Planetary Science Conference, .

Gaidos, E. J. 2001. Cryovolcanism and the recent flow of liquid water on mars. *Icarus* 153 (1): 218-23.

Gilmore, M. S., and E. L. Phillips. 2002. Role of aquicludes in formation of martian gullies. *Geology* 30 (12): 1107.

Grimm, R. E., E. Heggy, S. Clifford, C. Dinwiddie, R. McGinnis, and D. Farrell. 2006. Absorption and scattering in ground-penetrating radar: Analysis of the bishop tuff. *J.Geophys.Res* 111 : E06S02.

Heggy, E., SM Clifford, RV Morris, P. Paillou, and G. Ruffie. 2004. On the dielectric properties of the martian-like surface sediments. Paper presented at Lunar and Planetary Institute Science Conference Abstracts, .

Heggy, E., P. Paillou, F. Costard, N. Mangold, G. Ruffie, F. Demontoux, G. Grandjean, and JM Malézieux. 2003. Local geoelectrical models of the martian subsurface for shallow groundwater detection using sounding radars. *J.Geophys.Res* 108 (E4): 8030.

Heldmann, J. L., O. B. Toon, W. H. Pollard, M. T. Mellon, J. Pitlick, C. P. McKay, and D. T. Andersen. 2005. Formation of martian gullies by the action of liquid water flowing under current martian environmental conditions. *J.Geophys.Res* 110 (10.1029).

Iverson, RH. 1997. The physics of debris flows. *REVIEWS OF GEOPHYSICS-RICHMOND VIRGINIA THEN WASHINGTON*- 35 : 245-96.

Knauth, L. P., and D. M. Burt. 2002. Eutectic brines on mars: Origin and possible relation to young seepage features. *Icarus* 158 (1): 267-71.

Kossacki, K. J., and W. J. Markiewicz. 2004. Seasonal melting of surface water ice condensing in martian gullies. *Icarus* 171 (2): 272-83.

Lucas, A., and A. Mangeney. 2007. Mobility and topographic effects for large valles marineris landslides on mars. *Geophysical Research Letters* 34 (10): 10201.

Lucchitta, B. K. 1979. Landslides in valles marineris, mars. *Journal of Geophysical Research* 84 (B14): 8097-113.

Malin, M. C., and K. S. Edgett. 2000. Evidence for recent groundwater seepage and surface runoff on mars. *Science* 288 (5475): 2330.

Mangold, N., F. Costard, and F. Forget. 2003. Debris flows over sand dunes on mars: Evidence for liquid water. *J.Geophys.Res* 108 (10.1029): 2002001885.

Miyamoto, H., J. M. Dohm, R. A. Beyer, and V. R. Baker. 2004. Fluid dynamical implications of anastomosing slope streaks on mars. *J.Geophys.Res* 109 (10.1029).

Parsons, RA, MA Kreslavsky, and F. Nimmo. 2008. Martian gully slope measurements made using HiRISE stereo pairs. Paper presented at Lunar and Planetary Institute Science Conference Abstracts, .

Picardi, G., J. J. Plaut, D. Biccari, O. Bombaci, D. Calabrese, M. Cartacci, A. Cicchetti, S. M. Clifford, P. Edenhofer, and W. M. Farrell. 2005. Radar soundings of the subsurface of mars. *Science* 310 (5756): 1925.

Reiss, D., and R. Jaumann. 2002. Spring defrosting in the russell crater dune field--recent surface runoff within the last martian year? Paper presented at Lunar and Planetary Institute Science Conference Abstracts, .

Rowe, P. W. 1962. The stress-dilatancy relation for static equilibrium of an assembly of particles in contact. *Proceedings of the Royal Society of London.Series A.Mathematical and Physical Sciences* 269 (1339): 500-27.

Seu, R., R. J. Phillips, D. Biccari, R. Orosei, A. Masdea, G. Picardi, A. Safaeinili, B. A. Campbell, J. J. Plaut, and L. Marinangeli. 2007. SHARAD sounding radar on the mars reconnaissance orbiter. *Journal of Geophysical Research* 112 (E5): E05S05.

Shinbrot, T., N. H. Duong, L. Kwan, and MM Alvarez. 2004. Dry granular flows can generate surface features resembling those seen in martian gullies. *Proceedings of the National Academy of Sciences of the United States of America* 101 (23): 8542.

Strangway, DW, and GR Olhoeft. 1977. Electrical properties of planetary surfaces. *Philosophical Transactions of the Royal Society of London.Series A, Mathematical and Physical Sciences* 285 (1327): 441-50.

Sullivan, R., P. Thomas, J. Veverka, M. Malin, and K. S. Edgett. 2001. Mass movement slope streaks imaged by the mars orbiter camera. *Journal of Geophysical Research* 106 (E10): 23607,23,633.

Thomas, PC, P. Gierasch, R. Sullivan, DS Miller, E. Alvarez del Castillo, B. Cantor, and MT Mellon. 2003. Mesoscale linear streaks on mars: Environments of dust entrainment. *Icarus* 162 (2): 242-58.

Treiman, A. H. 2003. Geologic settings of martian gullies: Implications for their origins. *J.Geophys.Res* 108 (10.1029).

Williams, KE, OB Toon, JL Heldmann, and MT Mellon. 2009. Ancient melting of mid-latitude snowpacks on mars as a water source for gullies. *Icarus* 200 (2): 418-25.

CHAPTER 6: DIELECTRIC AND HARDNESS MEASUREMENTS OF PLANETARY REGOLITH ANALOG ROCKS IN SUPPORT OF IN-SITU PLANETARY SUBSURFACE SAMPLING

6.1. Introduction

Dielectric properties as inverted from radar subsurface sounding are increasingly suggested to assess the ground mechanical properties as rock hardness, density and porosity for several planetary surfaces. Of particular interest is the in situ sampling from Mars, comets, asteroids and icy satellites as their shallow subsurface hold key information in understanding the volatiles occurrence, geological compositional and geophysical evolution of these planetary bodies. Conjugating penetrometer and/or drill with sounding radars have been widely suggested to optimize subsurface investigation and sampling (e.g. Kofman et al., 2004; Safaeinili et al., 2007). Radar sounders will be used to probe the subsurface and assign localities of high scientific interest with the minimum drill and penetration risk as the CONSERT radar supporting the MUPUS penetrometer and SD^2 drill on board the Rosetta lander (Biele, 2002) and the potential future ground penetrating radar experiment as the proposed WISDOM radar which will support ExoMars drill on future ExoMars mission to targets of investigations (Plettemeier et al., 2009; Winnendael et al., 2005; Ciarletti et al., 2009). In addition, drilling and subsurface sample returns has also been suggested for asteroid missions (Lauretta et al., 2012; Bowles et al., 2012). In all these different planetary surfaces the drilling capabilities strongly depend on identifying optimal locations where rock hardness permits penetration to subsurface sample. Such identification can be made using sounding radars radargrams where observed anomalic bulk dielectric constants can indicate locations with subsurface inclusion of ice and porous materials (Heggy et al., 2003;

Campbell et al., 2009). Hence an accurate assessment of the subsurface mechanical properties (i.e. rock hardness, density and porosity) and how they correlate to dielectric properties is crucial to future drill investigations.

While the porosity and density dependency of the dielectric property of planetary analogs have been explored (e.g. Ulaby et al., 1990; Heggy et al., 2004; Stillman and Olhoeft, 2008), their dependency on rock hardness remains poorly known for volcanic material that are considered as the more accurate analog to planetary regolith (Weren et al., 2004; Brady et al., 2005). Such ambiguities can compromise the accuracy of the dielectric inversion leading to miss assessment of ground hardness, reducing the performance of the drill and potentially missing or altering targets of interest especially those related to volatile exploration. Therefore, the main purpose of this research is to perform dielectric permittivity and hardness measurements for planetary analog volcanic rocks to provide a cross relation between these two parameters. These findings will help use the dielectric inversion from past, present and future radar experiments to assess the subsurface rock hardness to support and optimize the drill operation for sampling purposes as well as the physical characterization of the shallow subsurface.

6.2. Experimental method and sample description

6.2.1. Sample preparation and measurements procedure

To simulate the different mechanical properties of planetary analogs, we use eight different types of volcanic rocks for dielectric and hardness measurements. Of which, six were basaltic rocks (Belleville, flood, Olivine rich, Mojave, Saddleback and lava basalts), one sample of welded tuff and another for pumice. Core and thin sliced specimens are cut and prepared for each sample. Hardness and dielectric measurements are performed on each sample. Both

measurements are conducted at room temperature for desiccated and undesiccated samples. Moisture affects rock strength; rock strength decrease with increasing the moisture content (Rehbinder et al., 1948). For this reason measurements are performed on desiccated samples. Desiccation is carried by heating samples for 24 h at 100 ºC to eliminate residual moisture. The full description of the dielectric measurement setup and sample preparation can be found in (Heggy et al., 2001).

6.2.2. Hardness measurements

Hardness is a measure of the resistant of material when it is under confined stress by overcoming the mineral constituents of the rock and the bond strength that exist between the mineral grains (Parkhomenko and Keller, 1967). The mechanical behavior of volcanic rocks under stress forces is complex; therefore, there are different measurement techniques for hardness: scratch, indentation, and rebound hardness (Atkinson et al., 1978).

Our hardness measurements are performed for desiccated and undesiccated samples using the rebound technique as it is a non destructive technique which does not leave any imprints on the test sample and is sensitive in differentiating the hardness between two closely density related samples (Hucka, 1965; Brown, 1981; ASTM, 2001; Ericson, 2004; Goudie, 2006). We used Proceq Schmidt hammer type-L with hammer impact energy of 0.735 Nm. Core Specimens are checked to be free of visible cracks and representative of the rock mass. For data gathering, 10 rebound tests are recorded per sample and averaged to determine the rebound number (R) with a repeatability of ± 2 R.

6.2.3. Dielectric measurements

Laboratory dielectric measurements of thin sliced samples < 3mm in thickness carried at room temperature for desiccated and undesiccated samples using a dielectric capacitive cell and a test fixture attached to an impedance analyzer. The analyzer is connected to a central command unit to extract data and calculate, in real-time, the real and imaginary part of the complex dielectric constant. Samples are placed between the parallel plates of a guarded capacitive cell to reduce edge errors (ASTM, 1999). Sweeping over the frequency range of observation, the real and imaginary parts of the relative complex permittivity is calculated from the capacitance and admittance knowing the thickness of the sample. Values of relative permittivity are measured over the entire frequency range; 200 to 1500 MHz hence covering the frequency ranges of several of the previous, current and future sounding radar experiments.

6.3. Experimental Results

Dielectric and hardness measurements are carried out on desiccated and undesiccated samples (residual moisture ranges from 0.2 to 1.3% of mass) in order to determine the effect of minor volatile presence on hardness and dielectric properties.

Schmidt hammer hardness number ranged from R= 14.16 to 69.65 at the density of $\rho \sim 0.85$ and 3.018 gm/cm^3 for pumice and Olivine basalt, respectively for undesiccated samples. For desiccated samples, Schmidt hammer hardness number ranged from R= 12.8 to 68 at the density of $\rho \sim 0.83$ and 3.012 gm/cm^3 for pumice and Olivine basalt, respectively. For volcanic materials used in this study, the residual moisture is observed to have no-significant impact on the rock hardness. For each samples category, the lowest and highest R-values (pumice and Olivine basalt) correspond to the lowest and highest density of the samples. For volcanic rocks, we

observed that as the density increase, the hardness increases which implies the strong effect of density on hardness measurements (Table 6.1).

Dielectric measurements for undesiccated and desiccated samples with a given density are listed in Table 6.2 at three frequency ranges (100, 500 MHz and 1 GHz). Dielectric constant is observed to decrease with increasing the frequency and to increase with increasing the density of the rock samples. Desiccation was observed to decrease the dielectric constant with different amplitudes for the different samples. The dielectric constant decreased from ~12 to 6 for Saddleback basalt, corresponding to a 50 % variation due to desiccation eliminating the residual moisture which constitutes 1.1% of the sample mass. Such high variation is related to the presence of conducting iron oxides in the sample (Heggy et al., 2001). For lava basalt, we do not observe a significant change in the dielectric constant due to the minimal moisture content constituting 0.1% of the sample mass.

(Parkhomenko and Keller, 1967) suggested an inverse relation between molecular polarizability and binding energy of minerals, which suggests an inverse relationship between the dielectric constant and the hardness of minerals; hence the harder the mineral, the lower should be the dielectric constant; based on Mohs scale of hardness. Figure 6.1 shows the dielectric constant as a function of Schmidt hammer hardness number at room temperature for volcanic rocks at three frequency ranges (100, 500 MHz and 1 GHz). Dielectric constant was observed to increase with increasing rock hardness for volcanic material. Measurements suggest that for volcanic rocks and pyroclasts, the harder the rock, the higher is the dielectric constant. A possible explanation for this linear increase instead of a decrease as mentioned above is due to the variation of the density of the samples. We observed that both the hardness and the dielectric constant are linearly increasing with the increase of the density of the materials.

Table 6.1. Schmidt hammer hardness measurements of volcanic rocks for desiccated and undesiccated samples.

Rock types	ρ (gm/cm^3) [a]	R [a]	Slandered deviation	ρ (gm/cm^3) [b]	Moisture %	R [b]	Slandered deviation
Belleville basalt	2.73	51.4	2.5	2.71	0.51	66.43	3.7
Saddleback Basalt	2.75	68.14	1.5	2.73	0.72	64.45	2.8
Flood basalt	3.01	68.96	3.2	2.99	0.79	68	2.9
MMS	2.90	64.87	3.1	2.88	0.65	61.2	3.4
Olivine basalt	3.01	69.65	2.2	3.01	0.19	67.9	2.5
Welded tuff	1.60	33.37	3.3	1.59	0.35	39.7	2.8
Pumice	0.85	14.16	3.5	0.83	1.33	12.83	2.2
Lava basalt	2.23	20.22	3.4	2.22	0.29	18.30	1.9

[a] Undesiccated

[b] Desiccated

Table 6.2. Dielectric measurements of volcanic rocks for desiccated and undesiccated samples

Rock types	ρ (gm /cm^3) [a]	ε (100 MHz) [a]	ε (500 MHz) [a]	ε (1 GHz) [a]	ρ (gm /cm^3) [b]	ε (100 MHz) [b]	ε (500 MHz) [b]	ε (1 GHz) [b]	Moisture % [b]
Belleville basalt	3.25	8.56	7.89	7.73	3.22	6.48	6.46	6.49	0.37
Saddleback Basalt	3.29	12.23	10.65	10.26	3.25	6.87	6.86	6.89	1.01
Flood basalt	2.88	10.11	8.83	8.46	2.85	8.09	7.64	7.47	0.92
MMS	2.87	6.68	6.41	6.63	2.85	6.35	6.28	6.28	0.15
Olivine basalt	3.22	8.32	8.01	7.95	3.21	7.42	7.37	7.41	0.12
Welded tuff	1.43	2.73	2.73	2.72	1.42	2.58	2.57	2.57	0.33
Pumice	0.74	1.95	1.94	1.94	0.72	1.91	1.9	1.9	1.07
Lava basalt	2.23	4.73	4.58	4.49	2.22	4.56	4.41	4.31	0.10

[a] Undesiccated

[b] Desiccated

In order to validate our dielectric versus hardness measurements, we use (Aydin and Basu, 2005) Schmidt hammer rebound hardness (R) results, uniaxial compressive strength (σ_{UCS}) and dry density (ρ) for desiccated granitic rocks. We then apply the density model provided by (Olhoeft, 1979) to calculate the corresponding dielectric constant ($\acute{\varepsilon}$) for a given densities as provided by (Aydin and Basu, 2005) (Table 6.3).

$$\varepsilon' = 1.919^{\rho} \quad \text{(Olhoeft, 1979)} \quad (1)$$

Figure 6.2 shows the measured dielectric constant at three frequency ranges 100, 500 MHz and 1 GHz and hardness values after desiccating the basaltic samples at 100 ºC for 24 h as well as the calculated dielectric constant based on dry density measurements done by (Aydin and Basu, 2005). Our measurements suggest a linear correlation between the dielectric constant and the hardness (R) for both basalts and granitic samples. Dielectric constant varied from ~2 for a given hardness of ~12 to ~8 for hardness of ~ 68. Moisture removal by heating caused a decrease in the dielectric constant. The calculated values of the dielectric constant suggested a similar linear trend as supported by our laboratory measurements. Equation 2 describes the correlation between the dielectric constant and rock hardness based on our laboratory measurements and validation from Aydin and Basu, 2005.

$$\varepsilon' = (0.0674 \times R) + 2.126 \quad (2)$$

While this empirical equation can be used to describe the dielectric-hardness function for volcanic rocks, it cannot be applied as is to sedimentary rocks, loose sediments and icy surfaces. Further measurements will be needed to achieve such goal.

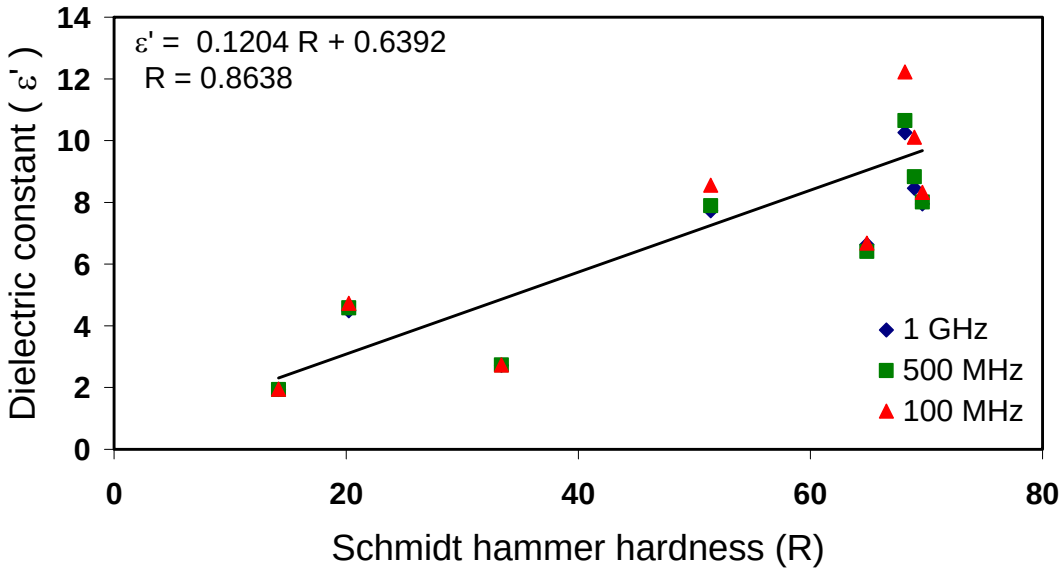

Figure 6.1. Dielectric constant versus Schmidt hammer hardness number (R) of volcanic rocks at different frequency ranges for undesiccated samples.

Table 6.3. Rebound values and some other physical properties of granitic rocks (Aydin and Basu, 2005).

Sample No	R	ρ (gm/cm^3) dry	σ_{ucs} (MPa)	ἐ (predicted)
1	64.67	2.69	196.45	6.111796
2	62.83	2.68	160.2	6.070805
3	62.6	2.63	157.22	5.869937
4	61.75	2.65	155.7	5.949474
5	61.42	2.57	148.36	5.63765
6	65.76	2.66	136.15	5.989646
7	61.84	2.59	133.55	5.714039
8	61.84	2.62	123.25	5.830569
9	62.13	2.63	139.45	5.869937
10	60.43	2.62	121.4	5.830569
11	60.24	2.58	116.3	5.675716
12	60.48	2.57	106.34	5.63765
13	61.4	2.65	88.2	5.949474
14	59.53	2.62	83.13	5.830569
15	58.02	2.49	68.21	5.342169
16	52.74	2.59	59.36	5.714039
17	49.15	2.57	53.19	5.63765
18	43.29	2.57	45.67	5.63765
19	42.45	2.42	32.16	5.096355
20	39.94	2.36	31.14	4.89468
21	48.86	2.47	26.83	5.270751
22	35.01	2.46	24.35	5.235401
23	34.91	2.42	22.96	5.096355
24	33.43	2.41	22.32	5.062175
25	43.99	2.52	14.7	5.451114
26	43.65	2.52	13.66	5.451114
27	36.39	2.37	13.61	4.92773
28	34.24	2.4	18.84	5.028223
29	32.24	2.26	17.3	4.576134
30	35.67	2.32	7.64	4.764684
31	33	2.24	23.15	4.514957
32	34	2.28	19.7	4.63814
33	34.91	2.36	25.14	4.89468
34	32.28	2.35	22.16	4.861852
35	34.39	2.34	11.67	4.829245
36	20	2.13	6.32	4.192812
37	50.33	2.55	33.86	5.562282
38	51.46	2.56	41.73	5.599839
39	48.48	2.47	25.38	5.270751
40	46.69	2.46	22.66	5.235401

6.4. Implication for future planetary sampling experiments

Sampling planetary bodies provide insight into their history of formation and evolution. The amplitude of the gravity field defines the optimal sampling mechanisms for planetary bodies. At micro-gravity environments such as asteroids and comets, anchoring the surface, and capturing surface samples is the most adequate technique as suggested for Rosetta in 2014. Additionally, other method such as firing the surface using bullets and collecting fragments is used on the Hayabusa mission. Drilling, penetrating and harpooning the surface and collecting or casing samples are suggested techniques for sampling bodies with substantial gravity field such as planets and satellites. All the above-mentioned sampling techniques require interaction with the surface and the shallow subsurface. Feasibility of accessing and sampling is function of the hardness of the investigated planetary body.

Sampling from unknown surfaces entitles challenges on the capability of the sampling technique; therefore, assigning localities of possible sampling using dielectric inversion from radar probing can provide an insight to subsurface hardness. This result in constraining drilling and sampling operational risks and maximise the scientific return from properly targeting the subsurface. As suggested by our laboratory measurements, the dielectric constant can be used to estimate the surface and subsurface hardness, which define the drilling rate to reach targets.

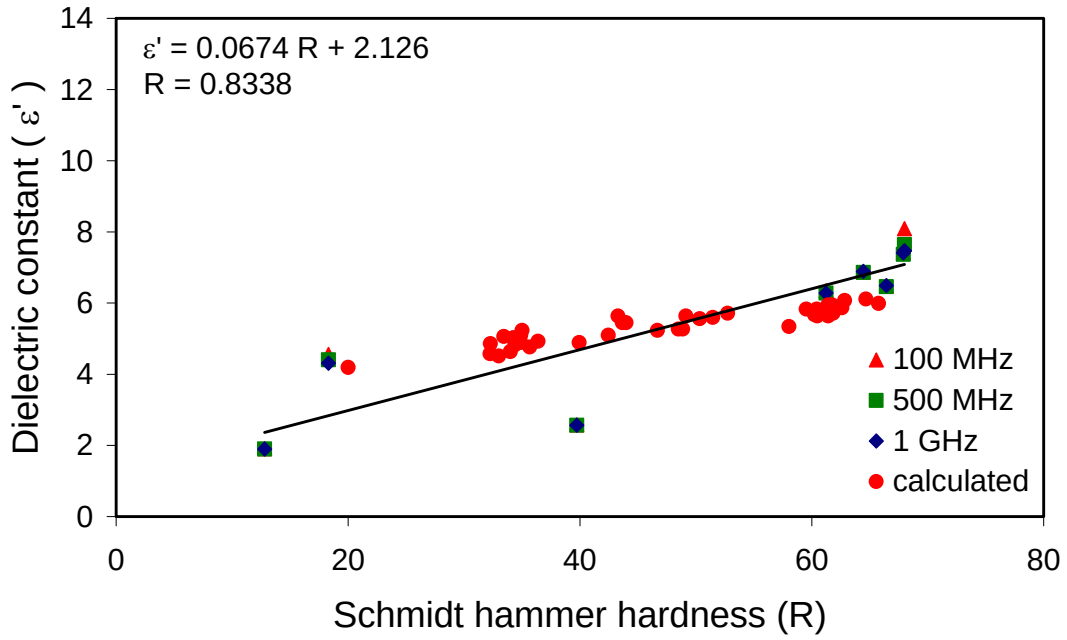

Figure 6.2. Dielectric constant versus Schmidt hammers hardness values for desiccated samples and the calculated dielectric constant (Aydin and Basu, 2005).

For a given weight on bit (WOB), as the subsurface hardness increases, the rate of penetration for the drill would decrease (Gstalder et al., 1966). Anttila (2005) conducted hardness and drill experiments on carbonates and volcanic rocks using a rotary drill. The drill operation power was 10 – 20 W and the WOB was in the range from 140 – 170 N. We converted (Anttila, 2005) hardness values from unconfined compressive strength (UCS) to Schmidt rebound hardness using equation 3 to determine the relation between the drill penetration rate and Schmidt hammer hardness method.

$$\boldsymbol{R = (0.2324 \times \sigma(MPa)) + 21.903}$$ (Kılıç and Teymen, 2008) (3)

Table 6.4 shows the UCS, drill penetration rate (DPR) (Anttila, 2005), sample density, calculated Schmidt hammer rebound number and computed dielectric constant of volcanic rocks (equation 2).

Figure 6.3 shows the drill penetration rate in cm/hr of (Anttila, 2005) samples as a function of the computed dielectric constant based on our relation (equation 2). A decrease in the drill penetration rate was observed with the increase in both rock hardness and the dielectric constant. Equation 4 shows the correlation between drill penetration rate using rotary drill and dielectric constant for volcanic rocks.

Table 6.4. Unconfined compressive strength, drill penetration rate, density, Schmidt rebound hardness number and dielectric constant of some volcanic rocks.

Rock types	σ_{ucs} (MPa)	DPR (cm/hr)	ρ (gm/cm^3)	R [a]	ε [b]
Calcite	50	8.1	2710	50.18826	4.38545
Diopside	120	5.75	3260	62.58867	5.481913
Diabase	220	3	3080	71.17416	7.048289
Mafurite	250	0.04	2545	72.98483	7.518202

[a] Calculated Schmidt hammer hardness based on (Aydin and Basu, 2005).

[b] Computed dielectric constant based on equation 2.

$$DPR = (-2.3561 \times \varepsilon') + 18.615 \quad (4)$$

Using our dielectric constant measurements of desiccated volcanic rocks and assuming a WOB of 100 – 200 N; we calculate the drill penetration rate based on equation 4 (Figure 6.4). Pumice and welded tuff have low dielectric constant and low hardness, therefore, they have high drill penetration rate of 12 and 14 cm/hr. Basalt from Lava sources have intermediate hardness and dielectric constant values where it's predicted drill penetration rate is about 8 cm/hr. The rest of the other types of basalts have high dielectric constant (6.4 – 7.5), higher hardness rebound number, which corresponded to low drill penetration rate (1 – 3.8 cm/hr). The future ExoMars rover will be weighting about 700 N on Mars (Brunskill et al., 2011); therefore, a WOB of 100 – 200 N, about 27% of the rover weight, will be stable and safe for drilling and sampling from the Martian subsurface.

6.5. Conclusions

In this research, we suggest a quantitative method to estimate ground hardness from radar dielectric inversion for drilling and sampling purposes. Radar probing is suggested to locate regions with highest drilling penetration rate in the subsurface based on retrieving low dielectric constant. The utility of such approach is crucial for not missing targets of opportunities such as shallow subsurface volatiles, losing drilling performance and saving power for the continuity of the investigation. An inverse correlation between drilling penetration rate based on rotary drill method and dielectric constant of volcanic rocks was concluded. This would minimize investigation ambiguities and enhancing sampling for future science return.

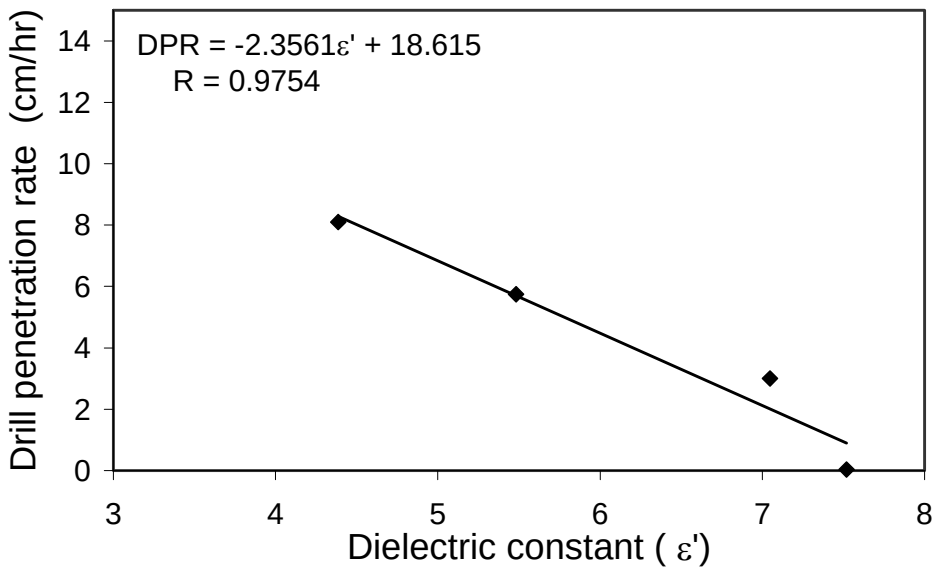

Figure 6.3. Drill penetration rate versus dielectric constant for carbonates and some volcanic rocks using rotary drill.

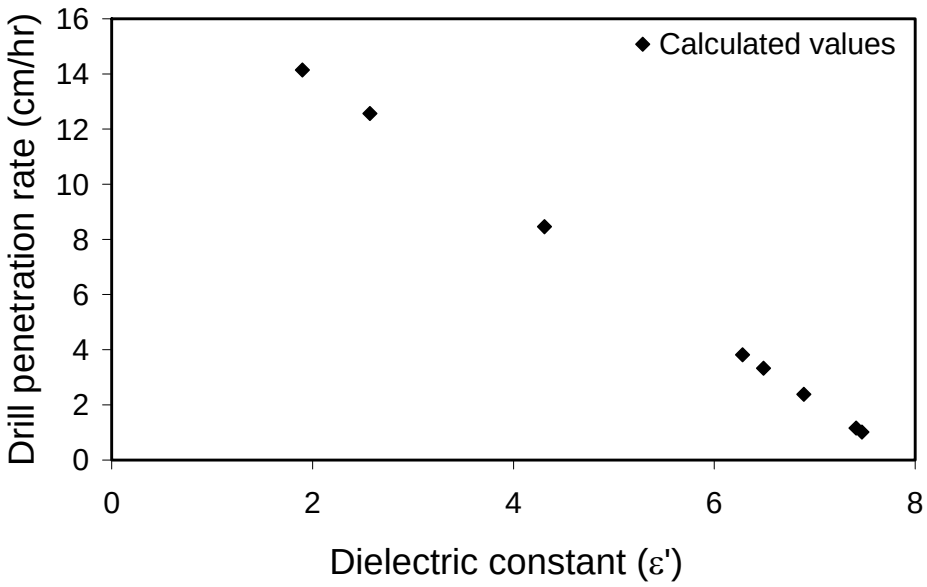

Figure 6.4. Calculated drill penetration rate for rotary drill versus dielectric constant of desiccated volcanic rocks.

6.6. References

Anttila, M. E. 2005. *Concept evaluation of mars drilling and sampling instrument*.

Aydin, A., and A. Basu. 2005. The schmidt hammer in rock material characterization. *Engineering Geology* 81 (1): 1-14.

ASTM, 2001. Standard test method for determination of rock hardness by rebound hammer method. ASTM Stand. 04.09 (D 5873-00).

Atkinson, RH, WE Bamford, E. Broch, DU Deere, and JA Franklin. 1978. Suggested methods for determining hardness and abrasiveness of rocks.

Biele, J. 2002. The experiments onboard the rosetta lander. *Earth, Moon, and Planets* 90 (1): 445-58.

Bowles, NE, SB Calcutt, and FM Reininger. 2012. The asteroid thermal mapping spectrometer: An imaging mid-IR spectrometer for the marco polo--R NEO sample return cosmic vision candidate mission. Paper presented at Lunar and Planetary Institute Science Conference Abstracts.

Brady, SM, SS Hughes, SEH Sakimoto, and TKP Gregg. 2005. Exploring the link between geochemistry and volcano morphology on the eastern snake river plain, a planetary analog to mars volcanism. Paper presented at 36th Annual Lunar and Planetary Science Conference.

Brown, ET. 1981. Rock characterization, testing and monitoring: ISRM. suggested methods.

Brunskill, C., N. Patel, T. P. Gouache, G. P. Scott, C. M. Saaj, M. Matthews, and L. Cui. 2011. Characterisation of martian soil simulants for the ExoMars rover testbed. *Journal of Terramechanics*.

Campbell, BA, JJ Plaut, JA Grant, and A. Freeman. 2009. Studying the near-surface geology of mars with imaging radar. Paper presented at AGU Fall Meeting Abstracts.

Ciarletti, V., C. Corbel, F. Cais, D. Plettemeier, SE Hamran, and M. Øyan. 2009. Performances of the WISDOM GPR designed for the shallow sounding of mars. Paper presented at Lunar and Planetary Institute Science Conference Abstracts.

Ericson, K. 2004. Geomorphological surfaces of different age and origin in granite landscapes: An evaluation of the schmidt hammer test. *Earth Surface Processes and Landforms* 29 (4): 495-509.

Goudie, A. S. 2006. The schmidt hammer in geomorphological research. *Progress in Physical Geography* 30 (6): 703.

Gstalder, S., and J. Raynal. 1966. Measurement of some mechanical properties of rocks and their relationship to rock drillability. *Journal of Petroleum Technology* 18 (8): 991-6.

Heggy, E., P. Paillou, G. Ruffié, JM Malezieux, F. Costard, and G. Grandjean. 2001. On water detection in the martian subsurface using sounding radar. *Icarus* 154 (2): 244-57.

Heggy, E., P. Paillou, F. Costard, N. Mangold, G. Ruffie, F. Demontoux, G. Grandjean, and JM Malézieux. 2003. Local geoelectrical models of the martian subsurface for shallow groundwater detection using sounding radars. *J.Geophys.Res* 108 (E4): 8030.

Heggy, E., SM Clifford, RV Morris, P. Paillou, and G. Ruffie. 2004. On the dielectric properties of the martian-like surface sediments. Paper presented at Lunar and Planetary Institute Science Conference Abstracts.

Hucka, V. 1965. A rapid method of determining the strength of rocks in situ. Paper presented at International Journal of Rock Mechanics and Mining Science & Geomechanics Abstracts, .

Kofman, W., and A. Safaeinili. 2004. Radar techniques applied to subsurface studies in solar system exploration. Paper presented at Tools and Technologies for Future Planetary Exploration.

Kılıç, A., and A. Teymen. 2008. Determination of mechanical properties of rocks using simple methods. *Bulletin of Engineering Geology and the Environment* 67 (2): 237-44.

Lauretta, DS, and O. R. Team. 2012. An overview of the OSIRIS-REx asteroid sample return mission. Paper presented at Lunar and Planetary Institute Science Conference Abstracts.

Olhoeft, G. R., and Geological Survey (US). 1979. Tables of room temperature electrical properties for selected rocks and minerals with dielectric permittivity statistics.

Parkhomenko, E. I., and G. V. Keller. 1967. *Electrical properties of rocks.* Plenum Press New York.

Plettemeier, D., S. Balling, W. S. Benedix, V. Ciarletti, S. E. Hamran, C. Corbel, and S. Linke. 2009. Ultra light-weight antenna system for full polarimetric GPR applications. Paper presented at EUROCON 2009, EUROCON'09. IEEE, .

Rehbinder, PA, LA Schreiner, and KF Zhigach. 1948. Hardness reducers in drilling. *Translated from Russian.) CSIR, Melbourne*.

Safaeinili, AA. 2007. Radar sounding at decameter wavelengths: Applying the lessons learned at mars to the investigation of icy bodies. Paper presented at AGU Fall Meeting Abstracts.

Stillman, D., and G. Olhoeft. 2008. Frequency and temperature dependence in electromagnetic properties of martian analog minerals. *J.Geophys.Res* 113 : E09005.

Ulaby, F. T., T. H. Bengal, M. C. Dobson, J. R. East, J. B. Garvin, and D. L. Evans. 1990. Microwave dielectric properties of dry rocks. *Geoscience and Remote Sensing, IEEE Transactions on* 28 (3): 325-36.

Van Winnendael, M., P. Baglioni, and J. Vago. 2005. Development of the ESA ExoMars rover. Paper presented at Proc. 8th Int. Symp. Artif. Intell., Robot. Automat. Space.

Weren, SL, SEH Sakimoto, SS Hughes, and TKP Gregg. 2004. Comparison of plains volcanism in the tempe terra region of mars to the eastern snake river plains, idaho with implications for geochemical constraints. Paper presented at Lunar and Planetary Institute Science Conference Abstracts.

CHAPTER 7: DISCUSSION

Penetration and sampling from planetary bodies provide insight into their formation and evolution history. The amplitude of the gravity field defines the optimal penetration and sampling mechanisms for planetary bodies. Sampling from the subsurface of planetary bodies (comets, asteroids, satellites and planets) is considered as one of the main objectives of planetary exploration missions since accessing the subsurface and obtaining pristine samples will enhances our understanding of the geology, morphology and history of the investigated planetary body. Anchoring the surface and capturing surface samples is the recommended technique for micro-gravity environments such as asteroids and comets. Additionally, other method such as firing the surface using bullets and collecting fragments is used on the Hayabusa mission. For planetary bodies which has substantial gravity field, Drilling, penetrating and harpooning the surface and collecting or casing samples are the suggested technique. All the above-mentioned sampling techniques require interaction with the surface and the shallow subsurface. Feasibility of accessing and sampling is function of the mechanical properties of the investigated planetary body.

The lack of knowledge of mechanical and physical regolith properties on other planetary bodies affected previous mission operation and will influence any future mission design and sampling activities. Due to the limited information about the lunar regolith before sending lander/rovers to investigate the Moon, there was a concern that the first lander/rover would sink into the lunar regolith. The Apollo Lunar Roving Vehicle (LRV) got bogged down in the lunar regolith during one of its traverse and the astronauts had to lift the vehicle and move it onto firmer ground (Carrier, 2008). The Soviet Lunokhod rover encountered a wheel sinkage up to 200 mm while roving on the Moon (Carrier, 2008). The MER Opportunity stuck in a regolith

trap on the surface of Mars but was able to free itself while the MER Spirit, got definitively stuck in the regolith in Gusev crater which led to the end of the rover (Showstack, 2010).

In order to assure the success of current and future mission, landing, roving, traversing, exploring and sampling the surface and the subsurface using in situ instruments, a considerable understanding of the nature of the regolith material and their behavior under planetary environmental conditions must be fully investigated. Therefore, discussion on the physical and mechanical properties of planetary regolith is grouped as:

1. Discussing the data provided by Lunokhod 2 on its mission to the Moon and testing our penetration model for better analyses the results.
2. Correlating the mechanical and electrical properties of planetary analogs to penetration testing for possible subsurface stratigraphy assessment.

7.1. Analysis of the penetration data provided by the Lunokhod rovers

Lunokhod 1 and 2 rovers were on-board Luna17 and 21 missions to the Moon. A 5 cm diameter penetrometer was equipped on Lunokhod 1 and 2, assigned to penetrate up to 10 cm deep with a maximum penetration mass of 23 kg in order to investigate the mechanical properties of the lunar subsurface (Leonovich et al., 1972). Along the traverse of Lunokhod 2 in the region of Lemonnier crater in the transitional zone from the sea region to the highland on the Moon; Lunokhod 2 conducted penetration testing using its cone penetrometer (Leonovich et al., 1972).

Figure 7.1 shows the penetration forces as a function of depth for various tests conducted on the Moon by the Lunokhod 2 penetrometer (Leonovich et al., 1976). Analysis of the

penetration curves suggested that curve 6 and the first part of curve 1 correspond to the maximum and minimum penetration forces on the Moon (Leonovich et al., 1976). These curves correspond to penetration into the hardest and loosest regolith materials (Leonovich et al., 1976). Up to that level of interpretation, no further analyses were reported about using the Lunokhod penetration forces to interpret the subsurface stratigraphy.

Luna 16 and 20 were equipped with a drill which was capable of drilling and sampling from the subsurface of the lunar regolith. These samples placed in a sealed capsule and sent to Earth for analysis. Table 1 shows mechanical and physical testing results performed on lunar regolith delivered to Earth by Luna 16 and 20 missions (Leonovich et al., 1976). Luna missions provided bulk density, angle of internal friction and void ratio for lunar regolith which correspond to the maximum and minimum penetration curves (curve 1 and 6) in Figure 7.1. Regolith bulk density found to have a minimum and maximum value of 1.04 and 1.798 kg m^{-3} corresponding to regolith void ratio of 1.88 and 0.67 and angle of internal friction of 25 and 50° respectively for Luna 20 samples and; a minimum and maximum bulk density of 1.115 and 1.793 kg m^{-3} with void ratio of 1.70 and 0.67 respectively reported for Luna 16 samples with minimum and maximum angle of internal friction of 25 and 50° (Table 1, Leonovich et al., 1976).

As shown in Figure 7.1, sudden changes in the penetration forces as a function of depth are observed from the character of the penetration curves which indicate inhomogeneities in the subsurface regolith. The main objective of this work is to theoretically reproduce the penetration forces as function of depth as in Figure 7.1 in order to estimate the subsurface densities which correspond to each penetration curve. The following theoretical frame work is used in the reproduction scheme:

The total penetration force (F_T) during probe insertion into the subsurface is the sum of two forces; the cone resistance (q_c) and the sleeve friction (f_s):

$$\boldsymbol{F_T = q_C A_C + f_S A_S} \tag{1}$$

Where A_c is the area of the cone, A_s is the buried area of the sleeve. The cone resistance can be calculated from (Puech et al*,* 2002):

$$q_C = \gamma \times Z \times Nq\left(1+\left(K \times \sin\varphi \times \frac{Z}{L}\right)\right) \tag{2}$$

Solving for the bearing capacity factor N_q (Puech and Foray, 2002):

$$N_q = \frac{q_c}{\gamma \times Z \times \left(1+\left(K \times \sin\varphi \times \frac{Z}{L}\right)\right)} \tag{3}$$

Where γ is the effective unit weight of the regolith (N m^{-3}), Z is the penetration depth (m), K is the coefficient of lateral pressure at rest (dimensionless), φ is the friction angle (degree) which is function of the relative density (Dr) and L is the lateral extension of the slip lines (m). The coefficient of lateral pressure is defined as (Harr, 1977).

$$K = 1 - \sin\varphi \tag{4}$$

The lateral extension of the slip lines L is defined as (Puech and Foray, 2002):

$$L = B \times \exp\left(\tfrac{\pi}{2} \times \tan\varphi\right) \times \tan\left(\frac{\pi}{4} + \frac{\varphi}{2}\right) \tag{5}$$

Where B is the cone diameter (m). The relative density (Dr) is an index that quantifies the degree of compaction (packing between loosest and densest state) of coarse-grained soils (Lunne et al., 1997):

$$D_r = \frac{e_{\max} - e}{e_{\max} - e_{\min}} \tag{6}$$

Where e is the void ratio of the sample. e_{max} is the maximum possible void ratio (loosest condition) and e_{min} is the minimum void ratio (densest condition) of the sand (Lunne et al., 1997).

In order to reproduce curves in Figure 7.1; we

1) Theoretically calculate the maximum and minimum bearing capacity factors using the penetration force curves 1 and 6; and their properties which are listed in Table 1 as input data and apply it into equation 3.
2) Correlate the maximum and minimum bearing capacity factors and regolith bulk densities to the angles of internal friction (Fig. 7.2).
3) Theoretically calculate the penetration forces using the estimated bearing capacity factors for curves 1 and 6 based on knowledge of the bulk density, void ratio and angle of internal friction (Table 1); and Plot them along the data provided by Lunokhood 2 (Fig. 7.3).
4) For the other curves (2 to 5) in Figure 7.1, we suggest a bulk density as input data in correlation with the mechanical properties in Figure 7.2 and apply it into equation 1 in order to calculate the theoretical penetration force at a specific bulk density. Once we get the theoretical force data, we plot it along the experimental data provided by Lunokhood 2 for each curve.
5) If there is no good matching between the theoretical force and the Lunokhood 2 data, we suggest another bulk density to get another theoretical force curve, until we get a good fit between the theoretical penetration forces and Lunokhood 2 data (Fig 7.4 to 7.8).

Curve 1 in Figure 7.4 showed two increasing trends of force as a function of depth, from 0 to ~5 mm, it is fitted and the bulk density is found to be 1798 kg m^{-3} and from ~ 20 to ~30 mm; it is fitted with a bulk density of 1570 kg m^{-3}. This indicates a decrease of density as a function of depth is at this location.

An increase in penetration force as a function of depth is observed for curve 2 (Fig. 7.5), the first 30 mm for curve 3 (Fig. 7.6) and the first 32 mm for curve 5 (Fig. 7.7). The fitted bulk density is 1650 kg m^{-3} for curve 2, 1350 kg m^{-3} for curve 3 and 1100 kg m^{-3} for curve 5.

Two density levels are observed for curve 4 (Fig. 7.8). From 0 to 30 mm the density is estimated to be 1200 kg m^{-3} while the rest of the curve is fitted with a density 1330 kg m^{-3}.

The rest of the penetration depth for curve 3 (~30 to 100 mm) and curve 5 (~38 to 43 mm) could not be reproduced using the model due to limitation in the model. Therefore, the density corresponding to the depth of ~30 to 100 mm in curve 3 is less than 1350 kg m^{-3} and the depth of ~38 to 43 mm for curve 5 is greater than 1100 kg m^{-3} since the data are below the fit for curve 3 and above the fit for curve 5.

Table 7.1. Bulk density and coefficient of porosity (void ratio) of lunar regolith (Leonovich et al., 1976).

Parameters	Luna 20		Luna 16	
	Losse	Packed	Losse	Packed
Bulk weight (g cm^{-3})	1.04	1.798	1.115	1.793
Coefficient of porosity (void ratio)*	1.88	0.67	1.70	0.67
Angle of internal friction (Deg)	25	50	25	50

*Assuming regolith specific weight of 3 g cm^{-3}

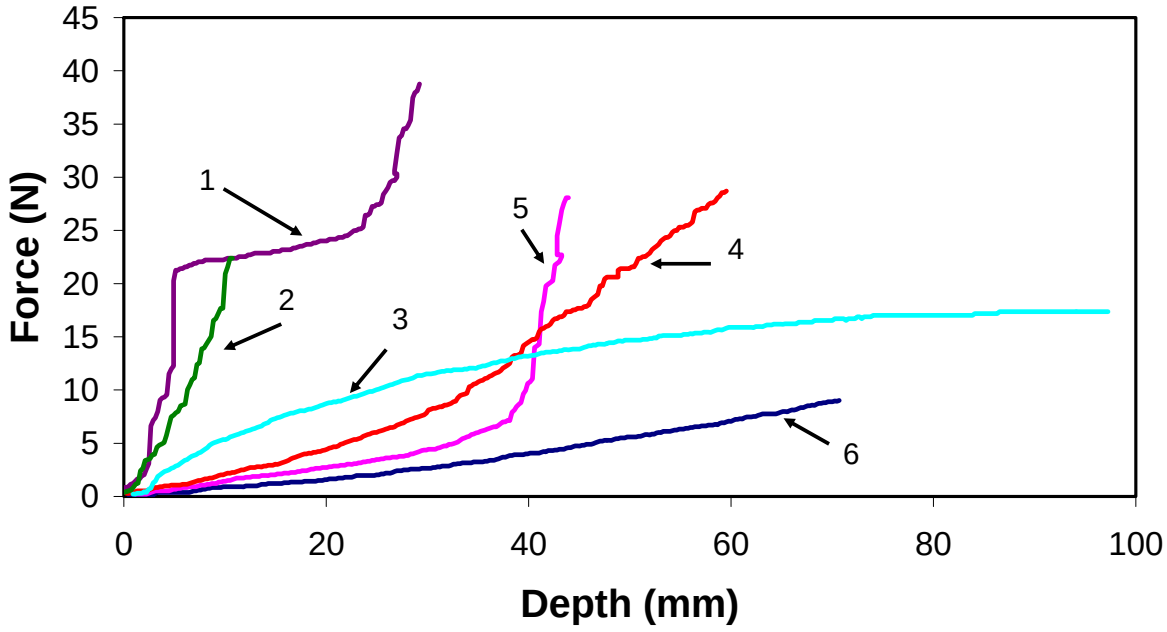

Figure 7.1. Penetration forces as a function of depth on the Moon conducted by Lunokhod 2.

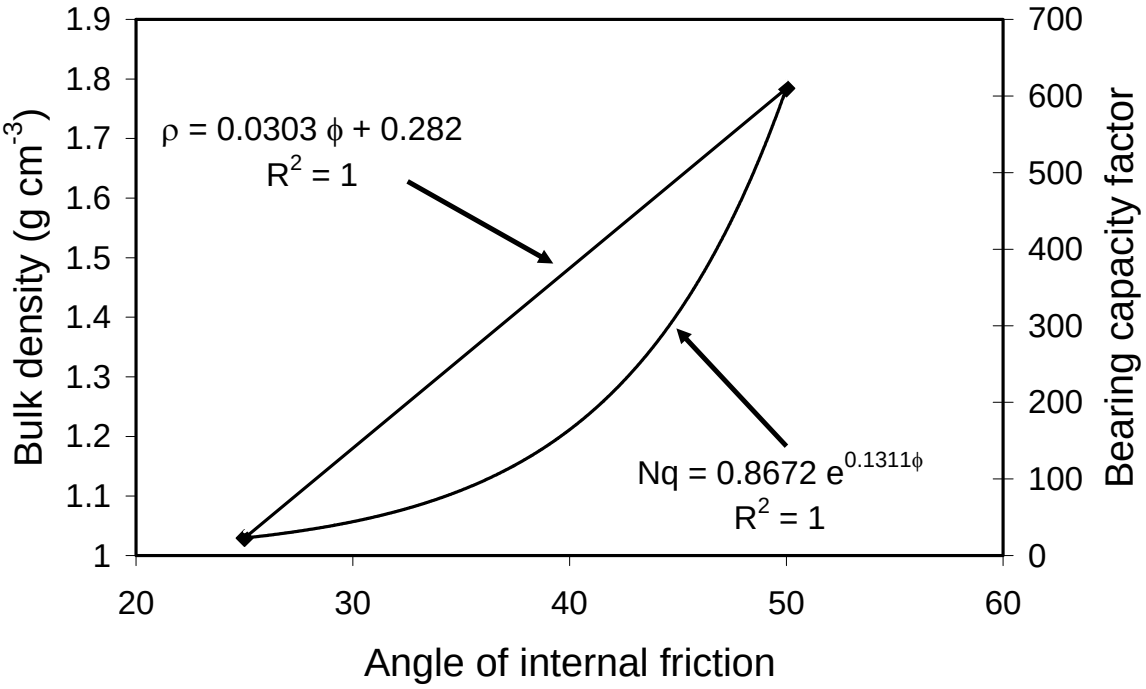

Figure 7.2. Regolith bulk density and bearing capacity factor as a function of the angle of internal friction for lunar regolith.

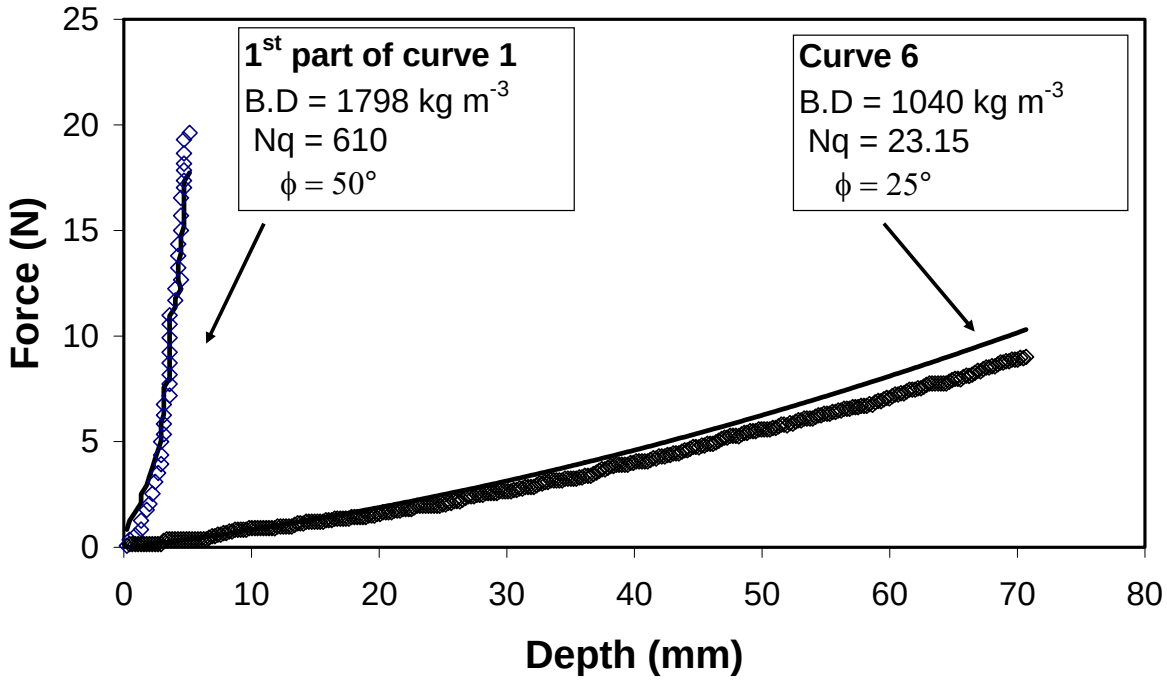

Figure 7.3. Maximum and minimum force as a function of depth conducted by Lunokhod 2 as well as the theoretical predicted force of penetration for part of curve 1 and curve 6.

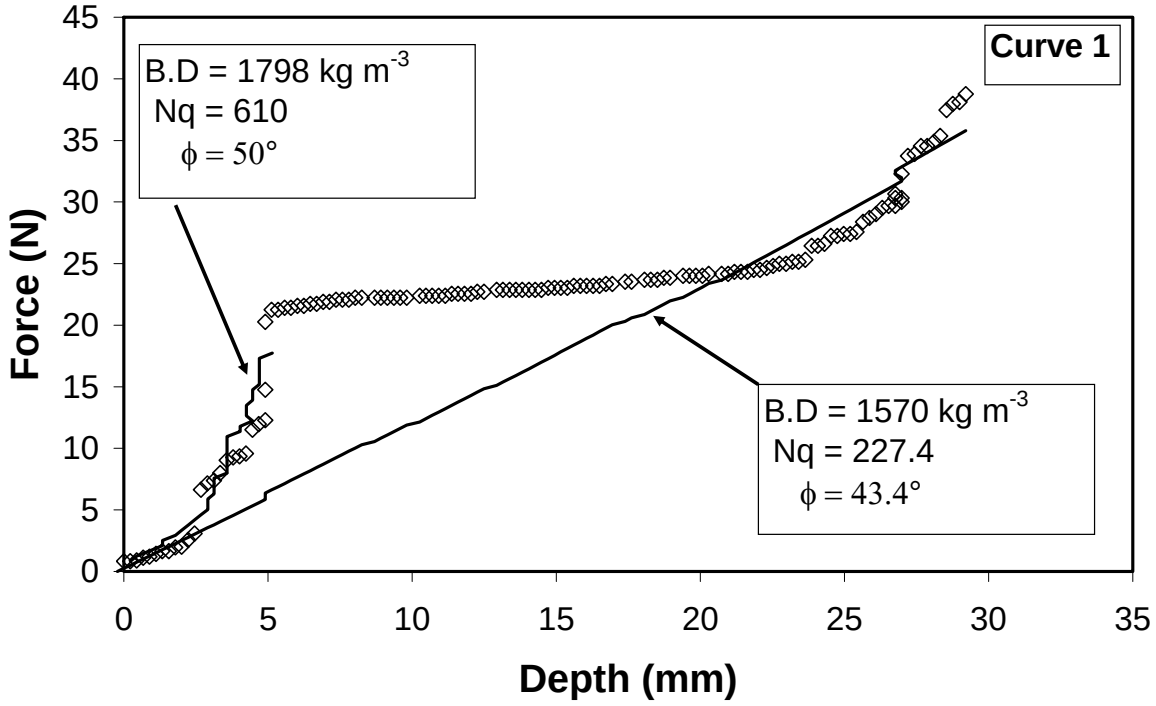

Figure 7.4. Cure 1 of penetration force as a function of depth conducted by Lunokhod 2 and its corresponding theoretical forces.

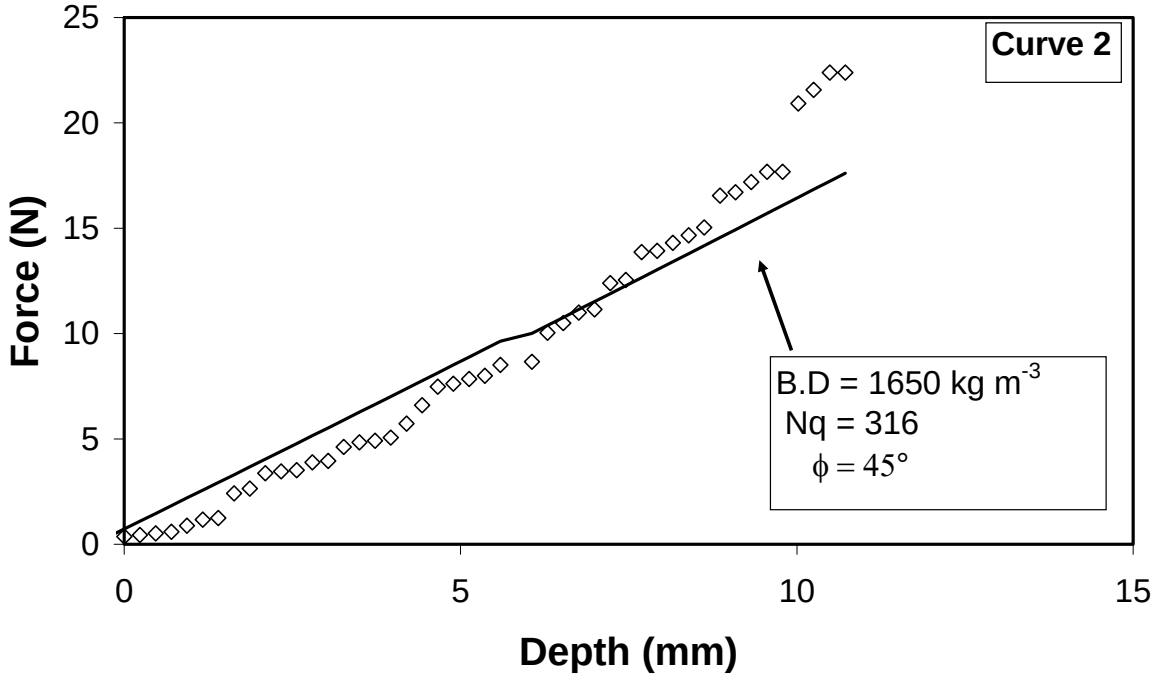

Figure 7.5. Cure 2 of penetration force as a function of depth conducted by Lunokhod 2 and its corresponding theoretical forces.

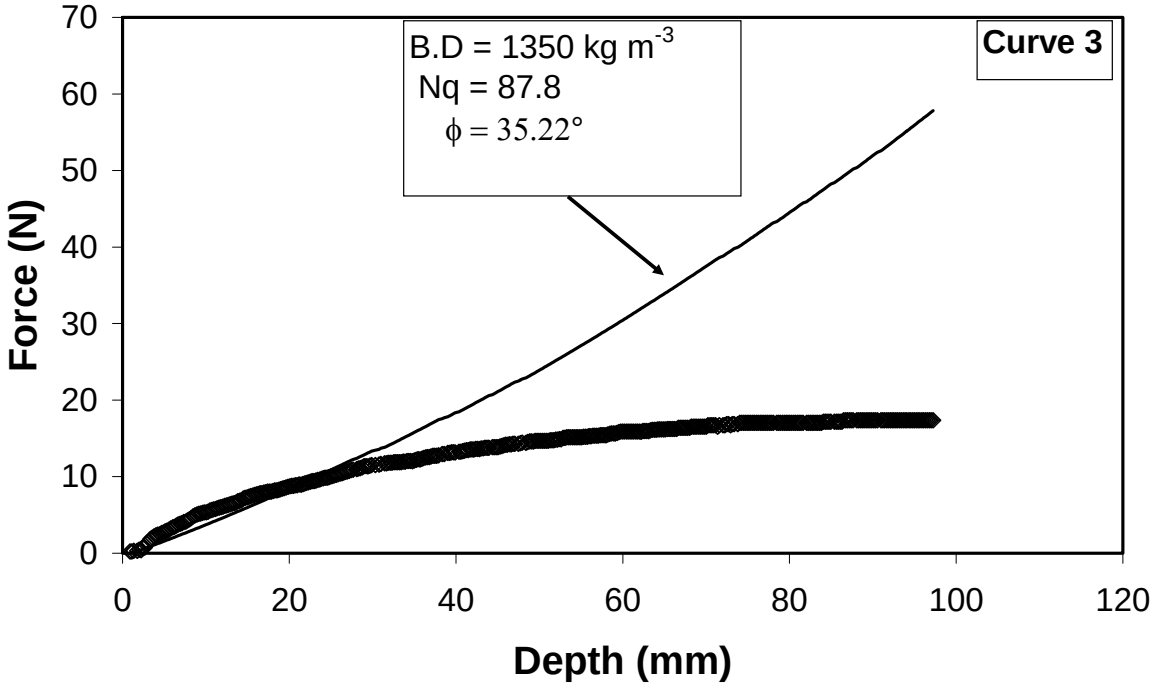

Figure 7.6. Curve 3 of penetration force as a function of depth conducted by Lunokhod 2 and its corresponding theoretical forces.

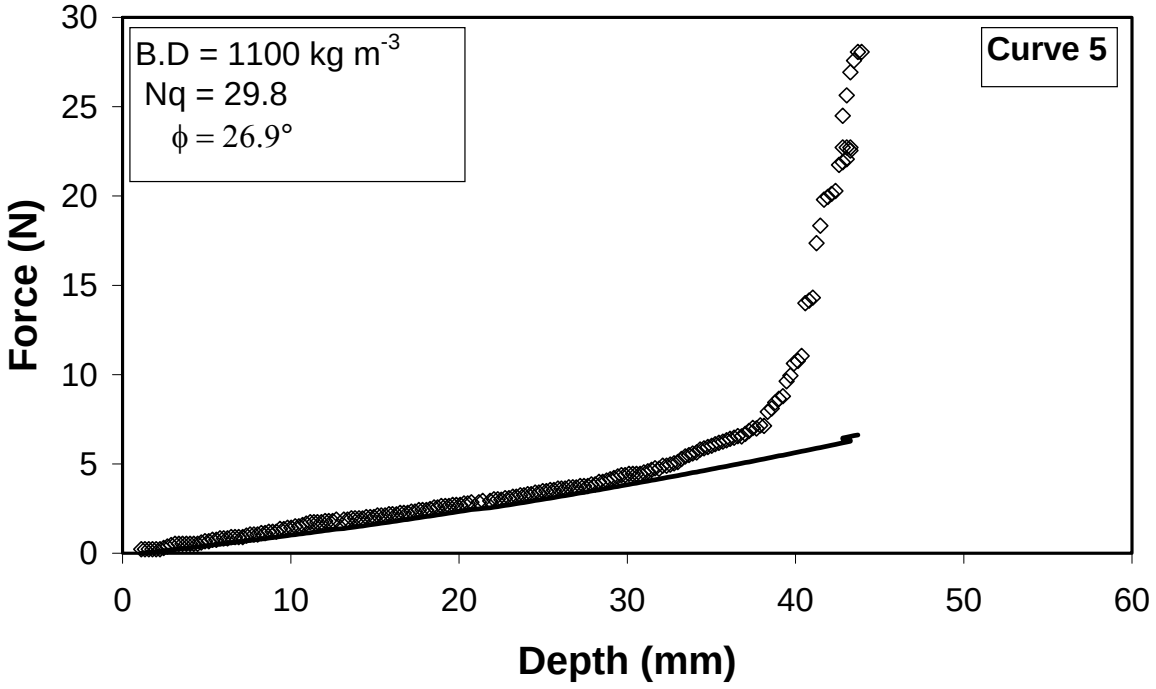

Figure 7.7. Curve 5 of penetration force as a function of depth conducted by Lunokhod 2 and its corresponding theoretical forces.

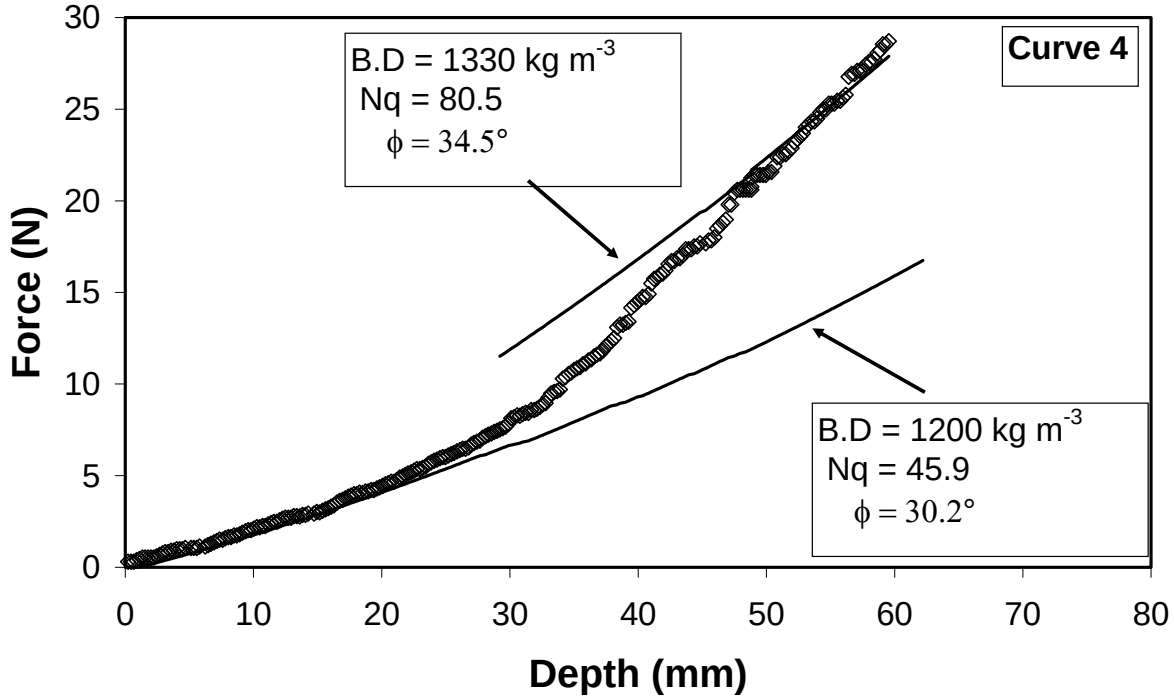

Figure 7.8. Curve 4 of penetration force as a function of depth conducted by Lunokhod 2 and its corresponding theoretical forces.

Table 2 shows the calculated density and porosity which correspond to curves 1 – 6 in Figure 7.1. The calculated porosity varied from a minimum of 0.4 to a maximum of 0.65 along a change in the density from a minimum of 1040 to a maximum of 1798 kg m^{-3}. Figure 7.9 shows a subsurface stratigraphic section of bulk density as a function of depth for curve 1 – 6 after processing the curves conducted by Lunokhood 2 penetrometer. As seen from Figure 7.9, the second part of curves 1, 5 and 3, 6 have a close bulk density values of ~ 1570 and ~ 1040 kg m^{-3}. Since curves 1 through 6 in Figure 7.1 are conducted at different locations along the path of Lunokhood 2. We can assume that a subsurface fault may be causing the similarity signatures seen on the second part in the penetration forces curves 1, 5 and 3, 6.

Based on the analysis of Lunokhod 2 data, increasing in the subsurface density correspond to an increase in the force of penetration. As shown in Figures 7.3 through 7.8, huge inhomogenitites of the subsurface are observed where density varied from a minimum of 1040 to a maximum of 1798 kg m^{-3} which are due to variation of subsurface porosity along the route of Lunokhod 2 at different depth. Therefore, it is possible to predict the subsurface density from penetration force curves.

Table 7.2. Processed density and porosity of curves 1 – 6 conducted by Lunokhood 2 penetrometer.

Curve No	Density (kg m^{-3})	Porosity
1	1798	0.40
	1570	0.47
2	1650	0.45
3	1350	0.55
4	1330	0.55
	1200	0.60
5	1100	0.63
6	1040	0.65

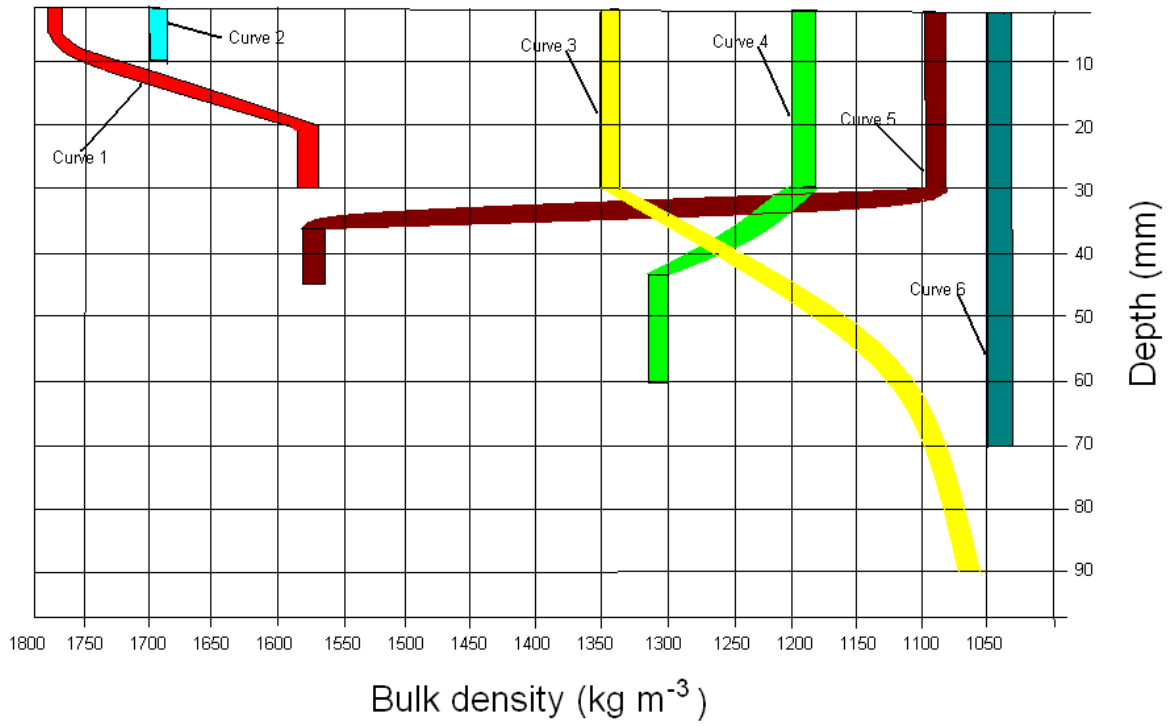

Figure 7.9. Stratigraphic section of the bulk density as a function of depth for curve 1 – 6 conducted by Lunokhood 2 penetrometer.

7.2. Correlating the mechanical and electrical properties to penetration forces

Penetrometer design can be adjusted to sample from the subsurface of planetary body with minimum disturbance into the subsurface layering. Uncertainty of the subsurface of planetary bodies, place a lot of constrains on the performance of the penetrometer especially if it is assigned for sampling. If the density of the formation where penetration will take place is high, this means more force for penetration is needed to compensate the high density. In such a case, penetration into this area may be over the penetrometer capability and there is a probability that the penetrometer may get stuck. Therefore, estimation the required force to penetrate and sample from the subsurface is mandatory for the success of the penetration and sampling mechanism.

Dielectric properties as inverted from radar subsurface sounding can be used to assess the ground mechanical properties as rock hardness, density and porosity. Penetration into the subsurface with emphasis on subsurface sampling return strongly depends on mechanical properties of the subsurface (density and porosity). Inversion of radargrams depends on the dielectric constant which is function of material density and porosity. Therefore, conjugating penetrometer supported by radar will enhance subsurface investigation and sampling. If we correlated between the forces required for penetration and sampling to dielectric properties of regolith materials, a pre-existed knowledge of the subsurface density can be drawn before taking the action of penetration. Radar can be used to probe the subsurface and assign localities of high scientific interest with the minimum penetration risk such as the CONSERT radar supporting the MUPUS penetrometer on board the Rosetta lander (Biele, 2002).

We here discuss the applicability of estimating the forces required for penetration and sampling based on knowledge of the dielectric constant of the investigated material. Based on

previous parts in the dissertation, it is observed that forces of penetration and dielectric constant of regolith material are both function of the density and porosity of the material under investigation.

In order to achieve our goal, we are going to:

1. Perform some penetration testing in JSC Mars-1 regolith analog at different prepared bulk densities.
2. Measure the dielectric constant of JSC Mars-1 at different bulk densities.
3. Correlate between the forces of penetration and dielectric constant of JSC Mars-1.

Figure 7.9 shows the dielectric constant of JSC Mars-1 measured at three frequency ranges (100, 500 MHz and 1 GHz) as a function of regolith bulk density. Dielectric constant is observed to increase from ~ 2 to ~ 9 along with an increase in regolith bulk density from 1200 to 1900 kg m^{-3}. Equation 1 shows the relationship between dielectric constant and bulk density of JSC Mars-1 regolith analog Figure 7.10.

$$\varepsilon = 0.0059\ \rho - 3.9217 \qquad (1)$$

Four different bulk densities of JSC Mars-1 are prepared for penetration testing and the used penetrometer is 1.2 cm in diameter. Figure 7.11 shows the effect of variation of regolith bulk densities on penetration forces. The forces of penetration increased from ~100 N at a bulk density of ~1120 kg m^{-3} to ~1600 N with bulk density of 1240 kg m^{-3}. The density effect is highly seen on penetration forces where it is observed to increase with increasing regolith bulk density.

Using equation 1, we calculated the dielectric constant of JSM Mars-1 regolith analog for the measured bulk densities used for penetration testing (Table 3). At the measured bulk densities, the calculated dielectric constant is found to increase from 2.68 to 3.39 corresponding

to an increase in bulk densities from 1120 to 1240 Kg m^{-3} which implies an increase in penetration forces (Fig 7.11).

Based on this investigation, estimating the regolith density and predicting the possible penetration forces for subsurface investigation can be assessed from knowledge of the dielectric constant. Combining a radar and penetrometer on a rover or lander will enhance subsurface exploration by assigning localities of high scientific return and minimization of penetration risks.

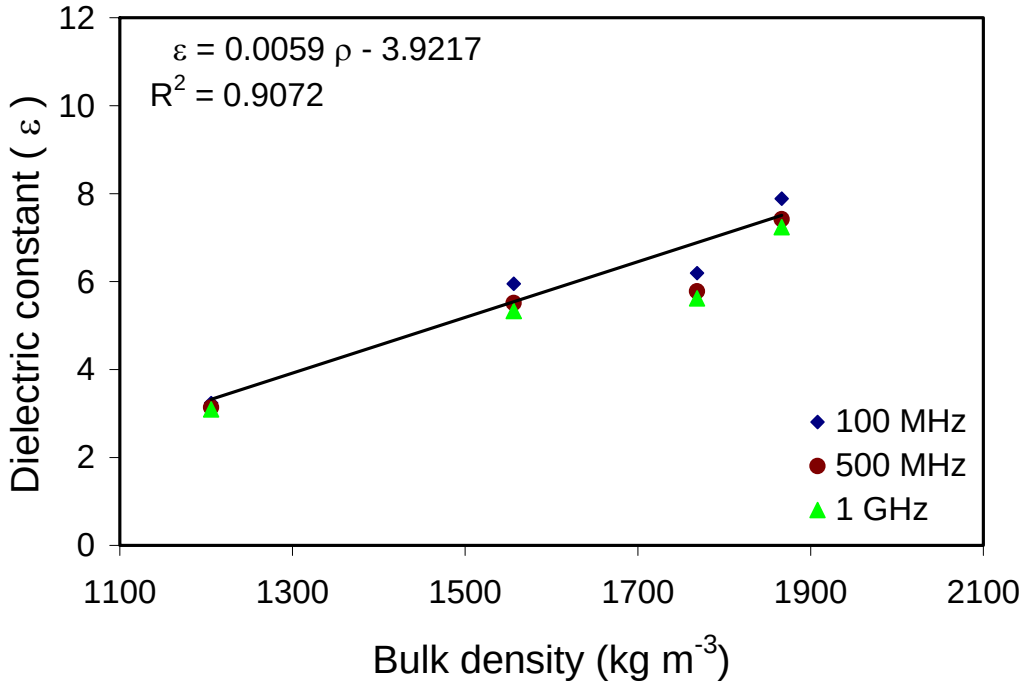

Figure 7.10. Dielectric constant versus regolith bulk density for JSC Mars-1.

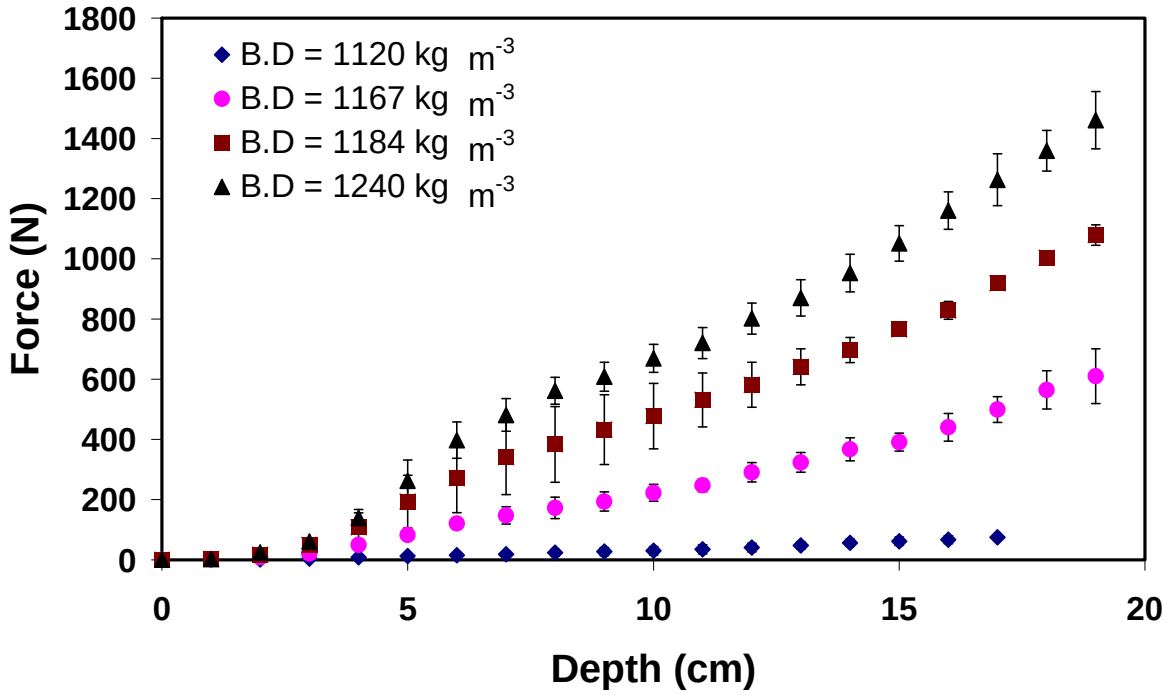

Figure 11. Variation of bulk density and dielectric constant for different penetration testing in JSC Mars-1.

Table 7.3. Bulk density and calculate permittivity for JSC Mars-1

Bulk density (Kg m^{-3})	Calculated permittivity
1120	2.68
1167	2.96
1184	3.06
1240	3.39

7.3. References

Biele, J. 2002. The experiments onboard the rosetta lander. *Earth, Moon, and Planets* 90 (1): 445-58.

Bulekov, VP, AS Buyalo, Y. V. Makarov, and VV Markachev. 1974. Results of an investigation of drilling instruments working aboard the automatic lunar stations luna 16 and luna 20. Paper presented at Metrologiya i metody optiko-fiz. izmerenij, p. 29-30.

Carrier, D., Lunar Geotechnical Engineering – Lessons Learned from Apollo, PTMSS conference, 9 June 2008, Sudbury, Ontario, Canada.

Harr, M. E. Mechanics of particulate media, 260, McGraw-Hill. 1977.

Leonovich, AK, VV Gromov, AD Dmitriev, VA Lozhkin, VN Penetrigov, PS Semionov, IN Grannik, VP Grushevskii, and VV Shvariov. 1976. Investigation of the physical and mechanical properties of the lunar sample brought by luna-20 and along the route of motion of lunokhod 2. *In: Space Activity Impact on Science and Technology.(A76-35711 17-12) Oxford, Pergamon Press, Ltd., 1976, p.321-332.* 1 : 321-32.

Leonovich, AK, VV Gromov, AV Rybakov, VN Petrov, PS Pavlov, II Cherkasov, and VV Shvarev. 1972. Investigations of the mechanical properties of the lunar soil along the path of lunokhod 1. Paper presented at Space Research.

Lunne, T., P. K. Robertson, J. J. M. Powell. Cone Penetration Testing in Geotechnical Practice, first ed. Blackie Academic and Professional, London, 1997.

Puech, A., and P. Foray. Refined model for interpreting shallow penetration CPTs in sands, Offshore Technology Conference, 6 -9 May 2002, Houston, Texas, 2002.

Showstack, R. 2010. Mars rover enters new phase of mission. *Eos Trans.AGU* 91 (5).

CHAPTER 8: CONCLUSIONS

This dissertation demonstrated that knowledge of the mechanical and electrical properties of planetary analogs is crucial for subsurface investigation, interpretation, and protection for future planetary exploration.

Penetration testing experiments in planetary regolith analogs showed that the total resistance penetration is affected by the mechanical properties of regolith. An increase in penetration force indicates an increase in the subsurface density. From assessment of the subsurface density, estimation of mechanical properties can be predicted such as porosity, void ratio and friction angle. An increase in the subsurface density indicates lower porosity, higher friction angle and higher bearing capacity. Using the penetration experiments conducted in JSC Mars-1 and Mojave soil as well as knowledge of their mechanical properties allowed correlating the mechanical properties to forces of penetration. This correlation will allow sensing and differentiating between different subsurface layers and inversion of subsurface density and porosity from penetration forces.

Estimation of the penetration forces on the Moon using penetrometers is possible using regolith analogs and the penetration model is verified with in-situ penetration experiments. Based on measurements of the density and void ratio of lunar regolith samples conducted on the Earth brought by Luna 20, we were able to reproduce the penetration testing performed by Lunokhod penetrometer and we estimated the subsurface density. Analysis of the results showed that the lunar subsurface is heterogeneous and a shift in the subsurface density as a function of depth is observed which may be due to faulting.

Penetration forces should not exceed the weight of the lander or the rover on the surface of the planetary body, otherwise, the whole lander or rover will lose its contact with the surface and place the whole mission in danger. Prediction of penetration forces for Mars can place a threshold to the weight of the lander or the rover. Therefore, simulating force of penetration on planetary analogs will constrain the mass of the lander or the rover which will prevent it from over penetration. Results of this investigation will improve future subsurface investigations of the Martian surface in terms of mission design, landing site selection and will be helpful the interpretation of physical, mechanical and geomorphological investigations as well.

Since penetration testing is highly affected by regolith bulk density as well as the dielectric constant, we correlated the penetration testing to regolith dielectric constant. An increase in penetration force is observed with an increase in the dielectric constant. Based on this correlation, estimation of the required penetration force or assessment of the subsurface dielectric constant is feasible. Therefore, combining radar and penetrometer on the same platform and coordination between both instruments will enhance subsurface exploration and will reduce penetration risks.

We simulated gully formation under different bulk densities with the objective of correlating mechanical and electrical properties of the regolith to gully shape. Simulation of gully experiments using JSC Mars-1 regolith analogs as a function of different bulk densities showed a correlation as function of gully total length existed. Gully total length, regolith dielectric constant and angle of internal friction found to be function of the density of the prepared sample. An increase in the subsurface density will correspond to an increase in gully

total length, regolith angle of internal friction and dielectric constant. Based on this investigation, geomorphological features such as gullies can be interpreted in terms of morphometrics, density and dielectric constant using orbital camera and radar which will enhance previous, current and future geomorphological investigation.

Drill penetration rate of planetary bodies for sampling purposes is function of subsurface hardness. Dielectric properties as inverted from radar subsurface sounding can be used to assess the ground mechanical properties as rock hardness, density and porosity. We suggest a quantitative method to estimate ground hardness from radar dielectric inversion for drilling and sampling purposes. We found the dielectric constant to increase with increasing rock hardness. An inverse correlation between drilling penetration rate based on rotary drill method and dielectric constant of volcanic rocks was concluded. The utility of such approach is crucial for not missing targets of opportunities such as shallow subsurface volatiles, losing drilling performance and saving power for the continuity of the investigation. This would minimize investigation ambiguities and enhancing sampling for future science return.

Appendices

Appendix A: Penetration Testing of the Optical Probe for Regolith Analysis (OPRA)

Available online at www.sciencedirect.com
ScienceDirect
Advances in Space Research 46 (2010) 327–336
ADVANCES IN SPACE RESEARCH (a COSPAR publication)
www.elsevier.com/locate/asr

Penetration testing for the Optical Probe for Regolith Analysis (OPRA)

A. ElShafie [a,*], V.F. Chevrier [a], R. Ulrich [a,b], L. Roe [a,c]

[a] Arkansas Center for Space and Planetary Sciences, University of Arkansas, 202 Old Museum Building, Fayetteville, AR 72701, USA
[b] Department of Chemical Engineering, University of Arkansas, Fayetteville, AR 72701, USA
[c] Department of Mechanical Engineering, University of Arkansas, Fayetteville, AR 72701, USA

Received 1 November 2009; received in revised form 9 March 2010; accepted 11 March 2010

Abstract

The Optical Probe for Regolith Analysis (OPRA) is a spike-shaped subsurface analytical probe that will be delivered to a planet, asteroid, or cometary body by a lander and/or rover. OPRA will be pushed down into the subsurface to record near infrared spectra as a function of depth down to maximum of 50 cm. Therefore, knowledge of the required penetration force to specific depths can be helpful in estimating the length of the probe. Test probes covering the anticipated diameter (2.5, 1.9, 1.2 and 0.9 cm diameter) and tip angle (T.A. = 30°, 60°, 90° and 120°) of OPRA were inserted mechanically into dry playground sand. The results showed that tip angle does not have a major effect, while probe diameter and density of the regolith are the most important parameters. Increasing probe diameter from 0.9 to 1.9 cm (i.e. a factor of 2) leads to an increase in penetration force from 200 to 1000 N (i.e. a factor of 5) at 20 cm depth. An increase in bulk density (B.D.) from 1550 to 1700 kg m^{-3} leads to an increase in penetration force from 10 to 200 N at 20 cm depth. Bearing capacity theory was used to explain the downward movement of the penetrometer through regolith and showed good agreement with the experimental results. This model was then used to take into account the effect of gravity on other planetary bodies. We observed a good agreement between the theoretical model and results from penetration testings on the Moon by the Apollo missions. Since the maximum allowed force for penetration is the weight of the lander/rover on their targeted planetary surface, our results put a strong constraint on the maximum reachable depth without endangering the whole mission.

Keywords: Penetrometry; Planets; Planetary probes

1. Introduction

Much of the history of rocky planetary bodies is revealed by studying the records of past events that are preserved in their surface geology. Younger layers are present on the top of older layers, based on the principle of superposition, which reveals the chronological order of geological events. According to the principle of original horizontality, each layer is formed horizontally but their orientation can be modified by various processes that can result due to uplifting and folding (Longwell and Flint, 1962).

Investigating microgravity planetary bodies (i.e. comets, asteroids) is of high interest since they are remnant of the primitive solar system. Not only could they provide information about the history of the solar system but also they could enhance our understanding of its evolution. Due to space weathering, surface compositions of asteroids are often altered compared to their internal structure (Chapman, 1996). Therefore, telescopic measurements of asteroids rarely match laboratory reflectance spectra (Binzel et al., 2010). Regolith layer on asteroids vary according to the size of the asteroids. Asteroids of moderate size (100–300 km diameter) have about 1 km depth of regolith material (Housen and Wilkening, 1982).

Layering has been observed on almost every solid body in the solar system with individual thicknesses from a few millimeters to hundreds of meters, and with bed depths up to kilometers in vertical extent. Penetrometry, hyper velocity impactors, excavators and drills are different methods which

* Corresponding author.
E-mail address: aelshafi@uark.edu (A. ElShafie).

0273-1177/$36.00 © 2010 COSPAR. Published by Elsevier Ltd. All rights reserved.
doi:10.1016/j.asr.2010.03.017

are used to investigate the subsurface structure and composition of planetary bodies (Glaser et al., 2008).

A penetrometer is a cone at the end of a cylinder which is used to investigate the surface and subsurface of planetary bodies by pushing it into granular material (Lunne et al., 1997). Cone Penetration Testing (CPT) is the technique of measuring the resistance force which is encountered by a penetrometer which increases with depth. CPT is widely used for terrestrial applications. CPT was earlier named the static penetration test, quasi-static penetration test and Dutch sounding test. The first Dutch cone penetrometer test was made in 1932 by P. Barentsen in Holland and it was pushed down by hand. The penetrometer had a cone surface area of 10 cm^2 and a 60° tip angle. CPT can be used to determine subsurface stratigraphy, estimate some geotechnical parameters and predict future changes of the soil due to loading (Lunne et al., 1997). In fact, two American Society for Testing and Materials (ASTM) standards (ASTM D3441-05) and (ASTM D5778-07) are describing the methodology of CPT.

In the second workshop on penetrometry in the solar system, Kargl et al. (2006) divided penetrometers into two main categories: fast and slow penetrometers. Fast penetrometers are released from a spacecraft and hit the planetary surface with enough velocity so that their kinetic energy provides the required penetration force. Slow penetrometers are released from landers or rovers on the surface of the target body and penetrate the subsurface through forces applied by mechanical means. Slow penetrometers are divided into static penetrometers, which utilize a steady penetration force, and dynamic penetrometers, which apply periodic impact such as hammering.

The Apollo Simple Penetrometer (ASP) was part of the Apollo 14 Lunar Surface Experiment Package (ALSEP) and was used to investigate soil mechanics on the moon. The ASP was a metal rod 68 cm long and 0.95 cm in diameter with a 30° cone angle. The ASP was used in three penetration tests by manually pushing it into lunar soil. The ASP reached depths of 42, 44 and 50 cm and the penetration force was in the range of 70–135 N using one hand. A second deployment of the ASP reached a depth of 62 cm and required a force of 225 N using both hands (Mitchell et al., 1971).

A Self-Recording Penetroemter (SRP) was used on the Apollo 15 and 16 missions. This instrument was connected to a drum which recorded the force versus depth. At a maximum depth of 76 cm, the Apollo 15 SRP recorded a force of 111 N and the Apollo 16 SRP recorded a maximum force of 215 N (Mitchell et al., 1974).

The ACC-E, a piezoelectric force sensor (impact penetrometer) which was part of the Surface Science Package (SSP) onboard the Huygens probe, is used to investigate the subsurface of Saturn's moon Titan (Lorenz et al., 1994). From the impact force profile of the thumb-size sensor (mass of 15 g) the density, cohesion and particle size distribution of the subsurface materials were estimated during the first 40 mm of penetration (Zarnecki et al., 2002). The results indicated that the surface has a weak crust and, beneath that, a structure consisting of wet sand and embedded pebbles (Zarnecki et al., 2005).

The Planetary Underground Tool (PLUTO) mole, was an instrument on board the Beagle 2 lander, as part of the Mars Express mission (Richter et al., 2002). It was considered as a dynamic penetrometer (Stoker et al., 2003). The mole was capable of delivering a maximum force of 50 N per shock where it reached to a depth of 3.9 mm in loose sand and 0.8 mm in stiffish sand on Earth (Kochan et al., 2001).

OPRA (Optical Probe for Regolith Analysis, Fig. 1A) is a static penetrometer with vertically stacked windows that would be inserted from either a lander or rover into regolith or unconsolidated ices on the surface of a planet, asteroid, moon or comet (Pilgrim et al., 2009). These windows are connected by fiber optics to an IR spectrometer located in the body of the spacecraft. The spectrometer will address each window individually, providing swept frequency illumination to the subsurface material outside the window and simultaneously returning the reflected signal to the unit. The result will be a spectral composition profile of the subsurface material sampled every couple of centimeters down to a maximum depth of about 50 cm. If a borehole is already available, OPRA could be lowered into it. The accuracy of the subsurface investigation will depend on the diameter of the borehole, and in turn the distance between the embedded sensors inside OPRA and the borehole wall. Because the probe will be thin (around 1 cm in diameter) and since the heat-producing electronics are in the spacecraft, disturbance of the subsurface layers should be minimal. There are no moving parts in the probe and all electronics will be located in the warm-box within the rover or spacecraft body. The spectral range of the instrument is nominally 0.5–5 μm (20,000–2000 cm^{-1}) which is suitable for mineralogical and chemical characterization of the subsurface, including the water band at ~3 μm and various ices (CO_2, clathrates).

In order to meet the intended science objectives, OPRA will have the shape of a penetrometer with windows placed laterally along the side (Fig. 1B). These windows will protect the fiber optic cables from being in direct contact with the subsurface materials. Some fibers will carry illumination to the windows and others will carry the returning signal to the IR instrument. The number of windows is a function of the probe diameter, length and fiber optic diameter (Pilgrim et al., 2009).

The principal objective of the experiments described in this paper is to determine the optimized diameter, tip angle which correspond to minimum insertion and withdrawal forces for OPRA for unconsolidated surfaces. This is done by measuring the amount of force needed to insert and extract various probes covering a range of these key variables into a regolith analogue. Sand was our choice of analogue material because it is a well-studied material and has a bulk density and particle size distribution similar to that is found on some planetary bodies such as Mars and the

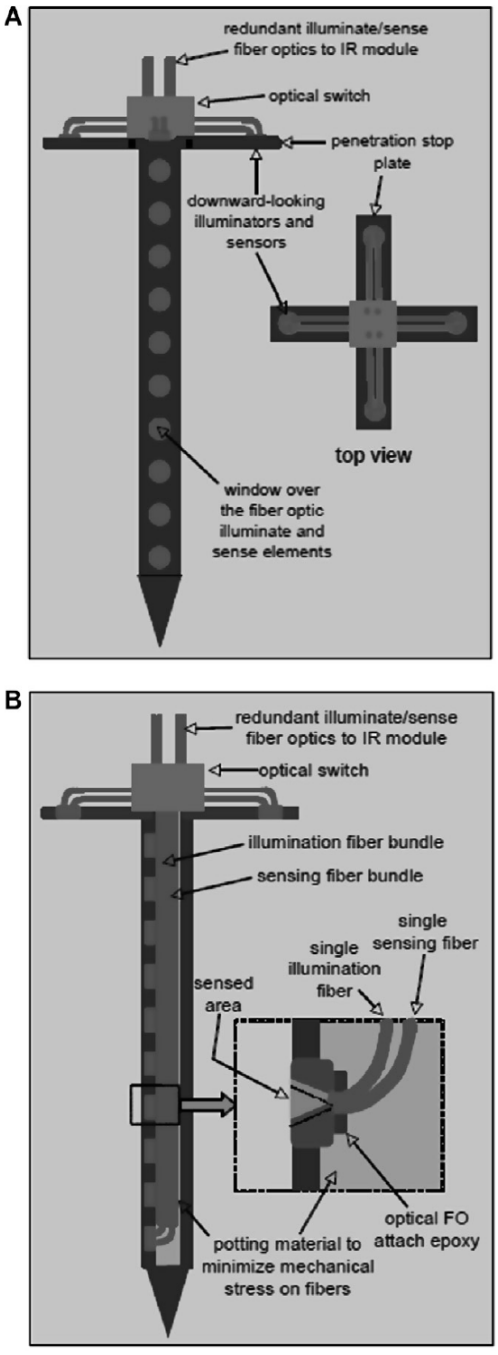

Fig. 1. Schemes of the Optical Probe for Regolith Analysis (OPRA). (A) Front view. (B) Side view.

Moon. Apollo 11 reported minimum and maximum bulk densities of 1360 and 1800 kg m^{-3} on the Moon (Mitchell et al., 1974). On Mars, an average bulk density of 1520 kg m^{-3} is indicated by Mars Pathfinder rover (Matijevic et al., 1997). The knowledge of regolith mechanical parameters allows theoretical applications such as the bearing capacity model to be used in geotechnical engineering and applied to the penetration resistance in sand (Terzaghi, 1943; Vesic, 1963; Hansen, 1970; Puech and Foray, 2002). In addition to the engineering requirements to minimize the force necessary to insert the probe, key properties of the regolith can be inferred from the force measurements,

Table 1
List of symbols used in the paper.

Symbol	Def.
A_c	Area of the cone (m^2)
A_s	Area of the sleeve (m^2)
B	Cone diameter (m)
D	Probe diameter (cm)
D_r	Relative density (dimensionless)
e	Void ratio (dimensionless)
e_{max}	Maximum possible void ratio (loosest condition)
e_{min}	Minimum void ratio (densest condition)
f_s	Sleeve friction (N m^{-2})
F_T	Total resistance force (N)
K	Coefficient of lateral pressure at rest (dimensionless)
K_p	Passive coefficient of lateral stress (dimensionless)
L	Lateral extension of the slip lines (m)
m_s	Mass of sand (kg)
N_q	Bearing capacity factor (dimensionless)
q_c	Cone resistance (N m^{-2})
V_S	Volume of solid particles (m^3)
V_T	Total volume (m^3)
V_v	Volume of voids (m^3)
Z	Penetration depth (m)
γ	Effective unit weight of sand (N m^{-3})
φ	Friction angle of sand (°)
ρ_s	Particle density of sand (kg m^{-3})

Table 2
List of probes and experimental parameters.

Series	Diameter (cm)	Length (cm)	Tip length (cm)	Tip angle (°)
Series 1				
Probe 1	0.9	50.8	1.8	30
2	0.9	50.8	0.9	60
3	0.9	50.8	0.6	90
4	0.9	50.8	0.3	120
Series 2				
Probe 1	1.2	51	2.4	30
2	1.2	51	1.2	60
3	1.2	51	0.7	90
4	1.2	51	0.4	120
Series 3				
Probe 1	1.9	50.8	3.4	30
2	1.9	50.8	1.7	60
3	1.9	50.8	1	90
4	1.9	50.8	0.6	120
Series 4				
Probe 1	2.5	51	4.6	30
2	2.5	51	2.2	60
3	2.5	51	1.35	90
4	2.5	51	0.8	120

including density, compaction and porosity. Table 1 shows symbols used through the paper and their definition.

2. Experimental apparatus

A list of probes was used to simulate OPRA in the penetration tests. We used 16 different probes categorized into four groups (Table 2). These probes vary in diameter, length and tip apex angle to envelop most of the variables potentially affecting the penetration force. They cover the expected size ranging from 0.9 to 1.9 cm in diameter, and tip angle of 30°, 60°, 90° and 120°.

A specific apparatus was designed and built to measure the insertion and withdrawal forces of the OPRA probe in unconsolidated materials. A general illustration of the setup is shown in Fig. 2. A parallel shaft gear motor drives a lead screw. The lead screw housing is made of steel with an outside diameter of 4 cm, thickness of 5 mm and length of 80 cm. The role of the housing is to move up and down in correspondence with the forward and backward movement of the motor. The housing is equipped with two reflective laser sensors, one at the top of the housing and the other one at the bottom (Fig. 3A), to stop the automated program if one of the lasers hits the reflective plates. This constraints the range of positions (depth) in which our apparatus can be safely operated. The motor is capable of working in reversible modes. The coupling between the motor and the lead screw is realized by using a two-way metal sleeve connector. The coupling piece provides high holding capacity between the motor shaft and the lead screw (Fig. 3B).

A Transducer Techniques compression load cell (MLP-1K), with a capacity of 4000 N, is attached at the bottom of the housing. A DPM-3 output panel is used as the load cell meter and calibrated to give output reading in Newton (N) with an accuracy of 0.01%. An ultrasonic depth sensor is

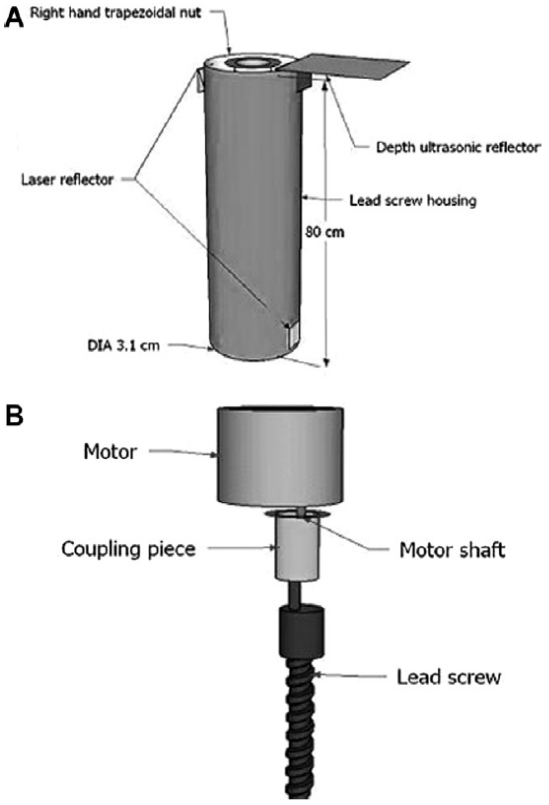

Fig. 3. (A) The lead screw housing with the laser reflectors, trapezoidal nut and depth reflector. (B) Coupling piece connecting the gear motor to the lead screw.

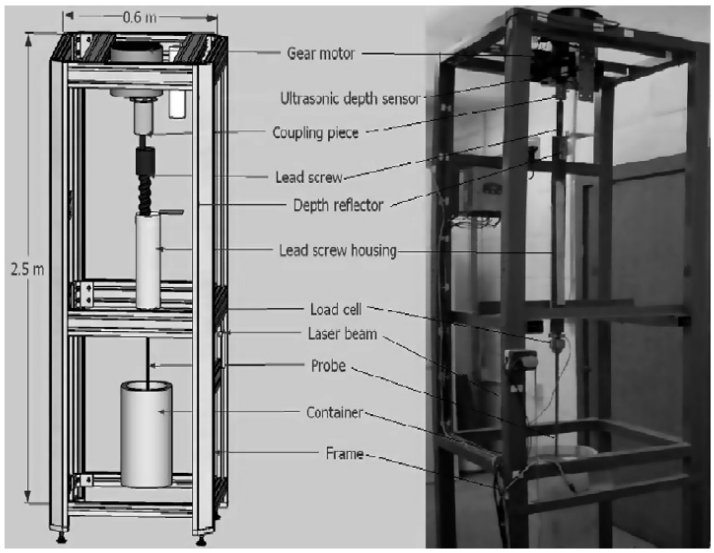

Fig. 2. OPRA penetration testing apparatus (left: scheme, right: picture).

placed on the top of the penetration stand. By measuring the distance between the sensor and the top of the regolith, the penetration distance of the probe into the regolith is measured continuously. At the top of the housing, a reflective aluminium surface is mounted in order to reflect the ultrasonic waves generated by the sensor (Fig. 3).

An automated control system was designed using a Programable Logic micro-Controller (PLC) programmed using a ladder logic program Proficy HMI/SCADA-CIMPLICITY [IC200UAL006] which has a Human Machine Interface (HMI) where the whole penetration experiment can be monitored and controlled through a personal computer. During penetration two parameters are being monitored: the penetration force and penetration depth. The Graphical Human Interface (GHI) of the data collecting software is composed of one main screen with three other sub-screens. Three outputs are shown in the main screen, the motor speed in mm s^{-1}, the penetration depth in cm and the corresponding penetration force in Newton (Fig. 4). The Insert/Remove buttons activate the probe downward and upward movement. The insert probe condition is deactivated when the probe reaches a desired depth configured by the user. The remove probe button stops its functionality when the probe is fully removed. The results of the penetration experiment are automatically saved in an Excel file.

3. Experimental procedures

Before starting the experiments, the force displayed on the GHI screen is calibrated by comparing it to the compression forces measured out of a balance. The balance output reading in kg is converted into Newton. A probe attached to the load cell is pushed down at different forces against a 200-kg capacity balance placed on the floor. The plot of the force measured by the load cell (GHI screen) versus the force measured by the balance shows a slope equal to 1 (Fig. 5), indicating that the load cell gives accurate readings and is thus perfectly calibrated for further experiments. Moreover, the error from the load cell is small enough (~1% of the measured value) to be ignored.

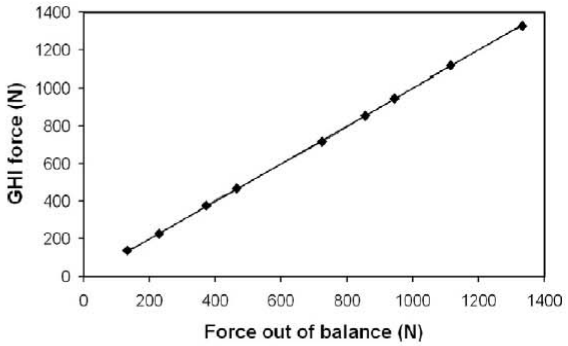

Fig. 5. Calibration of the readings out of the load cell (GHI) with the balance reading.

Samples are prepared by filling a 25 cm diameter and 65 cm deep cylindrical bucket with dry playground sand. The particle size distribution of sand was determined by sieving (Fig. 6). The results show that the sand contains 36% medium size particles (>0.5 mm) and 64% fine grained particles (<0.3 mm). The sand is poured in the bucket in 5 kg layers and the bucket is vigorously shaken in order

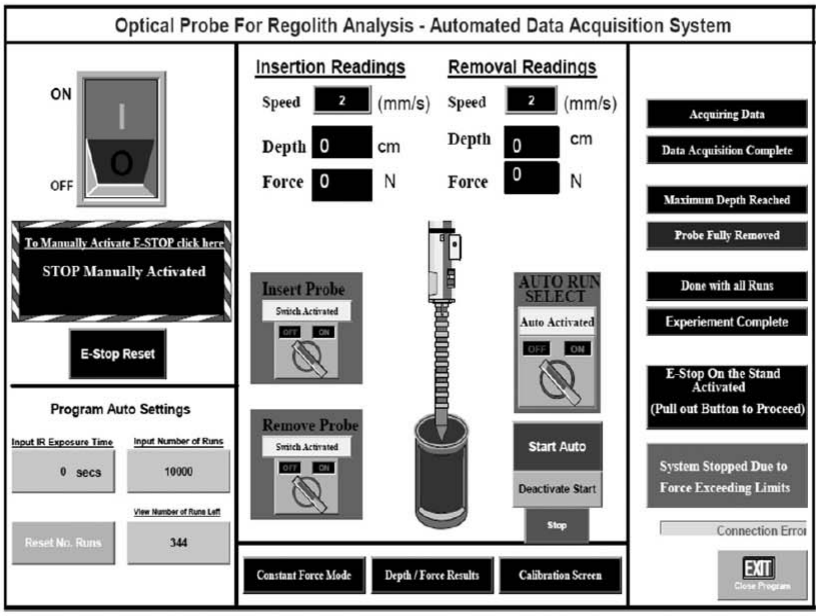

Fig. 4. Graphical Human Interface (GHI) screen.

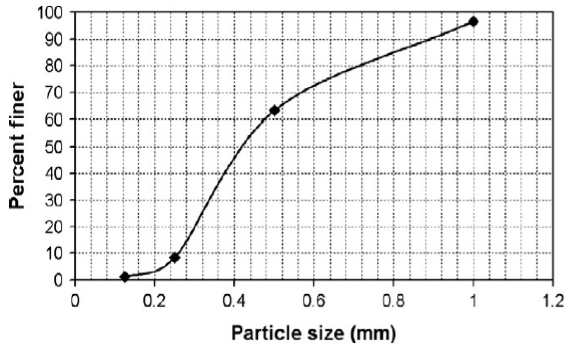

Fig. 6. Particle size distribution curve for playground sand.

to homogenize and compact the regolith. The height is measured after each compaction step to be sure that each layer has the same bulk density. Except when noticed (see Section 4.2), penetration experiments were run at a constant speed of 2 mm s^{-1}. All results are presented as measured force as a function of penetration depth.

4. Experimental results

4.1. Effect of compaction

In regolith materials, the required insertion force is generally a strong function of the density and thus of compaction (Murthy, 2002). To test the effect of compaction, a minimum bulk density of about 1550 kg m^{-3} (similar to what is indicated on Mars, Matijevic et al., 1997) and a maximum value of about 1700 kg m^{-3} (similar to what is indicated on the Moon, Mitchell et al., 1974) were chosen. Starting with a measured bulk density of 1550 kg m^{-3}, three insertions and removals were conducted and subsequently averaged. The standard error of the three runs was determined to be about 24%. The container was then shaken in order to compact the material to a higher bulk density, followed by three more penetration measurements. This procedure was repeated three times and the bulk density was determined at each step. The insertions and withdrawals of the probes themselves did not seem to compact the sand to a measurable degree. At a bulk density of 1550 kg m^{-3}, the 0.9 cm diameter, 60° tip angle probe required about 50 N to penetrate to a depth of 50 cm while it took about 1000 N to reach the same depth when the bulk density was 1700 kg m^{-3} where the standard error % was 13% (Fig. 7). Thus, a change of about 9% in the bulk density between 1550 and 1700 kg m^{-3} induces a factor 20 increase in the penetration force. The effect of compaction did not appear in the first 10 cm of the regolith, since all measured forces were in the same range for all four tested densities. Below 10 cm deep, the effect of compaction became significant according to each bulk density. The penetration forces increased with depth for 1550, 1600 and 1660 kg m^{-3} because of pore spaces where sand particles can expand. Below 45 cm deep for 1700 kg m^{-3}, the penetration forces suddenly increase with depth because of the high level of compaction making it hard for sand particles to move, especially since the probe is getting closer to the bottom of the container preventing the sand from moving. Therefore, compaction has a profound impact on the forces required for probe penetration.

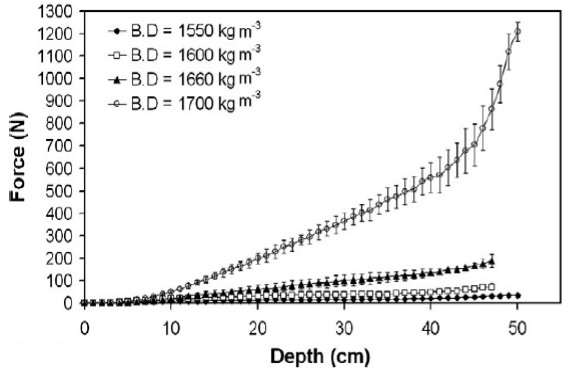

Fig. 7. Penetration force as a function of depth in sand under different bulk density ($D = 0.9$ cm, T.A. = 60°).

4.2. Effect of penetration speed

Four different motor speeds were tested (Fig. 8): 1, 2, 3 and 4 mm s^{-1} in sand with a bulk density of 1700 kg m^{-3} using the same 0.9 cm probe with a tip angle of 60° from the previous experiment. In the first 30 cm, the penetration force data for all speeds overlapped, and reached 380 N at a depth of 30 cm. We did not observe any significant difference in the required forces between each speed up to 50 cm, especially when considering the 13% error on the force value for a density of 1700 kg m^{-3} (±150 N at 50 cm depth). Thus, for the rest of the experiments, we decided to use an insertion speed of 2 mm s^{-1} since the actual penetration rate from a planetary lander or rover will probably be slow.

4.3. Effect of tip angle

Each probe was made with four tip angles: 30°, 60°, 90° and 120° since we expected that the tip angle would influ-

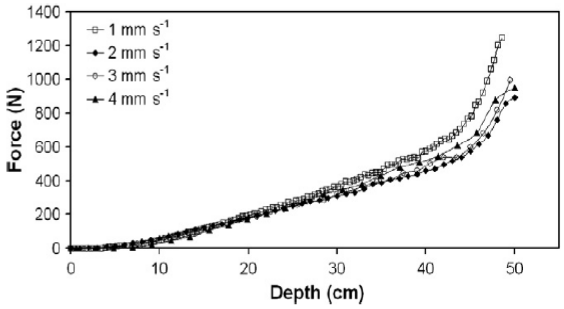

Fig. 8. Penetration force as a function of depth in sand for different motor speeds ($D = 0.9$ cm, T.A. = 60°).

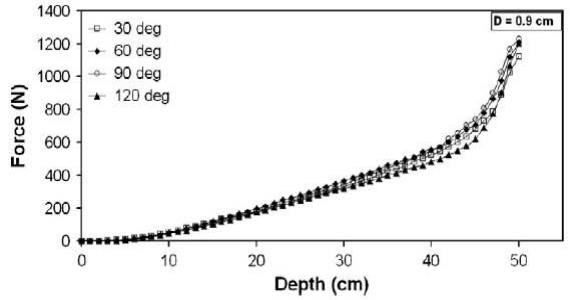

Fig. 9. Penetration force as a function of depth in sand for different tip angles and the same probes diameter ($D = 0.9$ cm).

ence the penetration force to reach a given depth. We found that the required forces were insensitive to tip angle (Fig. 9), since the four values for the tip angles at each depth are falling under the standard error (13%), their difference is not statistically significant. Therefore, the tip angle does not have any effect on the penetration force up to 50 cm depth.

4.4. Effect of diameter

Four different circular probes were made with different diameters (2.5, 1.9, 1.2 and 0.9 cm) and tested. A 30° tip angle was fixed in each experiment. The results show that the diameter strongly affects the penetration force (Fig. 10). Indeed, to reach a depth of 20 cm, a 0.9 cm probe requires about 200 N while the 1.9 cm probe needs about 1000 N. Thus, doubling the diameter (increasing the area by a factor of four) results in an increase of penetration force by a factor of five.

5. Discussion

5.1. Bearing capacity theory

The axial downward movement of the penetrometer through regolith is closely related to the problem of CPT

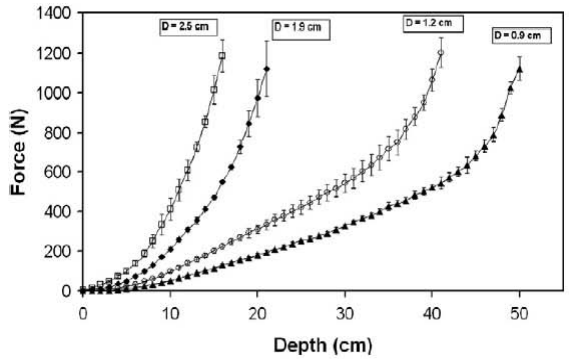

Fig. 10. Penetration force as a function of depth in sand for different diameter probes (T.A. = 30°; B.D. = 1700 kg m^{-3}).

in geotechnical engineering where it uses bearing capacity theory (Mitchell et al., 1974). The total resistance force (F_T) during probe insertion into the subsurface is the sum of two forces; the cone resistance (q_c) and the sleeve friction (f_s):

$$F_T = q_C A_C + f_S A_S \tag{1}$$

where A_c is the area of the cone, A_s is the buried area of the sleeve. For sand, the cone resistance can be calculated from (Puech and Foray, 2002):

$$q_C = \gamma \times Z \times N_q \left(1 + \left(K \times \sin\varphi \times \frac{Z}{L}\right)\right) \tag{2}$$

where γ is the effective unit weight of sand (N m^{-3}), Z is the penetration depth (m), N_q is the bearing capacity factor (dimensionless), K is the coefficient of lateral pressure at rest (dimensionless), φ is the friction angle of sand (°) and L is the lateral extension of the slip lines (m) (the lateral distance where sand was moved due to penetration).

The friction angle is defined as (Harr, 1977)

$$\varphi = 25 + (0.15 \times D_r) \tag{3}$$

where D_r is the relative density.

The coefficient of lateral pressure is defined as (Harr, 1977)

$$K = 1 - \sin\varphi \tag{4}$$

The bearing capacity factor N_q is defined as (Puech and Foray, 2002)

$$N_q = a \times e^{b\tan\varphi} \tag{5}$$

For sand, $a = 1.0584$ and $b = 6.1679$ (Puech and Foray, 2002).

Finally, the lateral extension of the slip lines L is defined as (Puech and Foray, 2002)

$$L = B \times e^{\left(\frac{\pi}{2}\times\tan\varphi\right)} \times \tan\left(\frac{\pi}{4} + \frac{\varphi}{2}\right) \tag{6}$$

where B is the cone diameter (m). The relative density (D_r) used in Eq. (3) is an index that quantifies the degree of compaction (packing between loosest and densest state) of coarse-grained soils (Lunne et al., 1997):

$$D_r = \frac{e_{max} - e}{e_{max} - e_{min}} \tag{7}$$

where e is the void ratio of the sample. e_{max} is the maximum possible void ratio (loosest condition) and e_{min} is the minimum void ratio (densest condition) of the sand (Lunne et al., 1997). The void ratio is the ratio between the volume of void (V_v) and the volume of solid (V_s):

$$e = \frac{V_v}{V_s} \tag{8}$$

From the knowledge of particle density of sand, the volume of solid particles can be calculated from:

$$V_s = \frac{m_s}{\rho_s} \tag{9}$$

where V_s is the volume of solid particles (m^3), m_s is the mass of sand (kg) and ρ_s is the particle density of sand ($kg\ m^{-3}$). The particle density (ρ_s) determination for sand is carried out by filling a beaker with water to a specific volume, pouring a weighted amount of sand into the beaker and measure the change in volume. The resulting sand particle density is $\rho_s = 2556\ kg\ m^{-3}$ (density of quartz, the main mineral of sand) and the values of e_{max} and e_{min} are found to be 0.71 and 0.34, respectively. From the volume of solid particles (V_s), the volume of voids (V_v) is calculated by:

$$V_v = V_T - V_s \tag{10}$$

where V_T is the total volume of regolith.

Using the previous values for e_{max} and e_{min}, and combining with the value of e, we determine (D_r). The theoretical friction resistance of the sleeve (f_s) is defined as (Harr, 1977):

$$f_s = \frac{K_p \times \gamma \times Z \times A_s}{3} \tag{11}$$

where γ is the effective unit weight of sand ($N\ m^{-3}$), Z is the penetration depth (m), A_s is the area of sleeve (m^2) and K_p is the passive coefficient of lateral stress (Harr, 1977):

$$K_p = \frac{1 + \sin\phi}{1 - \sin\phi} \tag{12}$$

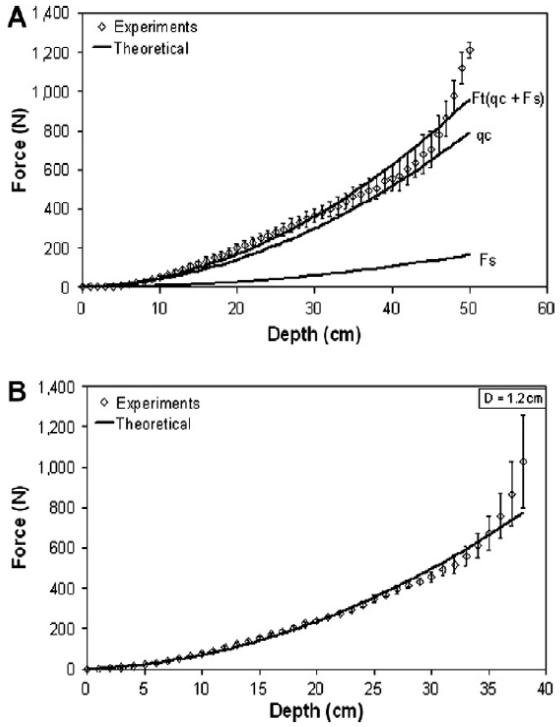

Fig. 11. (A) Theoretical verses experimental data in sand ($D = 0.9$ cm). (B) Theoretical verses experimental data in sand ($D = 1.2$ cm).

Then we calculate the total force (F_T, Eq. (1)) to insert the probe in the regolith simulant. The results are displayed in Fig. 11 and compared to the experimental data for two different diameter probes ($D = 0.9$ cm and $D = 1.2$ cm). Theoretical results fit very well the experimental data and show that cone resistance is about four times higher than sleeve friction. We observe a divergence between the model and the experimental data around 45 cm depth. Because we are reaching the bottom of the cylinder and there is no place for the regolith to expand which increases the resistance force.

In the model, the relative density of the tested samples and the probes diameter are the most dominant effects which affect the cone resistance. Experimental data are in agreement with the theoretical model regarding these two dominant effects.

5.2. Application to other planetary bodies

Gravity plays an important role in the performance of penetrometers whether they are fast or slow. Fast penetrometers may not be able to obtain sufficient kinetic energy from free-fall in the gravity field to achieve the desired degree of penetration. Therefore, there may be a need for added propulsion to increase the impact velocity. Also, a body with weak gravity would likely lack an atmosphere that could be used to orient the falling penetrometer with respect to the surface. Gravity also affects the mechanical properties of the subsurface material. A low gravity environment such as that found on asteroids and comets reduces the required penetration force because the required force is proportional to the overburden pressure and thus to gravity. Results from Deep Impact mission revealed a low-density material on comet Temple 1 (Kerr, 2005) which would ease the penetration process. On the other hand, an anchor system may be used in order to hold the lander or the rover with the body of the asteroid during penetration.

The maximum force for penetration would be the weight of the lander/rover on their targeted planetary surface. Table 3 shows the weight for past, present spacecrafts on their respective planets, which represents the maximum applicable force before tilting the rover. Penetration forces

Table 3
List of planetary landers and rovers and their weights on the target planetary body.

Vehicle	Planetary body	Weight (N)
Luna 13	Moon	184
Surveyor	Moon	480
Lunakhod	Moon	1360
Viking	Mars	2210
Sojourner	Mars	39
Beagle 2	Mars	123
Spirit/opportunity	Mars	683
Mars Science Lab	Mars	3320
Venera 13	Venus	6740
Huygens	Titan	431

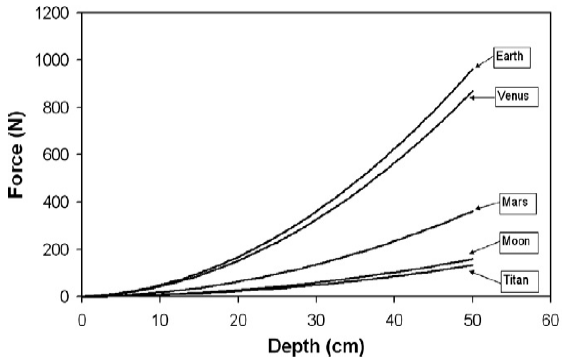

Fig. 12. Theoretical penetration forces as a function of depth for different planetary bodies under their own gravity.

are directly proportional to the lithostatic pressure which is affected by gravity. Fig. 12 shows the theoretical penetration forces as a function of depth which are needed to penetrate Earth, Venus, Mars, Moon and Titan. In this model, we assume that sand with its characteristics covers about the first meter of the subsurface of these planetary bodies and has a bulk density of about 1800 kg m^{-3} and the gravity is scaled according to each planetary body. When the gravity of the planetary body decreases, density, porosity, friction angle and relative density will decrease and therefore, force needed for penetration will decreases as well. A spacecraft weighing about 200 N on the Moon or Titan is capable of delivering penetration forces for a 1 cm diameter probe to reach a depth of about 0.5 m; a rover weighting about 500 N on Mars would reach the same depth. For the planetary bodies of interest (mostly Mars, Titan and the Moon), the maximum force to penetrate down to 0.5 m is below 400 N (Fig. 12). This means that most landers/rovers would be able to do penetration experiments on their respective planetary bodies. The only exceptions would be the smallest rovers like Sojourner and Beagle 2 (Mars). This also demonstrates that the weight of static

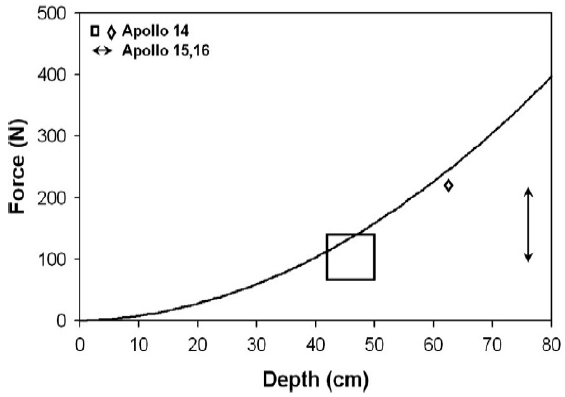

Fig. 13. Theoretical penetration force as a function of depth for the moon along with Apollo 14, 15 and 16 lunar data. Thick black line is the theoretical calculation.

landers (Phoenix and Huygens, for example) would be enough to insert a probe in the subsurface during landing.

Penetration forces have been measured successfully on the Moon using the Apollo Simple Penetrometer (ASP) on Apollo 14 which was pushed manually by the astronaut and the Self-Recording Penetrometer (SRP) which was connected to a drum to record the force versus depth on board Apollo 15 and 16 (Mitchell et al., 1971). Having these results is a good opportunity to verify the model on another planetary body. Fig. 13 shows the moon theoretical model and the results obtained by Apollo 14, 15 and 16 lunar data. Results from Apollo 14 are in good agreement with the theoretical model (using the previously determined parameters for sand and a density of 1800 kg m^{-3}) while the data of ASR on board Apollo 15 and 16 are less than the theoretical model by about 145 N. The reason for that difference is that the subsurface of the moon is not homogenous all over and its subsurface layers vary in thickness from one place to another. Fig. 13 supports our assertion that the driving factor for penetration on other planetary bodies is gravity.

6. Conclusions

This research was conducted to investigate and quantify different factors which affect the insertion process of different small probes in sand. To capture most of the effects, probes of different diameter, length, penetration speed and tip angle were used.

It was found that compaction levels play an important role on the required forces for probe penetration. An increase in bulk density from 1550 to 1700 kg m^{-3} resulted in increase in penetration force from 10 to 200 N at 20 cm depth.

The diameter of the probes is the second most dominant effect. It was found that by increasing the diameter of the probe, the corresponding penetration force increases linearly which was in agreement with (Terzaghi, 1943; Vesic, 1963).

No noticeable effect was found relating the speed and probe tip angles to the corresponding forces of penetration. Since there is no significant effect of tip angle, we can add a down looking hemispherical window in place of the tip which can provide spectra of the material directly under the probe.

Bearing capacity theory was used to explain the experimental sand data. Applying the model to sand was possible due to the knowledge of the bearing capacity factor N_q and showed a good agreement with the experimental results. The model was used to predict the force due to penetration on other planetary bodies such as Venus, Mars, Titan and the Moon where we are taking the effect of gravity into our considerations. From the extrapolation of the results on other planetary bodies, gravity showed that it is a primary factor driving the penetration resistance. A comparison between the theoretical model of the Moon and Apollo lunar was performed. The predicted force of penetration

was in agreement with Apollo 14 penetration lunar data while it was higher than Apollo 15 and 16 by 145 N at 76 cm depth which may be due to the non-homogenous structure of the subsurface of the Moon. Mars Science Lab (MSL) will be weighting about 3320 N on Mars. A 9 mm probe would be a good choice for OPRA to safely reach to about 0.5 m down into the subsurface of Mars or the Moon.

Acknowledgments

The authors would like to thank the National Aeronautics and Space Administration (NASA) and its Planetary Instrument Definition and Development Program (PIDDP) for the funding for this project under Grant No. NNX07AM86G. We would like to thank Obadiah Kegege and Lauren Foster for their automated program design. Finally, we would like to thank the anonymous reviewers and Dr. Kris Zacny for their comments which largely improved the quality of our manuscript.

References

Binzel, R.P., Morbidelli, A., Merouane, S., DeMeo, F.E., Birlan, M., Vernazza, P., Thomas, C.A., Rivkin, A.S., Bus, S.J., Tokunaga, A.T. Earth encounters as the origin of fresh surfaces on near-Earth asteroids. Nature 463, 331–334, 2010.

Chapman, C.R. S-type asteroids, ordinary chondrites, and space weathering: the evidence from Galileo's fly-bys of Gaspra and Ida. Meteorit. Planet. Sci. 31, 699–725, 1996.

Glaser, L.D., Andrew, J.B., Zacny, K.A. A review of penetrometers for subsurface access on comets and asteroids. Meteorit. Planet. Sci. 43, 1021–1032, 2008.

Hansen, J.B.. A revised and extended formula for bearing capacity. Bulletin, vol. 28. Danish Geotechnical Institute, Copenhagen, 1970.

Harr, M.E.. Mechanics of Particulate Media, vol. 260. McGraw-Hill, 1977.

Housen, K.R., Wilkening, L.L. Regoliths on small bodies in the solar system. Annu. Rev. Earth Planet. Sci. 10, 355–376, 1982.

Kargl, G., Kömle, N.I., Ball, A.J., Lorenz, R.D. Penetrometry in the solar system II, in: Proceedings of the International Workshop Held in Graz, Austria, September 25–28. Austrian Academy of Sciences Press, Vienna, 2006.

Kerr, R.A. Deep impact finds a flying snowbank of a comet. Science 309, 1667, 2005.

Kochan, H., Hamacher, H., Richter, L., Hirschmann, L., Assanelli, S., Nadalini, R., Pinna, S., Gromov, V.V., Matrossov, S., Yudkin, E.N., Coste, P., Pillinger, C., Sims, M. The mobile penetrometer (mole) – a tool for planetary sub-surface investigations, in: Kömle, N.I., Kargl, G., Ball, A.J., Lorenz, R., Graz, D. (Eds.), Penetrometry in the Solar System. Space Research Institute, Austrian Academy of Sciences, Austria, pp. 212–243, 2001.

Longwell, C.R., Flint, R.F.. Introduction to Physical Geology, vol. 324–345. John Wiley & Sones, Inc., New York and London, 1962.

Lorenz, D.R., Bannister, M., Daniell, P.M., Krysinski, Z., Leese, M.R., Miller, R.J., Newton, G., Rabbetts, P., Willett, D.M., Zarnecki, J.C. An impact penetrometer for a landing spacecraft. Meas. Sci. Technol. 5, 1033–1041, 1994.

Lunne, T., Robertson, P.K., Powell, J.J.M. Cone Penetration Testing in Geotechnical Practice, first ed Blackie Academic and Professional, London, 1997.

Matijevic, J.R., Crisp, J., Bickler, D.B., Banes, R.S., Cooper, B.K., Eisen, H.J., Gensler, J., Haldemann, A., Hartman, F., Jewett, K.A., Matthies, L.H., Laubach, S.L., Mishkin, A.H., Morrison, J.C., Nguyen, T.T., Sirota, A.R., Stone, H.W., Stride, S., Sword, L.F., Tarsala, J.A., Thompson, A.D., Wallace, M.T., Welch, R., Wellman, E., Wilcox, B.H., Ferguson, D., Jenkins, P., Kolecki, J., Landis, G.A., Wilt, D. Characterization of the martian surface deposits by the Mars Pathfinder Rover, Sojourner. Science 278, 1765, 1997.

Mitchell, J.K., Bromwell, L.G., Carrier, W.D., Costes, N.C., Scott, R.F. Soil Mechanics Experiment. Apollo 14 Preliminary Science Report. NASA SP, NASA SP-272, pp. 87–108, 1971.

Mitchell, J.K., Houston, W.N., Carrier, W.D., Costes, N.C. Apollo Soil Mechanics Experiment S-200. Final Report, NASA Contract NAS 9-11266, Space Science Laboratory Series, vol. 15, no. 7. University of California, Berkeley, 1974.

Murthy, V.N.S. Geotechnical Engineering: Principles and Practices of Soil Mechanics and Foundation Engineering (Civil and Environmental Engineering). CRC Press, 2002.

Puech, A., Foray, P. Refined model for interpreting shallow penetration CPTs in sands, in: Offshore Technology Conference, May 6–9, Houston, Texas, 2002.

Richter, L., Coste, P., Gromov, V.V., Kochan, H., Nadalini, R., Ng, T.C., Pinna, S., Richter, H.E., Yung, K.L. Development and testing of subsurface sampling devices for the Beagle 2 Lander. Planet. Space Sci. 50, 903–913, 2002.

Pilgrim, R., Ulrich, R., Leftwich, M. Subsurface spectroscopic probe for regolith analysis, in: Poster at 40th LPSC Conference, Houston, TX, 1219, 2009.

Stoker, C.R., Richter, L., Smith, W.H., Lemke, L.G., Hammer, P., Dalton, J.B., Glass, B., Zent, A. The Mars underground mole (MUM): a subsurface penetration device with insitu infrared reflectance and Raman spectroscopic sensing capability, in: Sixth International Conference on Mars, 3007, 2003.

Terzaghi, K. Theoretical Soil Mechanics. John Wiley, New York, 1943.

Vesic, B.A. Bearing Capacity of Deep Foundations in Sand. High Way Research Record No. 39, pp. 112–153, 1963.

Zarnecki, J.C., Leese, M.R., Garry, J.R.C., Ghafoor, N., Hath, B. Huygens surface science package. Space Sci. Rev. 104, 593–611, 2002.

Zarnecki, J.C., Leese, M.R., Hathi, B., Ball, A.J., Hagermann, A., Towner, M.C., Lorenz, R.D., McDonnell, J.A.M., Green, S.F., Patel, M.R., Ringrose, T.J., Rosenberg, P.D., Atkinson, K.R., Paton, M.D., Banaszkiewicz, M., Clark, B.C., Ferri, F., Fulchignoni, M., Ghafoor, N.A.L., Kargl, G., Svedhem, H., Delderfield, J., Grande, M., Parker, D.J., Challenor, P.G., Geake, J.E. A soft solid surface on Titan as revealed by the Huygens surface science package. Nature 438, 792–795, 2005.

ELSEVIER LICENSE
TERMS AND CONDITIONS

Mar 29, 2012

This is a License Agreement between Ahmed ElShafie ("You") and Elsevier ("Elsevier") provided by Copyright Clearance Center ("CCC"). The license consists of your order details, the terms and conditions provided by Elsevier, and the payment terms and conditions.

All payments must be made in full to CCC. For payment instructions, please see information listed at the bottom of this form.

Supplier	Elsevier Limited The Boulevard,Langford Lane Kidlington,Oxford,OX5 1GB,UK
Registered Company Number	1982084
Customer name	Ahmed ElShafie
License number	2878331194864
License date	Mar 29, 2012
Licensed content publisher	Elsevier
Licensed content publication	Advances in Space Research
Licensed content title	Penetration testing for the Optical Probe for Regolith Analysis (OPRA)
Licensed content author	A. ElShafie,V.F. Chevrier,R. Ulrich,L. Roe
Licensed content date	3 August 2010
Licensed content volume number	46
Licensed content issue number	3
Number of pages	10
Start Page	327
End Page	336
Type of Use	reuse in a thesis/dissertation
Portion	full article
Format	both print and electronic
Are you the author of this Elsevier article?	Yes
Will you be translating?	No
Order reference number	
Title of your thesis/dissertation	Subsurface Planetary Investigation Techniques
Expected completion date	May 2012
Estimated size (number of pages)	120